UNIVERSITÀ DEGLI STUDI DI PADOVA

Department of Information Engineering

Doctoral Thesis in
Information and Communications Technology

XXXII Series

Energy Management Strategies for Sustainable 5G Mobile Networks

PhD Candidate
ÁNGEL FERNÁNDEZ GAMBÍN

Supervisor
Prof. Michele Rossi

Coordinator
Prof. Andrea Neviani

Academic Year 2018/2019

To my family and supervisor for their invaluable support.

Abstract

The massive use of Information and Communications Technology (ICT) is increasing the amount of energy drained by the telecommunication infrastructure and its footprint on the environment. With the advent of the smartphone, mobile traffic is massively growing driven by both the rising number of user subscriptions and an increasing average data volume per subscription. This is putting a lot of pressure on the mobile network operators side, which are enforced to boost their infrastructure capacity by densifying the network with more Base Stations (BSs) and resources, which translates to a growth in the energy consumption and related costs. Hence, any future development in the ICT sector and its infrastructure has definitely to cope with their environmental and economical *sustainability*, where energy management is essential.

In this thesis, we discuss the role of energy in the design of eco-friendly cost-effective sustainable mobile networks and, in particular, we elaborate on the use of Energy Harvesting (EH) hardware as a means to decrease the environmental footprint of the 5G network. Specifically, we investigate energy management strategies in 5G mobile networks with the main goals of: (i) improving the energy balance across base stations and other network elements, (ii) understanding how the energy can be exchanged either among network elements and the electrical grid, and (iii) investigating how renewable energy sources can be utilized within network elements to maximize the utility for the overall network in terms of better performance for the users (e.g., throughput, coverage, etc.), and lower energy consumption (i.e., carbon footprint) for the 5G network infrastructure.

Therefore, we address, formulate and solve some of the problems related to the *energy management* in different scenarios within the 5G mobile network. The main covered topics are: (i) *Wireless Energy Transfer* where we investigate the tradeoffs involved in the recharging process from base stations to end users; (ii) *Energy Cooperation in Mobile Networks* where we target deployments featuring BSs with EH capabilities, i.e., equipped with solar panels and energy storage units, that are able to transfer energy among them; (iii) *Energy Trading with the Electrical Grid* where energy management schemes to diminish the cost incurred in the energy purchases from the electrical grid are pursued; and (iv) *Energy Harvesting and Edge Computing Resource Management* where EH and Mobile Edge Computing (MEC) paradigms are combined within a multi-operator infrastructure sharing scenario with the goal of maximizing the exploitation of the network resources while decreasing monetary costs. Online learning techniques, such as Gaussian Processes and Machine Learning Neural Networks, and adaptive control tools, like Model Predictive Control, are put together to tackle these challenges with remarkable results in decreasing costs related to energy purchases from the electrical grid and energy efficiency among network elements.

Contents

Abstract **iv**

List of Figures **x**

List of Tables **xii**

List of Acronyms **xiii**

1 Introduction **1**
1.1 Thesis Outline 3

2 State of the Art **5**
2.1 Introduction 5
2.1.1 Chapter Outline 5
2.2 Wireless Power Transfer 5
2.2.1 Wireless Energy Transfer 5
2.2.2 Simultaneous Wireless Information and Power Transfer 6
2.2.3 Wireless Powered Communication Network 9
2.2.4 State-of-the-Art of RF and Microwave Energy Conversion Efficiencies 10
2.2.5 Conclusions 10
2.3 Energy Cooperation in Mobile Networks 12
2.3.1 Energy Sharing 13
2.3.2 Communication Cooperation 15
2.3.3 Conclusions 16
2.4 Energy Trading with the Electrical Grid 17
2.4.1 A Review of Energy Trading in Smart Grids 17
2.4.2 Cellular Networks meet SG 19
2.4.3 Conclusions 21
2.5 Conclusions 22

3 Energy Transfer from Base Stations to End Users **24**
3.1 Introduction 24
3.1.1 Contributions 25
3.1.2 Chapter Outline 25
3.2 Related Work 25
3.3 System Model 27
3.3.1 Channel Models 27
3.3.2 Transmission Beamforming for WPT 28
3.3.3 Energy Consumption and Efficiency Metrics 29

3.3.4 Mobility Models . . . 30
3.4 Wireless Power Transfer Policies . . . 31
3.4.1 Policy 1 (genie-based, metric M_1) . . . 32
3.4.2 Policy 2 (heuristic, metric M_1) . . . 32
3.4.3 Policy 3 (genie-based, no metric) . . . 33
3.4.4 Policy 4 (heuristic, no metric) . . . 33
3.4.5 Policy 5 (genie-based, metric M_2) . . . 33
3.4.6 Policy 6 (heuristic, metric M_2) . . . 34
3.5 Numerical Results . . . 34
3.6 Conclusions . . . 39

4 Energy Cooperation among Energy Harvesting Base Stations 42
4.1 Introduction . . . 42
4.1.1 Contributions . . . 44
4.1.2 Chapter Outline . . . 44
4.2 Related Work . . . 45
4.2.1 Energy Transfer in Mobile Cellular Networks . . . 45
4.2.2 Pattern Learning along with Multi-step Optimization Techniques . . . 47
4.2.3 Novelty of the Present Work . . . 48
4.3 System Model . . . 48
4.3.1 Power Packet Grids . . . 48
4.3.2 Harvested Energy Profiles . . . 49
4.3.3 Traffic Load and Power Consumption . . . 49
4.3.4 Energy Storage Units . . . 49
4.4 Optimization Framework . . . 51
4.4.1 Overview of the Online Optimization Framework . . . 52
4.4.2 Pattern Learning . . . 53
4.4.3 Model Predictive Control . . . 57
4.4.4 Energy Allocation . . . 59
4.4.5 Energy Routing . . . 61
4.5 Numerical Results . . . 64
4.5.1 Performance Evaluation of the Pattern Learning Scheme . . . 64
4.5.2 Performance Evaluation of the Optimization Framework . . . 68
4.6 Conclusions . . . 72

5 Energy Harvesting and Edge Computing Resource Management 75
5.1 Introduction . . . 75
5.1.1 Contributions . . . 76
5.1.2 Chapter Outline . . . 76
5.2 Related Work . . . 76
5.3 System Model . . . 79
5.3.1 Harvested Energy Profiles . . . 80
5.3.2 Traffic Load Profiles . . . 80
5.3.3 Energy Consumption . . . 81

5.3.4 Energy Storage Units 81
5.3.5 Electric Retail Pricing 82
5.4 Optimization Framework 82
5.4.1 Pattern Forecasting 84
5.4.2 Adaptive Control 86
5.4.3 Algorithm Steps: 87
5.5 Numerical Results 88
5.5.1 Performance Evaluation of the Pattern Forecasting 88
5.5.2 Performance Evaluation of the Optimization Framework 89
5.6 Conclusions 96

6 Conclusions **98**

Acknowledgments **100**

List of Publications **101**

References **103**

List of Figures

2.1 WPT architectures. Green arrows represent energy transmission, whereas red arrows indicate information transmission. In the figure, AP represents an Access Point, i.e., a BS, while U1 and U2 represent end users. 6
2.2 SWIPT receiver designs. 8
2.3 State-of-the-art RF and microwave conversion efficiencies from [1]. Several topologies are used under a variety of load conditions and technologies. 11
2.4 Energy sharing scenarios 13
2.5 Communication cooperation scenario 14
2.6 Diagram illustrating the two ways of interaction between mobile networks and the smart grid. 20

3.1 Example of node's movement in RWP [2]. (x_i, y_i), $i \in \{1, \ldots, 8\}$, are the destinations for 8 subsequent steps, (x_0, y_0) is the initial position. 31
3.2 Example of group movement in RPGM [2]. The dashed straight lines represent the followers' reference path in absence of deviations. Two topology snapshots are drawn: one at the w-th window, and one at the $(w+1)$-th window. 32
3.3 Power transfer efficiency η *vs* inter-base station distance d_{BS}. RWP mobility, $N =$ 100 UEs, $P_{\text{tx}} = 16$ W and $M = 4$ transmit antennas. 34
3.4 Power transfer efficiency η varying the transmit frequency f_{tx}. 36
3.5 Power transfer efficiency η varying the maximum UE speed $v_{\max}$. 37
3.6 Power transfer efficiency η *vs* number of transmit antennas, M. 37
3.7 Power transfer efficiency η *vs* α. 38
3.8 Normalized average energy per non-dead node per window *vs* α. 39
3.9 Fraction of dead nodes *vs* number of transmit antennas M. RWP mobility with maximum user speed $v_{\max} = 2.5$ m/s. 40

4.1 Power packet grid topology. 43
4.2 Overview of the optimization framework. 44
4.3 Load pattern profiles (two classes). 50
4.4 Example for the allocation of energy routes. 63
4.5 One-step online forecasting for two weeks of data. 66
4.6 Multi-step prediction with different kernels. 67
4.7 Numerical results over the cluster probability p. 70
4.8 Outage probability $\gamma(t)$ over a day. 71
4.9 Numerical results regarding purchased energy. 72

5.1 Example of the considered scenario where three operators (black, red and blue) share the EH and MEC infrastructure. 79
5.2 Traffic load patterns. 80

5.3 LSTM memory cell diagram. 85
5.4 LSTM network architecture. 85
5.5 Model predictive control framework. 86
5.6 LSTM forecasting examples. 90
5.7 Average computational load *vs* capacity in the MEC server. 91
5.8 Average difference between needed $\boldsymbol{R(t)}$ and allocated $\boldsymbol{M(t)}$ VMs *vs* capacity in the MEC server. 91
5.9 MPC behavior over one day. 93
5.10 Average purchased energy *vs* traffic load. 94
5.11 Average purchased energy *vs* EB losses factor. 94
5.12 Average purchased energy *vs* EH farm capacity. 95
5.13 Optimization horizon evaluation. 96

List of Tables

3.1 Battery discharge power P_d *vs* activity from [3]. 29
3.2 System parameters used in the numerical results. 35
3.3 Parameters used in the following plots. 36

4.1 Average $\mathrm{RMSE}_*^{(t)}$. 64
4.2 System parameters used in the numerical results. 68

5.1 System parameters used in the numerical results. 88
5.2 Average values of the performance evaluation regarding **P2**. 92

List of Acronyms

ANN Artificial Neural Network

AP Access Point

ARIMA Autoregressive Integrated Moving Average

ARPU Average Revenue Per Unit

BS Base Station

CO Convex Optimization

CoMP Coordinated MultiPoint

CPU Central Processing Unit

CSI Channel State Information

DC Direct Current

DR Demand Response

DSM Demand-Side Management

EB Energy Buffer

EH Energy Harvesting

EPN Energy Packet Network

FDMA Frequency Division Multiple Access

GP Gaussian Process

GPs Gaussian Processes

ICT Information and Communications Technology

ID Information Detection

ITU International Telecommunication Union

LSTM Long Short-Term Memory

MC Memory Cell

MDP Markov Decision Process

MEC Mobile Edge Computing

MIMO Multiple Input Multiple Output

MISO Multiple Input Single Output

ML Machine Learning

MPC Model Predictive Control

MSE Mean Squared Error

NFV Network Function Virtualization

PPG Power Packet Grid

QoS Quality of Service

RAN Radio Access Network

RF Radio Frequency

RFID Radio-Frequency IDentification

RMSE Root Mean Square Error

RNN Recurrent Neural Network

RPGM Reference Point Group Mobility Model

RSSI Received Signal Strength Indicator

RWP Random Waypoint Model

SG Smart Grid

SNR Signal-to-Noise Ratio

SWIPT Simultaneous Wireless Information and Power Transfer

TDM Time Division Multiplexing

TDMA Time Division Multiple Access

TIM Telecom Italia Mobile

UE User Equipment

UHF Ultra High Frequency

VM Virtual Machine

VNF Virtualized Network Function

WET Wireless Energy Transfer

WPCN Wireless Powered Communication Network

WPT Wireless Power Transfer

WSN Wireless Sensor Network

1

Introduction

We live in the digital era where humans and machines alike are globally connected through the Internet. With the advent of 4G technology and the smartphone, mobile traffic is massively growing driven by both the rising number of user subscriptions and an increasing average data volume per subscription, fueled primarily by a higher viewing time, online embedded video and streaming services, plus the evolution toward higher resolutions [4]. Actually, International Telecommunication Union (ITU) estimated that 750 million households are online and there exist almost as many mobile subscribers as people in the world [5]. This new era is undoubtedly opening up new possibilities for individuals as well as new opportunities for businesses and organizations. However, this is putting a lot of pressure on the mobile network operators side, which are enforced to boost their infrastructure capacity by densifying the network with more Base Stations (BSs) and resources, increasing the amount of energy drained by the telecommunication sector and its footprint on the environment. Forecast values for 2030 are that 51% of the global electricity consumption and 23% of the carbon footprint by human activity will be due to ICT [6], which also translates into electricity bills in the order of 10 billion for the operators worldwide [7]. Moreover, the ICT industry has to solve an economical problem, since operators' Average Revenue Per Unit (ARPU) is decreasing every year (see an example here [8]). One of the reasons of this is the annual increase of the OPerative EXpenditure (OPEX) of its network. Energy has been dominating these costs: it has been calculated that the energy bill equals the cost of the personnel required to run and maintain the network, for a western Europe company in 2007 [8]. Hence, any future development in the ICT sector and in its infrastructure has definitely to cope with their environmental and economical *sustainability*, where energy management is essential.

In this thesis, we discuss the role of energy in the design of eco-friendly cost-effective sustainable mobile networks, focusing on the use of Energy Harvesting (EH) hardware as a means to decrease the environmental footprint of the 5G network. Specifically, we investigate energy management strategies in 5G mobile networks with the following *objectives*:

i) Improve the energy balance across BSs and other network elements.

ii) Understand how the energy can be exchanged either among network elements and the electrical grid.

iii) Investigate how energy from ambient energy sources, i.e., harvested energy, can be utilized within network elements to maximize the utility for the overall network in terms of: better performance for the users (e.g., throughput, coverage, etc.), and lower energy consumption (i.e., carbon footprint) for the 5G network infrastructure.

Therefore, the prime goal is to address, formulate and solve some of the problems related to the energy management in different scenarios within the 5G mobile network. The main *topics* covered in this thesis are the following:

T1) **Wireless Energy Transfer:** we investigate the tradeoffs involved in the recharging process within a dense mobile network deployment, where mobile users can be wirelessly recharged through radio frequency transmissions. Our objective is to devise and compare several distributed charging schemes, that dictate *which* users have to be charged and *when*, depending on the residual energy level in their batteries, on their distance from the serving BS, on the radiating frequency and on their mobility behavior. The focus is on a distributed network deployment, considering explicitly user mobility.

T2) **Energy Cooperation in Mobile Networks:** we target deployments featuring small BSs with EH capabilities, i.e., equipped with solar panels and energy storage units. BSs can collect energy from the environment, and have a local energy storage, which they can use to accumulate energy when the harvested inflow is abundant. This local energy reserve can be utilized to serve the local traffic and can be transferred to other BSs (energy routing) to compensate for imbalance in the harvested energy or in the traffic load. Some of the BSs, referred to as *ongrid*, are connected to the power grid, whereas the others are *offgrid* and, as such, rely on either the locally harvested energy or on the energy transferred from other BSs. Within this setup, intelligent policies are to be designed to transfer the surplus energy to *offgrid* BSs, to ensure the self-sustainability of the mobile system.

T3) **Energy Trading with the Electrical Grid:** here only ongrid EH BSs are under investigation. The aim is to devise energy management schemes to diminish the cost incurred in the energy purchases from the electrical grid. This can be achieved by intelligently controlling the amount of energy that BSs buy from the power grid over time, accounting for the harvested energy, traffic load, and hourly energy prices.

T4) **Energy Harvesting and Edge Computing Resource Management:** EH and Mobile Edge Computing (MEC) paradigms are combined by considering an edge infrastructure shared among several mobile operators, and equipped with a solar EH farm for energy efficiency purposes together with an edge MEC server for low-latency computation. Two main goals are pursued: (i) maximize the exploitation of the available resources at the edge in a fair fashion among BSs belonging to different operators; and (ii) decreasing the monetary cost incurred by energy purchases from the power grid.

Although we focus on different applications and scenarios in every chapter, throughout this thesis we use similar techniques and methodologies to model, formulate and optimize the proposed problems. In particular, we leverage on pattern forecasting techniques, such as Gaussian Processes (GPs) and Machine Learning (ML) Artificial Neural Networks (ANNs), and adaptive control tools like Model Predictive Control (MPC). More details about these tools will be given in following chapters.

1.1. Thesis Outline

The rest of the thesis is organized as follows:

- **Chapter 2** presents the state of the art related to the covered topics. The content of this chapter is mainly based on publication [J1] and related to all publications listed at the end of Chapter 6.
- **Chapter 3** refers to Topic 1. It is mainly based on publication [C1].
- **Chapter 4** refers to Topic 2 and 3. This chapter is based on publications [J3], [C2], [C3] and [C4].
- **Chapter 5** tackles Topics 3 and 4. It is mainly based on publications [J2], [J5], [C5], [C6] and [C7].
- **Chapter 6** provides the final remarks and includes the list of publications summarized through this thesis.

Chapters 3, 4 and 5 can be read separately as they tackle different scenarios. Moreover, each of them defines its own notation, although some of it can be the same throughout the whole thesis.

2

State of the Art

2.1. Introduction

In this chapter, we elaborate on the topics presented in Section 1.1. The aim of the chapter is to introduce the topics and their related work, by discussing the existing literature, highlighting open issues, and presenting possible solutions and contributions that will be explained with more details in the following chapters.

2.1.1. Chapter Outline

The rest of the chapter is organized as follows. In Section 2.2, we analyze the possibility of wirelessly transferring energy to end-devices through different techniques. New network design paradigms in mobile networks, named energy cooperation and energy trading, are respectively described in Sections 2.3 and 2.4. There, it is shown that network nodes can collaborate for energy self-sustainability and even trade some energy with the electrical grid to make profit, in the presence of renewable energy sources. Insight and conclusions are provided at the end of each section. Our final remarks are given in Section 2.5.

2.2. Wireless Power Transfer

Wireless Power Transfer (WPT) [9] technology allows charging a mobile device without the need to connect it to any external power supply and, in some cases, without the user even being aware of it. In the following, we analyze WPT techniques that have been studied from different perspectives:

1) **Wireless Energy Transfer (WET):** concentrating on the energy transfer from BSs to User Equipments (UEs) (downlink);

2) **Simultaneous Wireless Information and Power Transfer (SWIPT):** where both energy and information are transferred in downlink;

3) **Wireless Powered Communication Network (WPCN):** where energy is transferred in downlink, while information is transferred in uplink.

2.2.1. Wireless Energy Transfer

First, we consider the case of a transmitter that wirelessly transfers energy to multiple receivers. In general, (power) senders and receivers are equipped with multiple antennas and the transmitted signal is modulated. The energy harvesting module at the receiving end is based on a rectifying

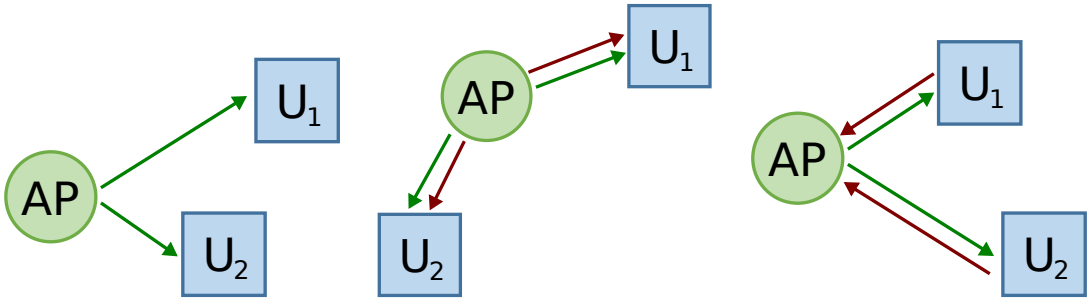

(a) WET. (b) SWIPT. (c) WPCN.

Figure 2.1: WPT architectures. Green arrows represent energy transmission, whereas red arrows indicate information transmission. In the figure, AP represents an Access Point, i.e., a BS, while U1 and U2 represent end users.

circuit that is composed of a diode and a low pass filter. This circuit converts the received RF signal into a DC one.

According to [10], the harvested energy per unit time is proportional to the received RF power. To improve it, one can increase the number of antennas at both transmitter and receiver, allowing a higher (combined) antenna gain. This solution, referred to as *energy beamforming*, effectively steers the transmit power towards a specific direction, with a subsequent improvement in the energy transfer efficiency. Furthermore, the width of the energy beam can be narrowed by increasing the number of antennas.

When considering the simultaneous charge of multiple energy receivers, a beamforming approach can lead to a *near-far* problem, where the users close to the transmitter receive more energy than those located further away. Furthermore, the use of beamforming requires an accurate knowledge of the channel state at the transmitter, but in many cases energy transmitters are simple devices, which do not possess signal processing capabilities. Including such capabilities comes at the cost of an increase in the device energy consumption and in its processing time. The acquisition of the Channel State Information (CSI) is investigated in [11], where the channel reciprocity is exploited to design an efficient channel acquisition method for a point-to-point Multiple Input Multiple Output (MIMO) WET system. In this paper, the antenna weights are set through a training phase, which is formulated as an optimization problem for the case of uncorrelated fading channels. Optimal solutions are derived for the special cases of MIMO Rayleigh and Multiple Input Single Output (MISO) Rician fading channels, with the aim of maximizing the net harvested energy at the energy receiver.

2.2.2. Simultaneous Wireless Information and Power Transfer

The SWIPT technique aims at transmitting energy and information through the same waveform, considering that information signals also carry energy that can be harvested by an energy receiver. Generally, Information Detection (ID) and EH receivers have different power sensitivities (-10 dBm for EH, -60 dBm for ID, according to [10]). This means that to work properly, EH receivers should be closer to the transmitter than ID receivers.

2.2. WIRELESS POWER TRANSFER

Since the design of the waveforms has a major impact on the performance of simultaneous energy and information transfer, a tradeoff between energy transmission and information transmission efficiencies has to be found. As for the energy transmission, the objective corresponds to maximize the power transferred to the end user, whereas, for the information transmission, it is the transmission rate that has to be maximized. In the literature, this tradeoff is explored through the definition of Rate-Energy (R-E) regions, which contain all the feasible rate (bit/s/Hz) and energy (J/s) pairs under a maximum transmit power budget. For any given technique, the optimal tradeoff between energy and information transfer rates is provided by the boundary of the corresponding R-E region, and depends on the receiver structure. An ideal receiver, that jointly decodes information and harvests energy from the same signal, using the full signal power for both tasks, is physically infeasible. Thus, the following practical receiver designs are proposed [10] (see Fig. 2.2 for further details):

1. *Time switching:* the transmitter sends data (ID) and energy (EH) using disjoint time slots. Within each time slot, the transmission can be optimized depending on its content (energy or information). The receiver, periodically switches between harvesting energy and decoding information.

2. *Power splitting:* the transmitter sends a single waveform to carry energy and information. The receiver splits the received signal into two streams: one stream with power ratio $0 \leq \rho \leq 1$ is used for energy harvesting, the other, with power ratio $1 - \rho$, is used to decode the data message.

3. *Integrated receiver:* the received signal is at first converted into DC current and then split into two streams. This solution allows using a passive rectifier for RF-to-baseband conversion, which entails a lower energy usage when compared to the active mixer that is required by the information decoder of the previous technique.

4. *Antenna switching:* this solution can be used when the receiver is equipped with multiple antennas. In this case, the receiver can use a number of antennas for energy harvesting and the remaining ones for information decoding. This simple solution reduces the hardware complexity at the receiver side, as it only needs to synchronize a switch.

In [12], a MIMO wireless broadcast system is investigated. In the considered setup, there are three nodes, one transmitter, one energy harvesting receiver and another receiver that decodes information. The cases of (i) disjoint and (ii) co-located receivers are explored. In the first case, the two receivers see two different channels, while, in the second, they experience the same channel. For the MIMO link between the transmitter and the energy harvesting receiver, the amount of energy harvested is maximized through beamforming. For the MIMO link between the transmitter and the data decoder, the transmission rate is maximized through spatial multiplexing. The R-E region is computed to assess the optimal broadcasting policy in the case of simultaneous wireless power and information transfer. In scenario (i), where the receivers are disjoint, the beamforming strategy is demonstrated to be optimal when considering MISO links (between the transmitter and the EH/ID receivers). It is also shown that increasing the correlation between the two channels widens the R-E region, proving that an increase in the antenna correlation is beneficial. In scenario (ii), where the two receivers are co-located, the optimal strategy is spatial multiplexing.

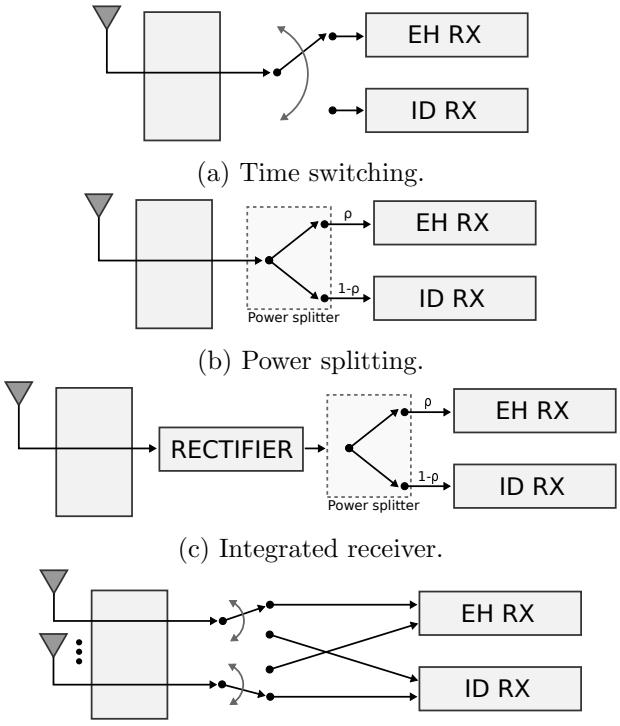

(a) Time switching.

(b) Power splitting.

(c) Integrated receiver.

(d) Antenna switching.

Figure 2.2: SWIPT receiver designs.

An improvement is proposed by [13], where the robust beamforming problem in a MIMO SWIPT wireless broadcasting system is investigated under the assumption of imperfect channel state information at the transmitter. The objective is to maximize the worst-case harvested energy for the energy receiver, while guaranteeing that the information transmission rate is above a given threshold, for all the possible channel realizations. This amounts to a non-convex problem, which is relaxed into a semi-definite programming formulation that can be solved efficiently. Simulation results show that neglecting the CSI in the system design leads to frequent violations of the target information rate.

The multi-user system case is investigated in [14], where a setup with two users and a receiver is considered. The first considerations are made on a scenario comprising a standard multiple access channel under the constraint that the energy received by the decoder is large enough. It is demonstrated that, as the required energy at the decoder increases, time-sharing is necessary to achieve optimal performance. This indicates the need for additional coordination between the two users. In a second scenario, a multi-hop channel is considered, where the relay is assumed to be capable of harvesting the energy received from the transmitter to forward packets to the receiver. It is shown that for small Signal-to-Noise Ratios (SNRs) in the second hop, it is desirable to maximize the energy transfer to the relay, while for sufficiently large SNRs in the second hop, it is optimal to maximize the information transfer to the relay. This means that the transmitter needs to adjust its transmission strategy according to the quality of the second link, with a subsequent need for

further coordination. A scenario with relay nodes is also considered in [15], where the performance limits of a two-hop multi-antenna amplify-and-forward relay system are investigated.

The employment of wireless energy harvesting in dense networks has been studied in [16]. Sensors are supplied by batteries and can harvest energy from neighbor packet transmissions. Two communication scenarios are considered: i) direct, where the sensors exchange messages directly, and ii) cooperative, where randomly deployed relays assist the message exchange. Simulation results indicate that the direct communication scenario presents better communication performance in randomly deployed dense network, whereas the cooperative scenario is superior in terms of network lifetime, providing higher harvested power. However, the wireless energy harvesting is not able to provide enough power to counterbalance the consumed energy in realistic scenarios, mainly due to the the path loss and the Radio Frequency (RF)-to-Direct Current (DC) conversion. A solution to this problem is tackled by the deployment of dedicated power transmitters of power beacons as done in [17], where a wireless powered sensor network with battery-less devices is considered. The authors provides results about the connectivity of the sensor network considering different routing mechanism (i.e, unicast, broadcast) and fading conditions.

2.2.3. Wireless Powered Communication Network

In this scenario, an Access Point (AP) transmits energy to multiple wireless devices. These devices use the harvested energy to transmit information in the uplink channel. Considering a transmission block of duration T, during a first phase of duration $\tau_0 T$ $(0 < \tau_0 < 1)$, the wireless devices harvest energy, while in the second phase, of duration $(1 - \tau_0)T$, they use the harvested energy to transmit information back to the AP. This protocol is termed *harvest-then-transmit*.

A typical issue of WPCNs is defined as *doubly-near-far* problem and it is quite similar to the near-far problem that was discussed in Section 2.2.1. In this case, a device placed further away from the AP harvests less energy than a closer device, due to the higher signal attenuation experienced by the former. For the same reason, it requires a smaller amount of power to transmit data to the AP. A solution to this problem is proposed in [18], where the cooperation among users is exploited in a two-user WPCN. The AP and the users are equipped with a single antenna. The user with the best channel, both for the EH downlink and the information transmission, uses part of its allocated uplink time and harvested energy to relay information. Simulation results show that this approach leads to improvements in the throughput and in the user fairness.

In [19], a scenario with a multi-antenna AP and a number of single-antenna users is considered. The minimum throughput among all users is maximized (max-min allocation problem) by a joint design of the downlink-uplink time allocation, the downlink energy beamforming, the uplink transmit power allocation, and the receive beamforming, while guaranteeing fairness. An optimal two-stage algorithm is proposed and two suboptimal designs, exploiting *zero-forcing* based receive beamforming, are also proposed. Numerical results show that the performance of suboptimal approaches is close to the optimal one when the distance from the AP is small, while the performance gap increases as this distance gets larger. Moreover, the max-min throughput is shown to increase significantly with the number of active antennas at the AP. The same scenario, with a multi-antenna AP and multiple single-antenna users, is considered in [20]. In this paper, the transmission time frame includes a slot for the channel estimation in the uplink. The users at first consume a fraction of the harvested energy to send pilots in the uplink. Then, the AP estimates the uplink channels

and obtains the downlink channel gains exploiting channel reciprocity. Hence, the scheme follows the classic steps of the harvest-then-transmit protocol described above. Even though a perfect CSI at the transmitter is not available, a more accurate CSI is shown to contribute to a higher energy transfer efficiency and to lead to a higher uplink information rate.

2.2.4. State-of-the-Art of RF and Microwave Energy Conversion Efficiencies

This subsection discusses the efficiencies of state-of-the-art energy harvesting devices, according to [1]. The contributions on this research field have been made essentially by two communities, focusing on space-based solar power harvesting and Radio-Frequency IDentification (RFID) systems. The first community deals with energy conversion at long distances and high powers, while the second with ultra-low power applications.

In Fig. 2.3, the state-of-the-art efficiencies from [1] are shown. Specifically, the input power is plotted versus the energy receiver efficiency for different energy transmission frequencies, in the 900 MHz, 2.4 GHz and 5.8 GHz bands. Efficiencies of applications working in bands above 5.8 GHz are also shown. Observing the curve for the 900 MHz band, we see that these systems are typically designed to work with low input levels. This is motivated by the fact that the research on Ultra High Frequency (UHF) energy harvesters have been engineered for RFID applications. Since RFID applications are designed to work in multipath environments, the available energy levels at the receiver are low.

Other studies consider WPT applications operating at microwave frequencies. Working in these bands permits the use of smaller antennas, thus reducing the required antenna aperture and making antenna beam steering easier. In particular, the availability of the unlicensed 5.8 GHz band has led researchers to focus on it. From Fig. 2.3, we see that most of the microwave frequency applications discussed in the literature, operate at high power levels. This is motivated by the fact that these works consider space-based solar power or pure WPT applications, which typically deal with high powers.

From this graph we see that as the transmitting power increases, the efficiency of energy harvesting devices increases too, whereas it decreases with an increasing frequency. This last fact can be motivated by the higher circuitry parasitic losses encountered at microwave frequencies.

2.2.5. Conclusions

The main findings of this section are described as follow:

1. The wireless transmission of energy has been studied in the literature considering different architectures, namely WET, SWIPT and WPCN.

2. The energy transmission efficiency depends on the distance between transmitter and receiver. Therefore, far users receive less energy and, in the case of WPCN, they are those that need it more to communicate. Cooperation schemes are a good solution to solve this problem.

3. Rate-Energy regions are used to find the optimal tradeoff between energy transmission and information rate in SWIPT.

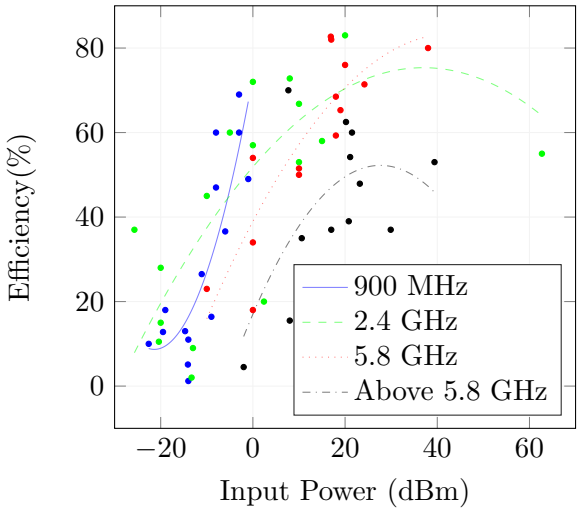

Figure 2.3: State-of-the-art RF and microwave conversion efficiencies from [1]. Several topologies are used under a variety of load conditions and technologies.

4. Different design for simultaneous transmission of information and power have been studied: time switching, power splitting, integrated receiver and antenna switching.

Future information and energy networks are likely to operate on overlapping portions of the spectrum, due its scarcity. For this reason, there is a need to manage the interference that will be dominated by the transmission of energy. It is also necessary to investigate scenarios with multiple users and, specifically, new ways of mitigating the interference, such as opportunistic WET with spectrum sensing and energy/information schedulers. In particular, when considering energy transmission, harmful interference can be turned into useful harvested energy. Hence, the problem of mitigating interference while facilitating energy transfer must be addressed.

The described literature analyses static scenarios, but nodes can also be mobile. In this case, the transmission of energy and information becomes time-variant, thus requiring dynamic and adaptive resource allocation policies. Further investigation is necessary to characterize the tradeoff between transmit power and distance from the receiver in mobile settings.

When considering the wireless transmission of energy, the intensity of microwaves can become a problem in some areas, especially when using massive MIMO and beamforming technologies. In particular, the power radiated by wireless devices must always satisfy the Equivalent Isotropically Radiated Power (EIRP) limitations dictated by existing regulations. To solve this problem, systems based on the concept of distributed antennas can be exploited. In this way, we have an omnidirectional and weak radiation for each antenna. The combined effect of this radiation is destructive everywhere, except for the desired location, where it is constructive. This solution should be further investigated taking into account the increased power consumption due to the use of multiple antennas. In particular, the tradeoff between the energy harvesting efficiency and the power consumption should be analyzed.

Finally, we underline that current studies are mainly theoretical and the achievable throughput performance for practical wireless information and energy transmission systems shall be assessed.

These studies should test the use of new technologies like mmWave, massive MIMO and distributed antenna arrays.

As we already discussed, the sensitivity of the receivers is a fundamental aspect to consider in the analysis of SWIPT schemes. Actually, the low sensitivity of energy receivers represents a problem, leading to situations where a device can only decode information without harvesting energy, with the consequent degradation of the SWIPT performance. For this reason, it is necessary to improve the energy receiver circuits in terms of hardware and design.

Overall, considering (i) the energy consumption sources, (ii) the energy efficiency of WPT receivers, (iii) the limited transmission powers due to regulations and especially to (iv) wireless channel losses, WPT is not deemed an effective technology yet to provide energy to mobile devices, as discussed in [21] and Chapter 3. Transfer efficiencies are in fact very small (often smaller than 10^{-4}) even when beamforming is exploited.

2.3. Energy Cooperation in Mobile Networks

We now consider a scenario where the BSs are supplied by energy harvesters and storage devices (rechargeable batteries) and may be disconnected from the electrical grid (*offgrid*). There, cooperation strategies can be conceived to make them *quasi* self-sustainable, i.e., to operate mostly relying on the harvested (and stored) energy.

In this context, geographical diversity shall be exploited to mitigate the well-known temporal and spatial variability in the energy harvesting process, especially when using renewable sources such as the wind. This aspect is partially investigated in [22], where a network made of two BSs equipped with energy harvesters and some limited energy storage capability is considered. The authors propose an offline linear programming algorithm, which limits the power drained from the power grid when the energy profiles are deterministic. Furthermore, an online algorithm is put forward for a more realistic scenario where they are stochastic and not known a priori. As expected, the best results are achieved when the harvested energy profiles at the two BSs are sufficiently uncorrelated. In fact, if the amount of energy harvested is highly correlated, we have a problem when the energy inflow is little, as this concurrently occurs at both BSs. When the correlation is low, it is instead very likely that one BS will experience an abundant energy inflow when the other one is in a low energy state. The former BS could then transfer some of its energy to the latter. The performance gap between the two algorithms in [22] is small, reaching the minimum value for anti-correlated energy profiles. We observe that a low correlation in the energy profiles can be more easily reached by using different renewable types, for example solar and wind, where the latter may be very useful to mitigate the shortage of energy from solar panels during the night.

In the following, two cooperation types are considered:

1) **Energy sharing:** in this case, BSs are interconnected with electric wires, forming a sort of microgrid that provides mechanisms to exchange the harvested energy among BSs. In Fig. 2.4 two deployment scenarios are depicted: direct connections among BSs (Fig. 2.4a) and BSs connected through an aggregator (Fig. 2.4b).

2) **Communication cooperation:** BSs are not interconnected via electric cables and their cooperation involves mechanisms to support the radio communication such as power control,

bandwidth control, sleep modes and traffic offloading. In this case, high-capacity mmWave backhaul connections [23] can be exploited to facilitate the deployment of *drop-and-play* devices, such as small cells. The scenario is depicted in Fig. 2.5.

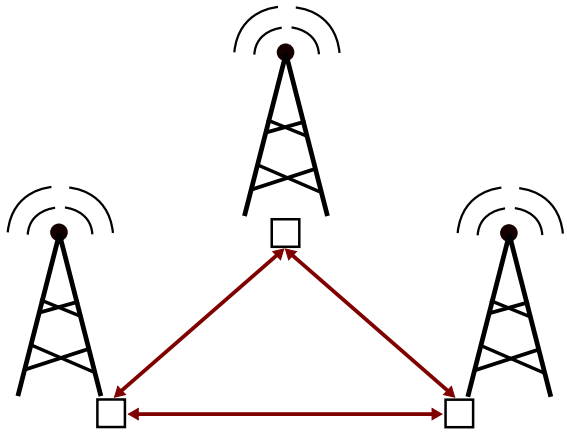

(a) Energy sharing through a microgrid.

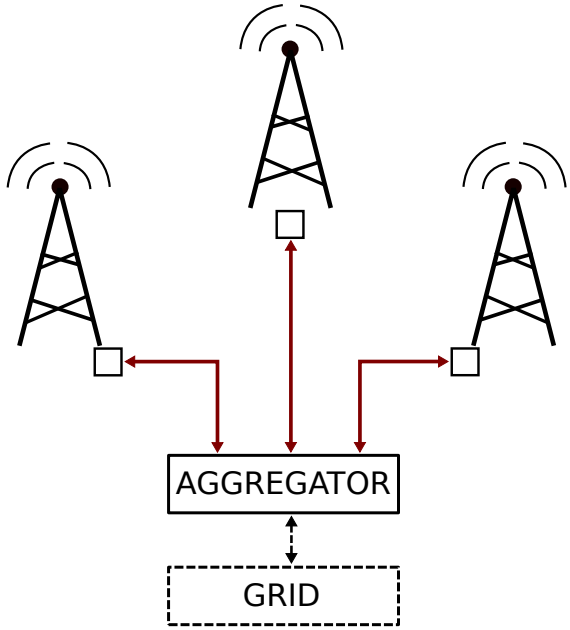

(b) Energy sharing through a microgrid with an aggregator.

Figure 2.4: Energy sharing scenarios

2.3.1. Energy Sharing

Energy sharing among BSs is investigated in [24] through the analysis of several basic multiuser network structures, namely, (i) an additive Gaussian two-hop relay channel with one-way energy

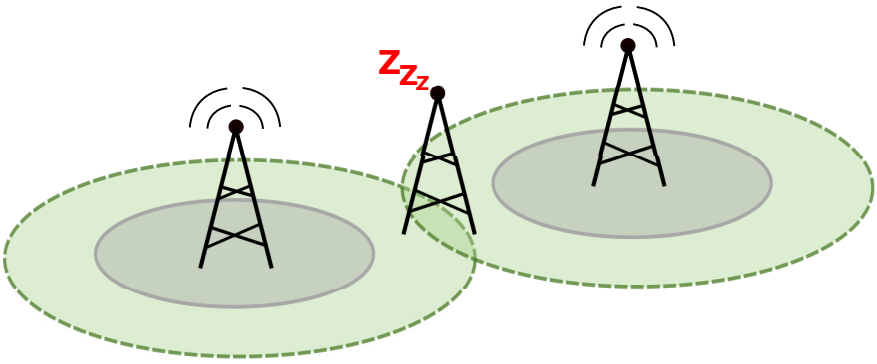

Figure 2.5: Communication cooperation scenario

transfer from the source to the relay node, (ii) a Gaussian two-way channel with one-way energy transfer and (iii) a two-user Gaussian multiple access channel with one-way energy transfer. A two-dimensional and directional water-filling algorithm is devised to control the harvested energy flows in both time and space (among users), with the objective of maximizing the system throughput for all the considered network configurations. The allocation algorithm is offline, relies on a priori information, i.e., the amount of energy harvested by sources and relays, and assumes unlimited data and energy buffers. However, these assumptions are unrealistic.

A very interesting energy sharing framework is presented in [25], where the concept of the *Energy Packet Network (EPN)*, also called *Power Packet Grid (PPG)*, is introduced. In an EPN, discrete units of energy, termed *energy packets*, can be exchanged among network elements or acquired from the environment through harvesting hardware. Accordingly, the harvested energy can be modeled as a packet arrival process, the energy storage as a packet queue and the energy consumption process as a queue of loads, i.e., one or more servers. These three components of the EPN are interconnected thanks to power switches. Electronic systems of this type, named *power packet systems*, have been recently experimented with. In some approaches, see [26], the packet takes the form of a pulse of current with fixed voltage and duration. Each energy packet is equipped with an encoded header, containing the information about the destination identity (i.e., its address), which is used to route the energy packet through the EPN.

The cost of deploying the micro-grid infrastructure that would be required by an EPN can be high. In [24,27], the use of wireless energy transfer is considered as a means to avoid the installation cost of electric cables. However, such technology has a low energy transfer efficiency nowadays, as we will demonstrate in Chapter 3 (see also [1, 21]).

A solution to reduce the costs of deploying electrical connections between BSs, is presented in [28], where a new entity named *aggregator* is introduced, as shown in Fig. 2.4b. The aggregator is in charge of mediating between the grid operator and a group of BSs to redistribute the energy flows.

In [29], the authors propose an algorithm that tries to jointly optimize the transmit power allocations and the transferred energy, so as to maximize the sum-rate throughput for all the users. This joint communication and energy cooperation problem is proven to be convex. Numerical simulation shows that this approach achieves better performance than *no cooperation* or *cooperation*

through communication in terms of average sum-rate.

Infrastructure sharing may be exploited to reduce power consumption by fairly distributing the harvested energy among mobile network operators [30]. The problem to capture the energy interactions among operators is stated as a bankruptcy game where fairness is pursued to further motivate cooperation. The results show that all cooperative operators could be provided with 6-7 hours of operation during non-solar hours, regardless the traffic demand. Furthermore, operators purchase energy from the grid at similar percentages when no green energy is available.

2.3.2. Communication Cooperation

The micro-grid deployment cost (i.e., the EPN installation cost) is one of the main aspects that motivate the introduction of this second cooperation mode. In this case, each BS has an energy harvester and may have a storage unit (*battery*), but it is not connected with the other BSs via electric cables and, in turn, cannot directly exchange energy with them, as shown in Fig. 2.5. This approach eliminates the costs related to the deployment of the micro-grid infrastructure (e.g., wires, converters and controllers). However, it may require harvesters and storage units with higher capacity, to achieve a certain Quality of Service (QoS). Ongoing research aims at finding the optimal size of harvesting devices and batteries to sustain the traffic demand through the available energy budget. In particular, methods that allow BSs to cooperatively optimize the network energy usage are proposed.

In [31], the fraction of time during which a BS cannot satisfy the traffic demand, due to energy scarcity is defined as *outage*. The authors compute the size of harvesters and batteries as a function of the outage probability. A photovoltaic panel is considered as the harvester and the size-outage region is obtained for different geographical locations. The authors conclude that full network self-sustainability may be feasible in locations with high solar irradiation, considering the cost and dimension of the energy harvesting hardware (panels and batteries). In [32], the authors define a system model of a K-tier heterogeneous cellular network, where BSs independently switch off when their energy reserve is insufficient. The authors determine the availability region, i.e., the uncertainty in BS availability due to the finite battery capacity and to the inherent randomness in the energy harvesting process. This provides a fundamental characterization of the conditions under which standalone BSs provide the same performance as BSs relying on traditional energy sources. The introduction of sleeping capabilities in some BSs in order to reduce the size of their harvesting and storage devices is explored in [33]. In this paper, sleep modes are enabled for 50% of the BSs, when the traffic is below 50% of its peak. Although simple, this scheme allows reductions in the power consumption from 10% to 40%, depending on the sleep policy, and to reduction in the size of batteries and photovoltaic panels. However, the impact of sleep modes on the user QoS is not assessed. In [34], an optimization problem that seeks to minimize delay and power consumption by turning off small BSs is investigated. The proposed algorithm is online and is based on the so called *ski rental framework*. Each agent operates autonomously at each small cell and without having any a priori information about future energy arrivals. The algorithm is compared against a greedy scheme that uses sleep modes when the battery level is below a fixed threshold. It is shown that the proposed solution outperforms the greedy approach in terms of power consumption and network cost. The performance is evaluated assuming that energy arrivals are Poisson. This assumption is however unrealistic in most energy harvesting scenarios, as demonstrated in [35],

where a stochastic Markov process has been derived for solar energy harvesting systems.

In [36], a two-tier urban cellular network is considered, where macro BSs are powered by the power grid and energy harvesting small cells are deployed for capacity extension. The authors propose a centralized optimal direct load control of the small cells based on dynamic programming. The optimization problem is represented using Graph Theory and the problem is stated as a Shortest Path search. The same scenario is considered in [37], where the authors propose an algorithm based on a multi-agent reinforcement learning that controls the energy spent according to the energy harvesting inflow and the traffic demand. Each node independently decides as to whether entering a sleep mode or serving the users within coverage. This algorithm is also shown to outperform a greedy scheme.

2.3.3. Conclusions

The main findings of this section are described as follows:

1. Energy cooperation between BSs can provide better results when exploiting different types of renewable energy sources and geographical diversity. However, this comes at expenses of higher deployment and infrastructure costs.

2. Energy sharing possibilities are limited by the cost of deploying a microgrid among BSs. Some architectural solutions have been provided. Specially, EPNs represent an interesting solution for future energy sharing deployments.

3. Communication cooperation between BSs avoids the deployment of a microgrid. Nonetheless, the dimension of energy harvesting and storage devices depends on the system outage constraints and on the deployment site.

Energy cooperation is a recent and open field of research. Moreover, the definition of cooperation methods is crucial in case of energy self-sustainability. A key aspect is the characterization of the network load that is still not precisely captured by current analyses. We also underline the lack of performance assessments for the user perceived quality in the presence of energy cooperation mechanisms.

The harvesting process is usually characterized by very intensive power generation periods, interleaved with cycles where the harvested energy is scarce of even absent. In the case of solar energy, for example, the generated power depends (among other things) on the season of the year. Since the system is designed for the worst case (e.g., winter months), the imbalance in the power generation across a full year may lead to an excess of energy during high power periods, which may be poorly handled. Investigations on an efficient use of the energy surplus shall be carried out to avoid this. The impact of energy storage devices still has to be investigated. In such a case, the adoption of energy storage leads to higher capital expenditure and the tradeoff between installation cost and network performance would also have to be assessed, taking into consideration the payback period.

Most of the work cited in this section solves offline optimization problems assuming a full knowledge of energy and load patterns. This is useful as a feasibility study and to obtain performance bounds, but it is still far from the design of a practical solution. In the literature, we see an

increasing interest in learning and distributed approaches for the design of online algorithms. However, these control methods are not yet mapped into the proposed 5G architecture. Concepts like network softwarization and virtualization should be included in their design and their performance should be evaluated considering real traffic (user demand) and energy harvesting traces.

Finally, a new research field is represented by the design of EPNs. There, energy packets would represent a flexible and convenient method to route energy when and where needed. However, the design of power switches, as well as the definition of proper energy routing protocols, are still open research directions.

2.4. Energy Trading with the Electrical Grid

In this section, we discuss a scenario where the 5G network trades energy with the Smart Grid (SG). In a SG, communication is provided across energy producers and consumers. Energy can be bought from the main power distribution network, but also from distributed users, if equipped with some energy harvester. Finally, these users can even sell their surplus energy, injecting it into the SG. A user may then concurrently act as an energy consumer and producer (often termed *prosumer* for short). In the scenario that we envision here, a BS with energy harvesting capability can be considered a *prosumer* of the SG. Next, we analyze the possible interactions that may occur between BSs within a mobile network and the SG, by reviewing the existing literature and discussing open challenges.

2.4.1. A Review of Energy Trading in Smart Grids

The energy supply system consists of energy *retailers* and *consumers*. The retailers offer a source-dependent energy price that varies over time. Consumers choose one or more retailers to buy energy from, depending on market prices.

The SG infrastructure is dimensioned to meet the peak energy demand and to avoid blackouts. This leads to an underutilization of the resources during off-peak periods. Furthermore, an increase in the peak demand requires investments in the distribution network and, possibly, in the power plants. For these reasons, grid operators are pushing the consumers to reduce their demand (the SG load) during peak hours (through dynamic pricing and economic incentives) or to shift their load to off-peak hours. The activities that target (i) reshaping the consumer's demand profile to make it match the power supply, (ii) eliminating blackouts, and (iii) reducing the operational costs and the carbon footprint are referred to as Demand-Side Management (DSM) in the literature. A practical way of achieving them is through Demand Response (DR), i.e., the energy provider issues some offers (incentives, etc.) over time and the users "respond" to these by adapting their behavior. Some researchers and practitioners use DSM and DR interchangeably [38], although DR can be seen as a way to implement DSM policies.

A real-time pricing scheme is presented in [39] to reduce the peak-to-average load ratio. The system is composed of several consumers and a single retailer. Each user reacts to the prices announced by the retailer and maximizes its payoff, which is the difference between its quality-of-usage and the cost of the energy bought from the retailer. The retailer designs realtime prices in response to the forecast user reactions to maximize its own payoff.

2.4. ENERGY TRADING WITH THE ELECTRICAL GRID

Game theory, and specifically Stackelberg games, has been widely used to find distributed solutions for dynamic pricing problems. This type of game models the behavior of two agents, one of them being the leader (having the first move advantage) and the other one being the follower, who plays a best response strategy to maximize his own utility. In energy trading scenarios, the retailer is usually the leader and sets energy prices according to market needs in an attempt to spur the participation of users, while also trying to maximize its own revenue [40]. A similar approach is presented in [41], where the authors propose a decision model for a retailer, who plays the role of an intermediary agent between a wholesale energy market and end-consumers. The response of the consumers with respect to the retailer price follows a two-stage Stackelberg game, while the market price uncertainty is modeled by a robust linear optimization model. The problem is reformulated as a mixed integer linear program and solved heuristically. A non-cooperative energy supply game is formulated in [42] to capture the competitive market within a multiple-supplier micro-grid. The authors of this paper propose an iterative algorithm to find the Nash equilibrium of the energy supply game and another one to form coalitions between micro-grids. Their results show that the pricing mechanism reduces the electricity imbalance inside the micro-grid and that the profit made by cooperating is higher than that made operating independently.

Collaborative schemes among consumers, designed to reduce the energy cost, are explored in [43]. There, two optimization problems are formulated with the goal of minimizing the peak-to-average ratio and the system energy cost. These problems are solved in a distributed manner through a scheduling algorithm based on game theory. Moreover, to encourage users to behave in a desired way (i.e., to minimize the energy cost) the authors propose a smart pricing tariff such that the interactions among the users automatically lead to an optimal aggregate load profile. Cooperation is also investigated in [44] for the case of urban buildings composing a micro-grid. The problem of deciding the optimal capacities of the harvesting equipment as well as of determining the optimal daily power operation plan is formulated as a mixed integer linear program. The objective function is optimized based on the Nash bargain method to enable equally distributed savings among the participants. Results show that power exchanges affect the required equipment size and viceversa. Furthermore, energy exchanges enhance the system self-sufficiency and reduce carbon emissions.

In [45], the social-welfare, defined as the difference between the total demand, the total cost experienced by all the generators and the wastage cost caused by transmission losses, is maximized through a distributed *demand and response* algorithm. The problem is formulated using convex optimization and solved in a distributed fashion applying the Lagrange-Newton method. In the computation of the optimal solution, each node (consumer or supplier) exchanges rounds of messages with its neighboring nodes. Although simulation results verify the correctness of the distributed algorithm, the computation rate and the entailed communication load are rather high. DSM is also a viable approach to control the temporal separation between energy generation and demand. In fact, load shifting allows demand flexibility without compromising the QoS [46]. This flexibility can be achieved thanks to energy storage devices, which can be used to accumulate renewable energy and use it when needed.

2.4.2. Cellular Networks meet SG

The interaction between cellular networks and the SG can be implemented in two different ways: 1) the SG is the only energy supplier, and 2) the energy harvesting BSs along with the SG are the energy suppliers.

1) The SG is the only energy supplier: in this scenario, several retailers operate within the SG to serve the consumers. An example of this can be found in [47], where a power allocation scheme, formulated as a non-cooperative game, is put forward to increase the network energy efficiency. Retailers offer different prices to the BSs and a multi-agent Q-learning scheme is proposed for the game to reach the optimal transmission power configuration. Along the same lines, in [48] a cognitive HetNet only powered by the SG is considered. In this paper, the authors formulate the problems of: (i) electricity price decision, (ii) energy-efficient power allocation and (iii) interference management, which are jointly and iteratively solved as a three-level Stackelberg game.

In [49], a DSM framework for cellular networks powered by multiple energy suppliers is proposed. The system model comprises a set of cellular operators, characterized by the QoS offered to their subscribers, and powered by a common pool of energy suppliers, characterized by energy prices and pollutant emission levels. Closed-form expressions for the amount of energy provided by each supplier to the operators are derived using stochastic geometry, accounting for user QoS, energy cost and carbon emissions.

2) The suppliers are the EH BSs and the SG: in this second scenario, BSs have energy harvesting capabilities, and act as *prosumers* of the SG, see Fig. 2.6. Different scenarios can be envisioned. For example, in [50] mobile operators are responsible for supplying power to their base stations. Each network operator has to procure energy from several SG retailers. The procurement decision is affected by two factors: the unitary price of energy and a penalty term depending on the amount of pollutant emissions from the energy source. Moreover, BSs are prosumers, i.e., they can procure energy from their own renewable energy sources, which are free of charge for the network operator. Using a two-level Stackelberg game, the authors of [50] formulate and find the optimal solution for an optimization problem that seeks to maximize the operator profit, as well as to reduce the emission of pollutants. We remark that, besides this centralized decision-making model, where the network operator decides the energy retailer for each of BSs, there are distributed scenarios where base stations are themselves responsible for carrying out the acquisition of energy in a distributed manner, choosing the most appropriate retailer according to their energy status, i.e., on their current energy income and reserve.

An adaptive power management for wireless BSs is studied in [51]. Here, each BS is a prosumer equipped with a solar panel and an energy storage unit, but is also plugged into the electrical grid. Due to the random nature of renewable generation, power prices and traffic load, the authors formulate a multi-stage stochastic optimization problem. This problem is then framed as a linear program and solved using standard tools. Energy management strategies are presented in [52, 53]. In these works, the authors also elaborate on the use of storage devices. In [52], simulations results show that a cost reduction can be attained through a higher battery capacity, but a greater cost reduction is possible by increasing the number of base stations. In [53], the authors get a critical battery capacity level above which no further cost reduction can be achieved. According to the

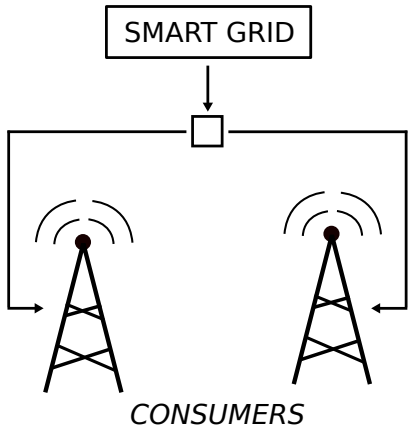

(a) One supplier.

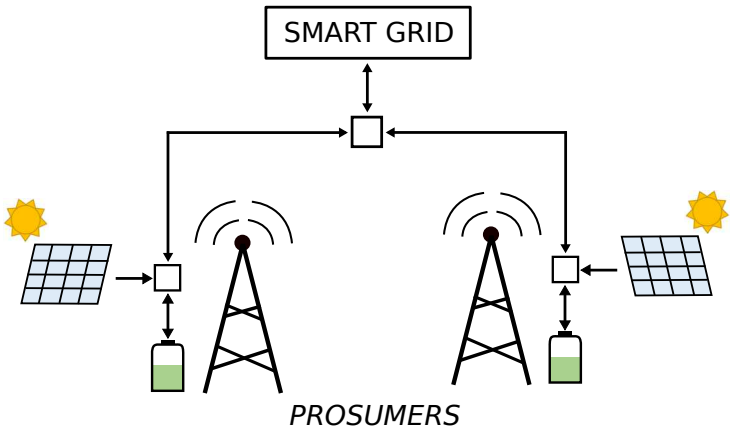

(b) Multiple suppliers.

Figure 2.6: Diagram illustrating the two ways of interaction between mobile networks and the smart grid.

authors, these results can be used as guidelines in the design of storage systems for BSs in a SG environment. Auctioning is explored in [54], where a double auction trading algorithm is proposed to incentivize BSs with extra harvested energy to share their energy surplus with BSs with a lower energy reserve. Auction mechanisms are the key elements of many applications in wholesale and retail electric power markets. Similar to traditional auction rules, the main goal of distributed energy trading is to find the lowest-cost match between the supply and the demand, so as to maximize the economic efficiency [40]. BS energy storage is studied in [55]. Batteries must operate within a guard range to avoid a rapid decrease of their performance (i.e., typically between the 20% and 90% of their capacity). The authors propose a fuzzy Q-Learning small cell energy controller to simultaneously minimize the electricity bought from the SG and enhance the life span of the storage device.

Finally, a hybrid energy sharing framework is proposed in [56], where a combination of physical power lines and energy trading with other BSs using smart grid is used. Algorithms for physical

power lines deployment between BSs are designed based on the renewable energy availability. An energy management framework is also formulated to optimally determine the quantities of electricity and renewable energy to be procured and exchanged among BSs, respectively. Results demonstrate considerable reduction in average energy cost thanks to the hybrid energy sharing scheme.

2.4.3. Conclusions

The main findings of this section are described as follows:

1. Collaborative schemes and energy cooperation among consumers in smart grids are effective techniques to reduce energy costs, while increasing network efficiency. Specifically, game theory and auctioning schemes have been widely investigated within DSM strategies, providing valuable outcomes for energy trading. Stackelberg games are the most popular approach.

2. The use of BSs with energy harvesting capabilities opens new scenarios in the smart grid market, where green network operators could trade their harvested energy with the SG.

3. Some initial papers dealing with the interaction between SGs and green network operators (managing EH BSs) have recently appeared. Initial results, for selected network scenarios, look promising. In particular, energy resources can be optimally allocated (and traded between BSs and the SG) to obtain monetary cost reductions and a higher energy efficiency for the BS network.

A few open issues are now identified. The basic scenario studied in the reviewed literature involves a single retailer (the SG), which offers hourly energy prices to the final consumers, i.e., the BSs. The energy price depends on the cost of production and on the expected demand. In this scenario, decision-making solutions shall be addressed to find the best energy-purchasing policies for the BSs taking into account: (i) current and forecast renewable energy income, (ii) current and forecast traffic load and (iii) the future evolution of the energy prices. In addition, the presence of energy storage devices makes the problem more involved, allowing the storage of energy for later use, when the market conditions are unfavorable. There is a vast literature on dynamic pricing and price forecast, but this is mostly limited to the smart grid domain, whereas the integration of prices, energy and load forecast for the control of base stations, when these act as *prosumers* within a SG, is still unexplored.

Further, existing papers study network scenarios where the BSs can harvest energy, use it locally (to serve their own mobile users) or purchase it from the SG. Few studies additionally consider BSs as possible energy sources, and allow them to sell energy to the SG retailer. However, more complex scenarios are possible, where BSs interact and are endowed with the capability of exchanging energy among themselves (using their local energy storage). According to this new paradigm, BSs can sell (buy) energy to (from) other BSs in the mobile network, besides using it locally or selling it to the main SG retailer. This amounts to green mobile networks, where BSs can self-organize and cooperate toward the overall reduction of the energy that the mobile network drains from the SG, reducing the carbon footprint of ICT.

Finally, stochastic optimization and adaptive control tools, involving, e.g., model predictive control, shall be considered to handle the integration of energy harvesting capabilities in mobile

networks where BSs can be considered as prosumers of the SG. Better load models (accurately tracking the spatio-temporal traits of mobile traffic) are needed, along with lightweight and flexible tools for pattern analysis and prediction, to be integrated into foresighted optimization techniques. Within these settings, micro-economic models should also be investigated when consumers (BSs) aim at maximizing their utility (e.g., combining energy, monetary cost and served traffic), subject to their monetary budget constraints; while SG retailers aim at maximizing their profit.

2.5. Conclusions

In this chapter, the topics tackled in this thesis have been presented. Moreover, existing literature has been discussed, highlighting open challenges and potential solutions. Some of those solutions are addressed throughout this work where the main goals and contributions are summarized in Section 1.1 and then, detailed on each of the following chapters. Furthermore, literature related to the application scenario is provided on each chapter. Note that we do not provide a general section in this chapter about Topic 4 but just related work in Section 5.2, since MEC paradigm is not intended to be the focus of this thesis, apart from its integration within a specific application tackled in Chapter 5. Actually, the combination of EH and MEC paradigms opens a wide research field that shall be addressed in future work. Moreover, EH resources are modeled, used, and managed throughout all chapters where extensive state of the art is provided.

3

Energy Transfer from Base Stations to End Users

3.1. Introduction

Nowadays, the Internet counts more than three billions active users in the world, sending more than two millions emails and watching more than 130 thousands YouTube videos per second [57]. The largest part of the overall Internet traffic is generated by mobile devices, which have almost completely replaced desktop computers and even laptops, to a large extent. These devices, either being smartphones, tablets or wearable ones, are battery-powered and tend to discharge quite rapidly. This fact usually forces their owners to plug them into power outlets during the day, maybe just for a short period of time, to gain some extra energy that permits the devices to safely reach the end of the day, when they will be plugged back in and be fully recharged. However, connecting a device to an energy source in the middle of the day is not always possible.

WPT [9] is a recent technique that allows charging a mobile device without the need to connect it to any external power supply and, in some cases, without the user even being aware of it. This technique relies on external tools, such as BSs that are capable of communicating with the UE and charging it by wirelessly sending energy to it, if necessary. This approach involves a transmitter, i.e., a BS that sends energy through the wireless medium, and at least one receiver, i.e., a UE that harvests this energy to replenish its battery.

In this chapter, we investigate the tradeoffs involved in the recharging process for a dense (e.g., inter-BS distances of about 20 meters) cellular network deployment, where mobile users can be wirelessly recharged through radio frequency transmissions. Our objective is to devise and systematically compare several distributed charging schemes, which dictate *which* users have to be charged and *when*, depending on the residual energy level in their batteries, on their distance from the serving BS, on the radiating frequency and on their mobility behavior. Most of the related literature focuses on a single BS that transmits energy to the users being served, designing techniques that entail the joint transmission of power and information (see Section 3.2). A distinctive trait of this work is that we look at a *distributed network deployment* and explicitly consider *user mobility*. We do not consider the transmission of information, but we are rather concerned with the allocation of power transfer slots from each BS according to the mobility patterns of the users and to the residual energy in their batteries. Our results shed some light on the actual effectiveness of WPT in future mobile networks, assessing whether it can be considered an effective means to charge terminals while they are on-the-go, considering real world system parameters, along with independent and group mobility models. Also, we provide useful results on the best WPT scheduling strategies. A somewhat counterintuitive finding from our study, is that the location of the mobile users is the sole metric that has to be taken into account in the design of WPT schedules, as this will steer the system toward higher transfer efficiencies and, at the same time, decrease the

number of dead nodes (whose battery is completely depleted). Designing for the battery level will lead to worse results in all respects.

In our numerical analysis, a *genie* is at first utilized to devise optimal charging schedules, where user locations and residual battery levels are exactly known by the BS controllers at all times. Hence, several heuristic policies are proposed and their performance is compared against that of genie-based approaches in terms of transfer efficiency and fraction of dead nodes. Our results reveal that: i) an even allocation of resources among UEs is inefficient, whereas even a rough estimate of their location allows heuristic policies to perform very close to the genie-based schemes, ii) mobility matters: group mobility leads to higher efficiencies and an increasing speed is also beneficial, iii) wireless charging can substantially reduce the fraction of dead nodes, due to their battery level dropping below a certain critical threshold. Nevertheless, this comes at the expense of constantly transmitting power and transfer efficiencies are low under any scenario.

3.1.1. Contributions

The main contributions of this chapter are:

- We investigate the tradeoffs involved in the energy transfer from BSs to UEs within a dense cellular network, where mobile users can be wirelessly recharged through radio frequency transmissions.
- We present and compare different distributed charging strategies, that dictate which users have to be charged and when, depending on the residual energy level in their batteries, on their distance from the serving BS, on the radiating frequency and on their mobility behavior. The focus is on a distributed network deployment, considering explicitly user mobility.
- We provide numerical results, revealing that: i) an even allocation of resources among UEs is inefficient, whereas even a rough estimate of their location allows heuristic policies to perform very close to the optimum; ii) mobility matters: group mobility leads to higher efficiencies and an increasing speed is also beneficial; iii) wireless charging can substantially reduce the fraction of nodes with depleted battery. However, this comes at the expense of constantly transmitting power and transfer efficiencies are low under any scenario.

3.1.2. Chapter Outline

The rest of the chapter is organized as follows. In Section 3.2, we discuss the related literature. Section 3.3 describes the system model. Then, WPT policies are proposed in Section 3.4. In Section 3.5, we present and discuss some selected numerical results. Finally, we conclude our work in Section 3.6.

3.2. Related Work

Due to the large diffusion of Wireless Sensor Networks (WSNs), involving relatively small and usually battery-powered devices, the study of WPT and EH has emerged as an interesting field of

research, including its application in future mobile networks. Below, we detail some of the main literature approaches.

In an early work [58], the authors show that it is possible to apply WPT with satisfactory results. There, they wirelessly transferred energy between a pair of devices by adopting self-resonant coils in a strongly coupled regime. The efficiency of the non-radiative transfer is demonstrated over higher distances than the radii of the two coils. A quantitative model, describing WPT, is also presented and the practical applicability of the system is discussed. It is also highlighted that specific materials and more elaborated geometries can be taken into account in order to improve the transfer efficiency. In this way, in [59], Kurs et al. exploit strongly coupled electromagnetic resonators to transfer energy from a transmitter to a receiver separated by a distance much larger than the size of the resonators. This technique can also be used to remotely power multiple devices from a single transmitting source. The power transfer efficiency is experimentally shown for cases involving coupling objects of different sizes. The authors also highlight that a single source powering many small devices, distributed over a large volume, achieves a good overall efficiency, even in scenarios where the transfer efficiencies of the single devices are quite low.

In [60], the SWIPT approach is tackled. The authors studied the tradeoff between the rates at which energy and information can be injected over a wireless channel affected by noise. A capacity-energy function of the channel was also found. According to this paper, by adopting the found tradeoff, it is possible to receive both large amounts of energy and information per unit time. Moreover, a three-node wireless MIMO broadcasting system for SWIPT is described in [61], involving two receivers and a single transmitter. In the described scenario, one of the two receiving devices harvests energy from the source, while the other one decodes the transmitted information. Two cases are studied: one where the information and energy receivers see two different channels from the transmitter, and another one in which they see the same channel. In the first case, strategies for maximum information rate versus energy transfer are derived. In the second case, instead, a performance bound outside of the rate-energy region is shown. This bound, though, is not reachable with existing technology, because circuits for harvesting energy from radio signals are not able to also decode information yet.

In [62], an optimal packet scheduling problem in a single-user energy harvesting wireless communication system is considered. In this network scenario, both the data packets and the harvested energy are modeled at the source node as random arrival processes, and the goal is to adaptively change the transmission rate according to the traffic load and to the available energy, such that the time by which all packets are delivered is minimized. Moreover, the authors of [63] propose an amplify-and-forward relay network, where an energy constrained relay node harvests energy from an acquired RF signal and uses it to forward the received information from the source to the destination.

The use of MIMO techniques along with beamforming allows for a considerable improvement in the transfer efficiency of energy and information. In [64], a MIMO beamforming scheme is considered to power mobile devices without needing them to be placed on apposite charging pads or with a particular orientation. This approach transfers energy by beamforming the nonradiated magnetic field and steering it toward the mobile device. Differently to what is doable using traditional inductive or resonating techniques, where the device to be charged has to be placed close to the charger, with this scheme a UE can be charged while inside the owner's pocket or a bag. Also, it does not require to modify the smartphones' hardware, but can be used with today's devices by

simply including a small receiver coil and circuit in a sleeve attached to the mobile device. A similar approach is presented in [65], where the authors consider a MISO femtocell cochannel overlaid with a macrocell to exploit the advantages of SWIPT, while promoting the energy efficiency. The femto BSs send information and simultaneously transfer energy to femto users via beamforming.

Finally, a recent work [66] presents a model for joint downlink and uplink transmission of K-tier heterogeneous cellular networks with SWIPT for efficient spectrum and energy utilization. In the downlink transmission, mobile users, equipped with power splitting receiver architecture, simultaneously decode information and harvest energy. In the uplink transmission, instead, UEs use the harvested energy to transmit information.

Novelty of the present work: the distinctive trait of our present work is that we explicitly consider user mobility in a distributed cellular system composed of several WPT-enabled BSs, investigating how mobility affects the charging efficiency of heuristic and optimal approaches.

3.3. System Model

We consider a cellular network covering a toroidal area of $M_1 \times M_2$ square meters. Within such an area, we randomly deploy $N > 0$ nodes, that represent the UEs in the network, as well as $B > 0$ BSs, with $B \ll N$. Each base station $i = 0, \ldots, B-1$ keeps track of the nodes that are located inside its coverage area A_i and, each node $n = 0, \ldots, N-1$, keeps track of all the surrounding base stations. Hence, each node will be associated with the BS that provides the highest Received Signal Strength Indicator (RSSI), which is referred to as the *serving* BS. For WPT, each BS uses $M \geq 1$ transmitting antennas, whereas each UE uses a single antenna, entailing a MISO power transfer channel. The UEs are free to move according to a certain mobility model, whose discussion is deferred to Section 3.3.4. In the following, we consider a target UE that is to be charged in a specific time slot by its serving BS and with d we mean their physical distance.

3.3.1. Channel Models

As for the channel model, we consider path loss and multi-path fading propagation phenomena. To model the path loss, we use the following simplified formula [67]: $P_{\text{rx}} = P_{\text{tx}} K (d_0/d)^{\gamma}$, where P_{tx} is the power transmitted by the BS, P_{rx} is the power received at the UE, d_0 is a reference distance for the antenna far-field, d is the distance between the WPT transmitter and the receiver, and γ is the path loss exponent. K depends on the antenna characteristics and is given by $K = (\lambda/(4\pi d_0))^2$, where λ is the wavelength. The power gain due to path loss is thus $f_{\text{pl}}(d) = K(d_0/d)^{\gamma}$.

Furthermore, for the considered dense network scenario, which is typical of network deployments in urban areas, we assume that a direct channel between the BS and the UE is unlikely to exist and for this reason the UEs receive a number of weak multi-path components, whereas the direct path is blocked. In such case, the received fading envelope is Rayleigh distributed. In order to model the Rayleigh fading, we use an improved version of the Pop-Beaulieu simulator based on Clarke's model [68]. According to this model, the normalized lowpass fading process $y(t) = y_c(t) + jy_s(t)$ is

obtained through a sum-of-sinusoids statistical simulation model, where:

$$y_c(t) = \frac{1}{\sqrt{P}} \sum_{p=1}^{P} \cos(\omega_d t \cos \alpha_p + \phi_p), \tag{3.1}$$

$$y_s(t) = \frac{1}{\sqrt{P}} \sum_{p=1}^{P} \sin(\omega_d t \cos \alpha_p + \phi_p), \tag{3.2}$$

with $\alpha_p = (2\pi p + \beta_p)/P$, $p = 1, 2, ..., P$, where P is the number of propagation paths, $\omega_d = 2\pi f_d$, f_d is the Doppler frequency, α_p and ϕ_p respectively represent the arrival angle (at the receiver) and the initial phase of the p-th propagation path. Finally, β_p and ϕ_p are statistically independent and uniformly distributed in $[-\pi, \pi)$, for all $p = 1, 2, \ldots, P$.

3.3.2. Transmission Beamforming for WPT

In the considered MISO scenario, beamforming techniques are utilized to increase the received power at the target UE. Here, we assume the channel gains are known at the transmitter and we use transmit beamforming [67] to maximize the amount of power that is transferred to the UE that is to be charged in the current time slot t. At the transmitter, the signal $s_i(t)$ that is to be transmitted from antenna i is multiplied by a complex gain $\omega_i = \rho_i e^{-j\theta_i}$, $\rho_i \in [0, 1]$. This multiplication implements co-phasing (θ_i) and weighting (ρ_i) relative to the channel gains. Let $g_i = \sqrt{f_{\text{pl}}(d)} y(t)$ be the complex lowpass channel gain (amplitude domain) between the i-th antenna at the BS and the receiving antenna at the UE, which depends on the path loss gain $\sqrt{f_{\text{pl}}(d)}$ and on the lowpass fading envelope $y(t)$ in the current time slot t. With perfect channel knowledge, co-phasing amounts to setting $\theta_i = \arg(g_i)$, $i = 1, \ldots, M$. Moreover, the combined lowpass signal at the receiver is:

$$r(t) = \sum_{i=1}^{M} \rho_i r_i s_i(t), \tag{3.3}$$

where $r_i = |g_i|$. For maximum power transfer, the (optimal) beamforming weights are obtained as [67]:

$$\rho_i = \frac{r_i}{\sqrt{\sum_{i=1}^{M} r_i^2}}, \tag{3.4}$$

which satisfies $\sum_{i=1}^{M} \rho_i^2 = 1$. With transmit beamforming and M transmit antennas at the BS, the power transmitted from antenna $i = 1, \ldots, M$, is $P_{\text{tx}}^i = P_{\text{tx}} \rho_i^2$, where P_{tx} is the total transmitted power. The harvested power Q at the target UE in slot t is proportional to the total received power in that slot, and is obtained as [65]:

$$Q = \xi \sum_{i=1}^{M} P_{\text{tx}} |g_i \omega_i|^2 = \xi P_{\text{tx}} \sum_{i=1}^{M} (\rho_i r_i)^2, \tag{3.5}$$

where $0 < \xi \leq 1$ is the power harvesting efficiency, which depends on the energy scavenging technology at the receiver. The channel gains g_i are obtained as a function of the path loss gain and of the multi-path fading envelope in the current time slot t. Moreover, we assume independently distributed fading processes across the transmitting antennas.

3.3.3. Energy Consumption and Efficiency Metrics

Time is slotted, slot times have a constant duration of T seconds, are grouped into windows, and each window contains W subsequent time slots. In each time slot, each UE consumes a certain power, P_d, which depends on the current task, i.e., emailing, Web browsing, calling, idling, etc. Assuming a constant power consumption in a time slot entails an energy drainage of TP_d.

The power consumption quantities, taken from [3], are measured using a Samsung Galaxy S3 smartphone and are shown in Table 3.1. In our numerical results, one activity from this table is picked with a certain probability at the beginning of each time window and is kept unchanged for its whole duration. The energy consumption for a time window is thus $E_d = WTP_d$.
Taking a specific UE $n = 0, \ldots, N-1$, and referring to its battery level at the beginning of window $w = 0, 1 \ldots$ as $E_{n,w}$, from window $w-1$ to w we have:

$$E_{n,w} = \begin{cases} E_{n,w-1} - E_{n,d} + E_{\text{rx},n,w-1}, & \text{if } E_{n,w} > 0 \\ 0, & \text{otherwise,} \end{cases} \tag{3.6}$$

where $E_{n,d}$ is the energy consumed by UE n due to the phone's activity and $E_{\text{rx},n,w-1}$ is the energy harvested by this user through WPT in window $w-1$. Note that, if the battery gets empty, i.e., $E_{n,w} = 0$, UE n is considered *dead* and cannot be wirelessly charged any longer.

Table 3.1: Battery discharge power P_d *vs* activity from [3].

Task	P_d [mW]
Audio	226
Email	1299
Phone call	854
Standby	24
Web	1080

WPT efficiency: for a given WPT scheduling policy, we measure the wireless power transfer efficiency $\eta \in [0, 1]$ as the ratio between the total energy harvested by the UEs and the total amount of energy that is transmitted by the BSs:

$$\eta = \lim_{L \to +\infty} \frac{\sum_{w=0}^{L-1} \sum_{n=0}^{N-1} E_{\text{rx},n,w}}{\sum_{w=0}^{L-1} \sum_{i=0}^{B-1} E_{\text{tx},i,w}}, \tag{3.7}$$

where L is the number of time windows, B is the number of BSs, N is the number of UEs, $E_{\text{tx},i,w}$ and $E_{\text{rx},n,w}$ respectively represent the total energy transmitted by BS i and the total energy har-

vested by UE n within time window w.

Charging metrics: at the beginning of a new window w, each BS i has to decide which ones of the users within its own coverage area A_i are to be charged and in which time slots: this is referred to as *power transfer schedule*. This decision is made in order to maximize one of the following global metrics. *Metric* 1 (M_1) jointly considers the transfer efficiency η and the residual battery level averaged over all UEs across all time slots, E, and is obtained by their linear combination through a weight $\alpha \in [0, 1]$:

$$M_1 = \alpha\eta + (1 - \alpha)E. \tag{3.8}$$

Here, $\alpha \in [0, 1]$ weighs the importance of the charging efficiency versus the residual energy level of the terminals. In fact, when $\alpha = 1$ the UEs providing the best transfer efficiency (i.e., the highest η) are charged, as these will have the largest M_1 metric, while when $\alpha = 0$ the devices whose battery is about to deplete are prioritized, as charging these will increase E. Intermediate cases occur for $0 < \alpha < 1$.

With *Metric* 2 (M_2), the previous quantities are multiplied:

$$M_2 = \eta E. \tag{3.9}$$

Here, the UEs with the lowest battery level, and that at the same time would benefit the most from the power transfer (leading to the highest η), are prioritized.

In the charging strategies that will be discussed in Section 3.4, we aim at maximizing the global metrics M_1 and M_2 by devising WPT schedules on a window-by-window basis. That is, at the beginning of any time window $w = 0, 1, \ldots$, each BS assesses the η and E metrics only for the users within its cell and for the entire window w. The best local schedule is then found through dynamic programming, by assessing all the possible allocation policies for the W time slots in the current window w [69]. The policies that we obtain through this approach are referred to as *genie-based* in Section 3.4, are not guaranteed to lead to the globally optimal metrics, but are preferred due to their practical and lightweight character.

3.3.4. Mobility Models

For the mobility, we consider the Random Waypoint Model (RWP) and Reference Point Group Mobility Model (RPGM). RWP allows the users to move freely and without restrictions around the network. In this model, first proposed by Johnson and Maltz [70, 71], UEs randomly choose their destination, speed and traveling direction and they do so independently of other users. RWP permits to study mobility scenarios where the users travel alone. At the beginning of the algorithm, each UE randomly chooses its destination and speed $\boldsymbol{v}$ such that its modulus is $|\boldsymbol{v}| \in [v_{\min}, v_{\max}]$, where $v_{\min}$ and $v_{\max}$ respectively are the minimum and maximum speed, then it chooses the movement direction in order to get closer to its destination. Upon reaching it, the user stops for a pause time T_{pause}, then he randomly chooses a new destination and the whole process repeats anew. A mobility path example for RWP is shown in Fig. 3.1.

RPGM [2], permits to study mobility scenarios where the movements of UEs are spatially correlated, i.e., users moving in groups, or carrying multiple devices. Nodes are divided into *group*

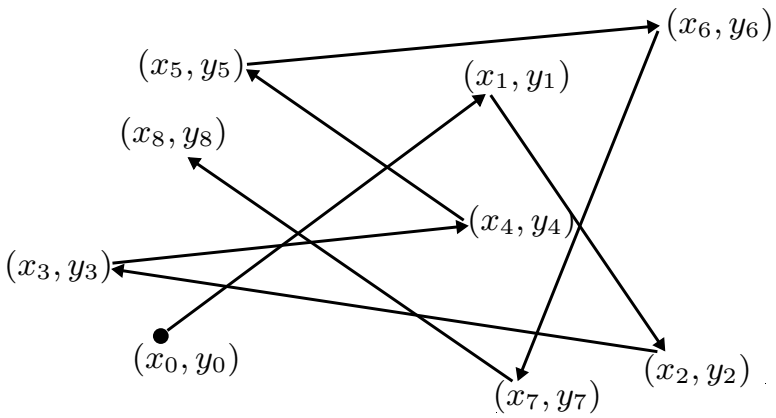

Figure 3.1: Example of node's movement in RWP [2]. (x_i, y_i), $i \in \{1, \ldots, 8\}$, are the destinations for 8 subsequent steps, (x_0, y_0) is the initial position.

leaders and *followers* and each group is composed of a group leader, that determines the direction of movement and speed for the whole group, and a certain number of followers, that tag along the leader of their group. At the beginning of the algorithm, each group leader behaves as an RWP node would do, i.e., randomly choosing his destination and speed and, at each round, he gets closer to his destination. The followers, instead, move in the same direction and with the same speed of their group leader, eventually deviating of a bounded distance from their reference point, i.e., the point they would reach traveling along the very same direction of their leader and with the same speed. This process goes on until the leader reaches his intended destination, then the whole group stops for a pause time, T_{pause}, after which the leader chooses another destination and the whole process repeats again. A group mobility example in RPGM is shown in Fig. 3.2.

3.4. Wireless Power Transfer Policies

Whenever the battery energy of any UE decreases below a certain threshold, $E_{\text{th}} \in (0, E_{\max}]$ ($E_{\max}$ is the UE's maximum battery energy), the UE sends a charging request to the BSs within coverage. The collection of charging requests and the decision of which UEs are to be charged is made on a window-by-window basis. Specifically, the requests that arrive during window $w-1$ are processed at the beginning of the w-th window, at which point the BSs decide which of the requesting users shall be charged during window w. Hence, a certain amount of power will be wirelessly transmitted to the selected users in their allotted time slots in a Time Division Multiple Access (TDMA) fashion. Note that the time slot allocation has to be made wisely, i.e., in order to maximize some selected metrics (see previous metrics M_1 and M_2). This means that, depending on the specific metric that is to be maximized, some users may be preferred as they are located within a shorter distance from the base station and thus the power transfer efficiency toward them is higher or other users may be given higher priority as their battery is about to deplete (i.e., energy level below E_{th}). Hence, in each window the number of time slots that is to be allocated by each BS to each user within coverage may change and may be uneven across different users, depending on their battery level and location. Next, we propose several policies to obtain suitable *power transfer schedules* by

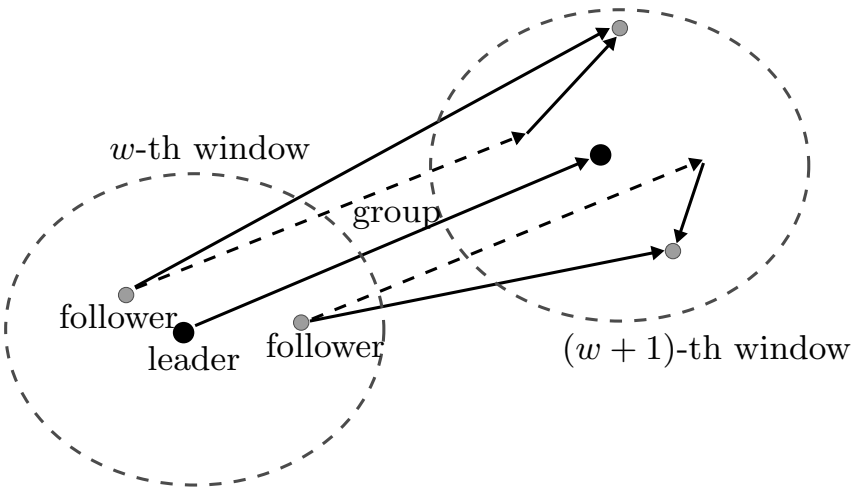

Figure 3.2: Example of group movement in RPGM [2]. The dashed straight lines represent the followers' reference path in absence of deviations. Two topology snapshots are drawn: one at the w-th window, and one at the $(w+1)$-th window.

adopting genie (optimal) or heuristic approaches and considering either metric M_1 or M_2.

3.4.1. Policy 1 (genie-based, metric M_1)

According to Policy 1 (P1), the BSs exactly know the position of all UEs throughout the entire simulation and optimally allocate TDMA (power transfer) time slots among the nodes that are to be charged, so as to maximize metric M_1 of Eq. (3.8).

Policy P1 uses a *genie* which knows the exact position of all users at all times. P1 is utilized as a benchmark for the *heuristic* policies that we detail below.

3.4.2. Policy 2 (heuristic, metric M_1)

With Policy 2 (P2), instead, the BSs estimate the positions of the UEs in the *current* time window. Any BS i, given that a UE is inside its coverage area A_i, and by observing at least two different positions of it, predicts its trajectory as we now describe. Consider UE $n \in \{0, \ldots, N-1\}$, and assume that we measure its position in time slots t and $t-k$, with $k \geq 1$, which we respectively call $\boldsymbol{p}_{n,t} = (p_{n,t,x}, p_{n,t,y})$ and $\boldsymbol{p}_{n,t-k} = (p_{n,t-k,x}, p_{n,t-k,y})$. The UE speed $\boldsymbol{v}_n = (v_{n,x}, v_{n,y})$ is then estimated as:

$$v_{n,x} = \frac{p_{n,t,x} - p_{n,t-k,x}}{Tk}, \tag{3.10}$$

$$v_{n,y} = \frac{p_{n,t,y} - p_{n,t-k,y}}{Tk}, \tag{3.11}$$

where T is the duration of a time slot. The BS can also estimate the future UE location at any time slot $t' > t$, $\hat{\boldsymbol{p}}_{n,t'} = (\hat{p}_{n,t',x}, \hat{p}_{n,t',y})$, as:

$$\hat{p}_{n,t',x} = p_{n,t,x} + v_{n,x}(t' - t)T, \tag{3.12}$$

$$\hat{p}_{n,t',y} = p_{n,t,y} + v_{n,y}(t' - t)T. \tag{3.13}$$

If BS i sees that the estimated future position of any UE n falls outside its coverage area, say, inside the one of BS j, with $i, j \in \{0, \ldots, B-1\}$, $i \neq j$, it notifies the latter BS of this fact, providing it with estimates of the UE arrival time and location. Given that each BS executes the above steps, estimates for UEs arrivals and departures are available to all BSs. After executing these estimations, which are made at the beginning of each window w, the BSs pick the power transfer slots as in P1, i.e., they determine the UEs to charge in order to maximize metric M_1 of Eq. (3.8) for each time slot. The only difference with respect to P1 is that in this case the estimated locations are used in place of the exact ones.

3.4.3. Policy 3 (genie-based, no metric)

With Policy 3 (P3), the BSs know the location of the UEs inside their coverage area A_i at the beginning of each time window. However, for the remaining time slots within the same time window they only know whether each of these UEs will remain inside their coverage area A_i. Hence, for any given time window, each BS $i = 0, \ldots, B-1$ only charges the UEs that have issued a charging request (with energy level below E_{th} at the beginning of the time window) and that remain inside its coverage area A_i for the entire window. For the charging schedule, the TDMA slots in the window are evenly split among these UEs. P3 is a *genie* policy as, although the exact position of the UEs is not known for all the future time slots, their serving BS is known beforehand for all the future slots in the current window, and since the beginning of it.

3.4.4. Policy 4 (heuristic, no metric)

With Policy 4 (P4), as with P3, the BSs only know the location of the UEs at the beginning of the current time window. Differently from P3, though, each BS i does not know those nodes that remain inside its coverage area A_i, but has to get an estimate for this using a method analogous to that of P2. After this, the TDMA time slots are evenly split among all the UEs that are estimated to remain within the coverage area A_i and that need to be charged, i.e., whose energy level is below E_{th} at the beginning of the time window.

3.4.5. Policy 5 (genie-based, metric M_2)

With Policy 5 (P5), the BSs exactly know the position of the UEs throughout the simulation and optimally allocate TDMA slots between the nodes to charge. Differently from P1, though, with P5 the BSs do this in order to maximize metric M_2, see Eq. (3.9). Analogously to P1, also P5 is a *genie* policy, designed to evaluate the performance of its corresponding heuristic policy, i.e., P6.

3.4.6. Policy 6 (heuristic, metric M_2)

With Policy 6 (P6), instead, each BS i has to estimate the future positions of the UEs inside its coverage area A_i and does so in the very same way as with P2. Differently from P2, though, the metric to maximize when choosing which UEs are to be charged is M_2, see Eq. (3.9).

3.5. Numerical Results

In this section, we present some selected numerical results for the WPT scenario of Section 3.3. The parameters that were used for the simulations are given in the following Tables 3.2 and 3.3. In all the graphs reported below, the network area is 1600 m^2 for an inter-BS distance of $d_{\mathrm{BS}} = 20$ m, except for Fig. 3.3, where it varies according to d_{BS}.

In Fig. 3.3, we show the transfer efficiency η obtained by the considered policies P1-P6 for $N = 100$ users, $P_{\mathrm{tx}} = 16$ W, $M = 4$, $v_{\max} = 2.5$ m/s and varying the inter-BS distance in $d_{\mathrm{BS}} \in [20, 100]$ m. As expected, for all the policies, the transfer efficiency increases with a decreasing inter-BS distance. This confirms that a densely deployed scenario, such as the one envisioned for next generation mobile networks, is beneficial to WPT. Further, we see that P1, P2, P5 and P6 behave similarly for the whole range of distances, with P1 and P2 being respectively the best and second-best. This fact was consistently verified across the whole parameter range, which means that metric M_1 has to be preferred to M_2. We also observe that P3 and P4 provide unsatisfactory performance, and this indicates that the user location (or at least a good estimate of it) is a valuable information for the considered WPT scheduling task. The inadequacy of P3 and P4 has been confirmed in all our numerical results. For these reasons, P3, P4, P5 and P6 will be dismissed and will no longer be considered in the following plots.

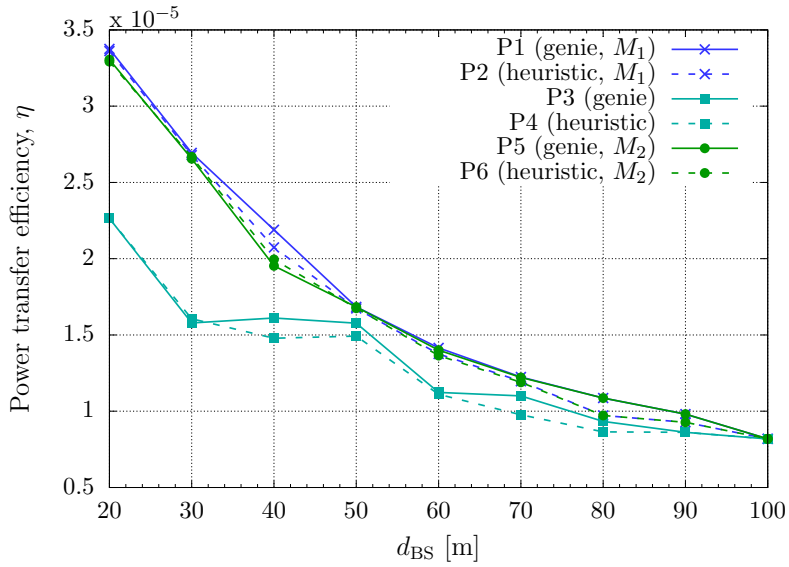

Figure 3.3: Power transfer efficiency η *vs* inter-base station distance d_{BS}. RWP mobility, $N = 100$ UEs, $P_{\mathrm{tx}} = 16$ W and $M = 4$ transmit antennas.

Table 3.2: System parameters used in the numerical results.

Parameter	Value
BS coverage range	10 m
Power harvesting efficiency, ξ	0.4
Energy threshold to issue a charging request, E_{th}	30% of E_{max}
Inter-BS distance, d_{BS}	$[20, 100]$ m
Minimum UE speed, v_{min}	0 m/s
Maximum UE speed, v_{max}	$[1, 4.5]$ m/s
Network area	$[1600, 40000]$ m^2
Number of antennas per BS, M	$[1, 8]$
Number of fading paths, P	8
Number of TDMA slots per window	10
Number of UEs, N	100
Number of UEs per group in RPGM	5
Number of windows in each simulation	28800
Path loss exponent, γ	3.5
Pause time, T_{pause}	2 s
Reference distance, d_0	1 m
Window duration	2 s
Total transmit power, P_{tx}	16 W
Transmit frequency, f_{tx}	$[100, 2000]$ MHz
UE battery capacity	2100 mAh
UE battery voltage	3.8 V

In Fig. 3.4, we explore the relationship between the power transfer efficiency η and the transmit frequency f_{tx}. As expected, lower frequencies are to be preferred and those commonly used for FM broadcasting (around 100 MHz) provide the highest transfer efficiencies within the considered frequency range, due to their lower path loss. As promptly inferred from this plot, the transfer efficiency that we may expect from this technology is rather small, but as we shall see in the following, when the network deployment is dense (e.g., $d_{\text{BS}} = 20$ m) the mobile users may still be able to charge their batteries (although at a low pace) and a good percentage of them to prevent their batteries from draining fast or being depleted. Moreover, in Fig. 3.4 we show results for random (RWP) and group (RPGM) mobility and we see that group mobility attains the best transfer efficiencies. In fact, we observe that when one user is in a favorable location (i.e., close to a WPT-enabled BS), with high probability his followers will also be favorably located. Hence, more users will be efficiently charged per unit time than with RWP mobility. This was consistently

Table 3.3: Parameters used in the following plots.

Figure	α	d_{BS} [m]	f_{tx} [MHz]	M	$v_{\max}$ [m/s]
Fig. 3.3	1	$[20, 100]$	100	4	2.5
Fig. 3.4	1	20	$[100, 2000]$	4	2.5
Fig. 3.5	1	20	100	4	$[1, 4.5]$
Fig. 3.6	1	20	100	$[1, 8]$	2.5
Fig. 3.7	$[0, 1]$	20	100	4	2.5
Fig. 3.8	$[0, 1]$	20	100	4	2.5
Fig. 3.9	1	20	100	$[1, 8]$	2.5

verified across all our experiments.

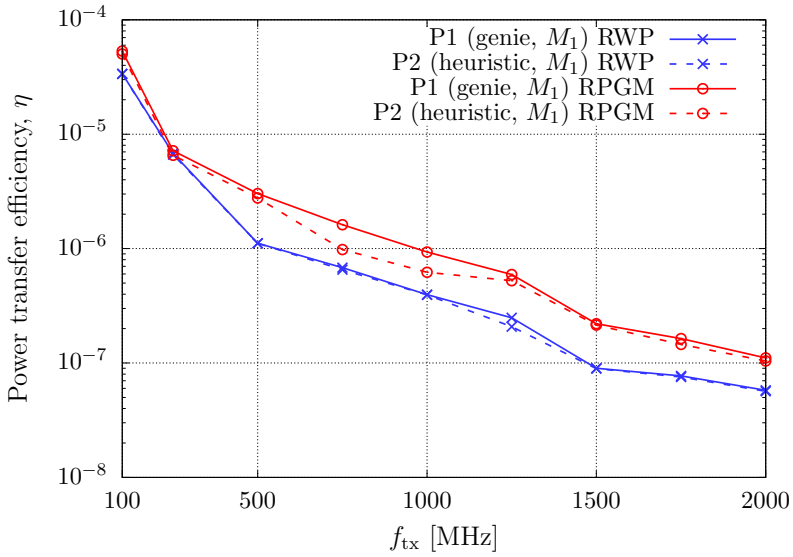

Figure 3.4: Power transfer efficiency η varying the transmit frequency f_{tx}.

Another interesting result is shown in Fig. 3.5, where we compare policies P1 and P2 for an increasing UE speed. From this plot, we see that mobility is actually beneficial in terms of η. This is because, through mobility, even users that are initially located far away from the WPT-enabled BSs eventually move closer to one of them and can thus benefit from WPT. Hence, the probability that there exist users in favorable positions, i.e., close to some WPT-enabled BS is higher in the presence of mobility and increases with an increasing maximum speed $v_{\max}$.

Although not shown in the plot for the sake of readability, the gap between P3/P4 and P1/P2 becomes substantial, which confirms that it is inappropriate to charge users without accounting for their distance from the charging BS. As for policies P5/P6, these still perform close to P1/P2, but their performance is always dominated. Also, an increasing speed leads to a higher gap between

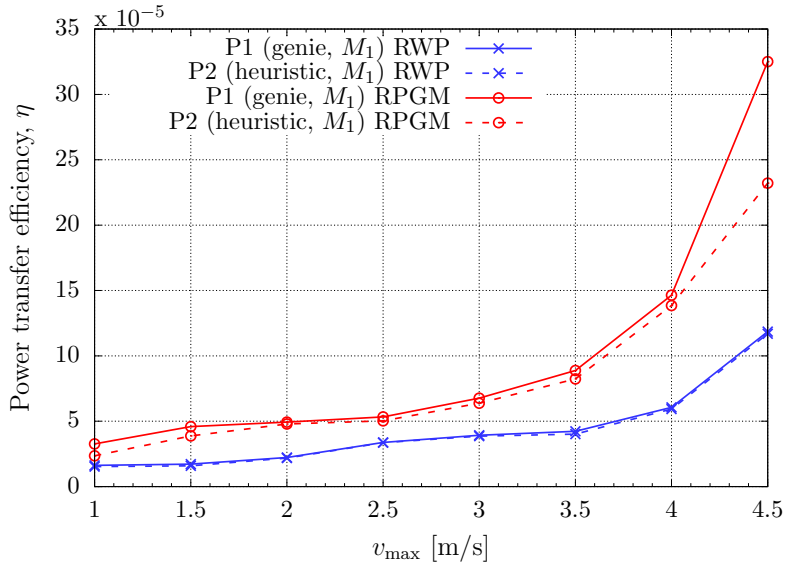

Figure 3.5: Power transfer efficiency η varying the maximum UE speed $v_{\max}$.

genie-based and heuristic policies and this is because the estimates obtained through Eq. (3.12) and (3.13) become less accurate. This is especially evident with RPGM mobility, as group mobility patterns are poorly described by these estimates (where the mobility of each terminal is independently assessed).

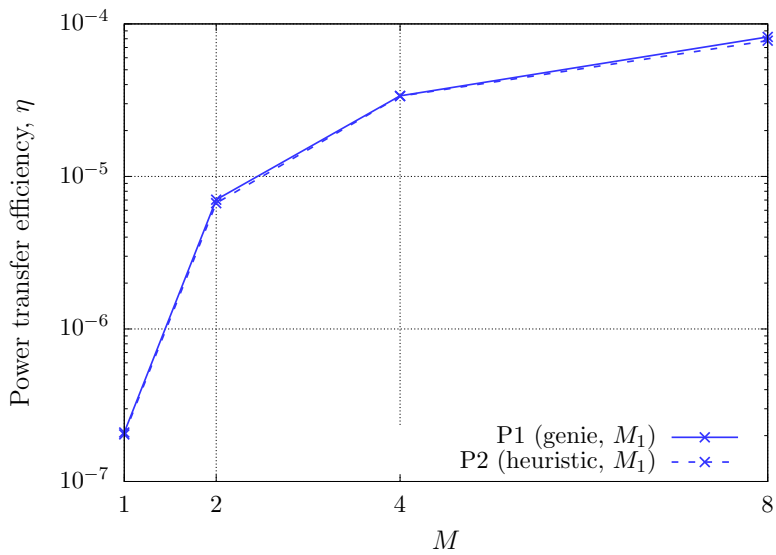

Figure 3.6: Power transfer efficiency η *vs* number of transmit antennas, M.

Fig. 3.6 shows the transfer efficiency η as a function of the number of transmit antennas M at the charging BS. When a single antenna is employed ($M = 1$, no beamforming) we obtain the

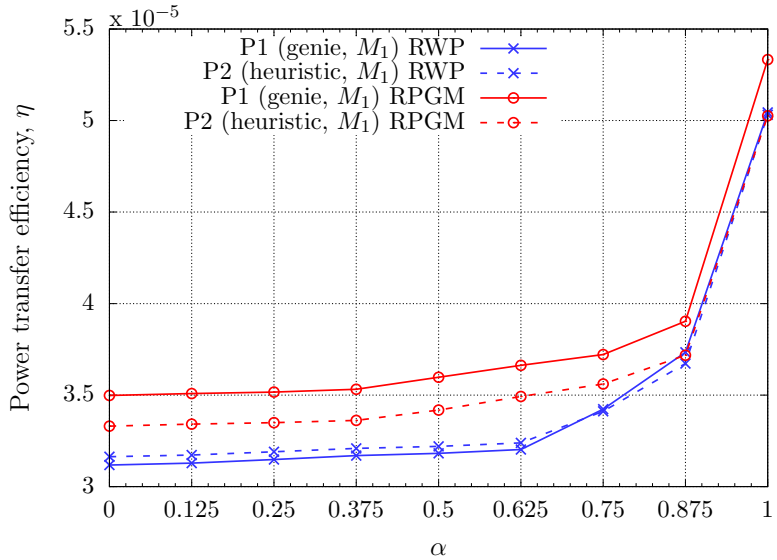

Figure 3.7: Power transfer efficiency η *vs* α.

lowest efficiency, which then improves by more than one order of magnitude for $M = 2$ and more than two for $M = 4$. Beyond $M = 4$, the additional improvement is marginal. We observe that, in theory, additional benefits may be possible by also using antenna arrays at the receiver side. Due to space constraints at the UEs, this is however only feasible at high frequencies (in the GHz range), due to the antenna size and the separation ($\approx \lambda/2$) that is required to ensure uncorrelated fading among antennas. Nevertheless, in the GHz range the efficiency appears too small to justify the use of WPT in the considered network scenario (see Fig. 3.4).

In Fig. 3.7, we show the efficiency η for the best policies P1 and P2 as a function of the weight α (see Eq. (3.8)). With $\alpha = 1$, metric M_1 puts more weight on η, which becomes the only performance indicator to be maximized. As seen from this graph, this is in fact what the policies do: as α goes from 0 to 1, the efficiency η correspondingly increases of about 50%. In this figure, we also show the impact of the mobility behavior, plotting results for the RWP and RPGM mobility models. Once again, group mobility leads to the highest efficiencies.

At this point, one might rightly wonder what happens to the energy metric E when we decrease α down to 0. This latter tradeoff is shown in Fig. 3.8, from which we get a somewhat counterintuitive result, i.e., that putting more weight on the residual energy level at the nodes ($\alpha \to 0$) does not lead to an increased energy metric E, but the residual energy is actually maximized when $\alpha = 1$, i.e., when the WPT schedules are solely computed based on the power transfer efficiency η. The reason behind this is that, when $\alpha = 0$, WPT slots will be assigned based on the residual energy level and disregarding the users' location. However, with this approach it may happen that users that are located far away from the BSs will be charged anyway as their energy level is below threshold, but the charging efficiency in this case will be very small and we would be better off by charging these users as they get sufficiently close to one of the WPT-enabled BSs. Overall, this means that the best strategy is to compute the charging schedules only based on the UE location, as the transfer efficiency will otherwise be too small. Besides, Fig. 3.8 confirms the fact that group mobility helps

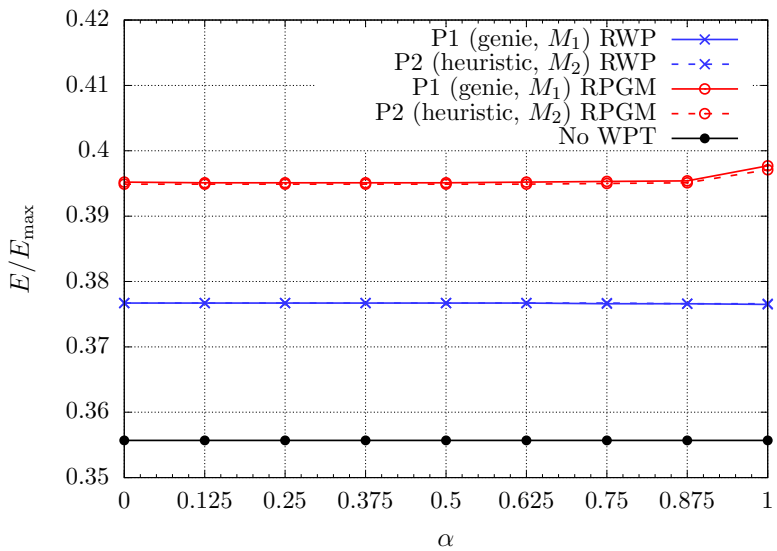

Figure 3.8: Normalized average energy per non-dead node per window *vs* α.

increase the nodes' energy level and that the heuristic policy P2 for $v_{max} = 2.5$ m/s performs very close to the genie-based policy P1.

In the last Fig. 3.9, we evaluate the fraction of UEs whose battery is depleted during the simulation for a pedestrian mobility scenario ($v_{\max} = 2.5$ m/s). Once again, we see that beamforming is quite efficient, lowering this fraction from 0.7 (i.e., 70% of the users) down to 0.53 for $M = 8$, which corresponds to a relative improvement of about 24%. This is considerable, especially in light of the very small efficiencies that are provided by WPT in the considered network scenario. Although not evaluated in this chapter, we foresee that in the near future BSs will be equipped with energy harvesting technology (e.g., solar panels), which will make it possible to collect ambient energy (see next chapters). Part of this energy, especially during daytime, could be used to charge mobile users. Although the charging efficiency is very low, this ancillary service is valuable to the users, who may be willing to pay for it, generating revenue for the mobile operators.

3.6. Conclusions

In this chapter, we have studied WPT techniques for sustainable mobile networks, using transmit beamforming to wirelessly charge mobile UEs in densely-deployed MISO femtocell networks. We have designed several policies to assess which users are to be charged and in which time slots, while prioritizing them based on their location and on their battery level.

Through numerical simulation, we have then analyzed the performance of these policies finding that heuristic approaches, that estimate the user locations, behave close to genie-aided ones, where locations are exactly known for all the future time slots. This is especially true for pedestrian scenarios, where the user speed is moderate and even simple linear approximations suffice to obtain accurate estimates. We have also assessed the impact of the mobility behavior, finding that mobility

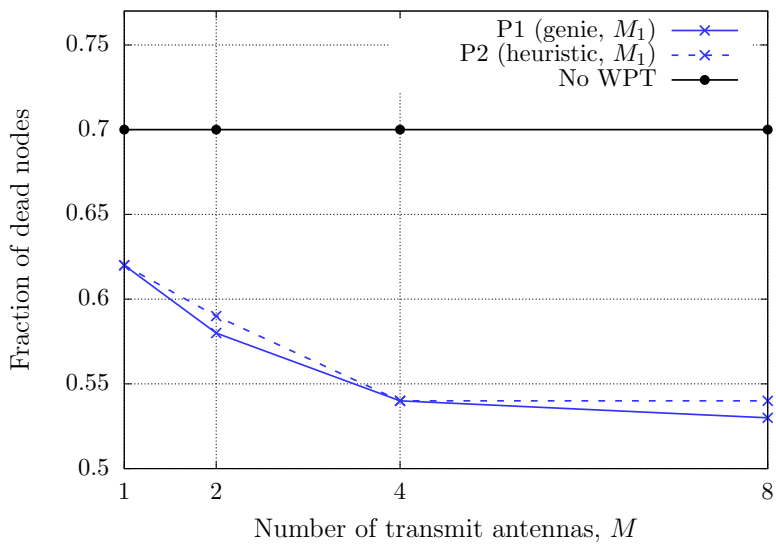

Figure 3.9: Fraction of dead nodes *vs* number of transmit antennas M. RWP mobility with maximum user speed $v_{\max} = 2.5$ m/s.

helps to increase the power transfer efficiency and also that the best results are achieved when users move in groups. Although typical WPT efficiencies are rather small in any scenario, our results indicate that the number of dead nodes, whose battery is depleted during the simulation, decreases of about 24% with WPT for an inter-BS distance of 20 meters.

Finally, it should be noted that although the considered setup in terms of configuration and network parameters might be far from conventional 5G deployments, the proposed methodology could be applied to the 5G air interface as well with minor modifications.

4

Energy Cooperation among Energy Harvesting Base Stations

4.1. Introduction

In this chapter, we advocate future networks where small BSs are densely deployed to offer coverage and high data rates, and EH hardware (e.g., solar panels and energy storage units) is installed to power them. BSs collect energy from the environment, and have a local energy storage, which they can use to accumulate energy when the harvested inflow is abundant. This local energy reserve can be utilized to serve the local traffic and can be transferred to other BSs (energy routing) to compensate for imbalance in the harvested energy or in the traffic load, see Fig. 4.1. Some of the BSs, referred to as *ongrid*, are connected to the power grid, whereas the others are *offgrid* and, as such, rely on either the locally harvested energy or on the energy transferred from other BSs. Within this setup, intelligent policies are to be devised to transfer the surplus energy to *offgrid* BSs, to ensure the self-sustainability of the mobile system.

Energy transfer is an important feature of EH mobile networks and can be accomplished in two ways: i) through WPT or ii) using a PPG [72]. For i), our previous studies (see Chapter 3 and [21]) have shown that its transfer efficiency is too low for it to be a viable solution when distances exceed a few meters, but ii) looks promising. In analogy with communications networks, in a PPG a number of power *sources* and power *consumers* exchange power (Direct Current, DC) in the form of "packets", which flow from sources to consumers thanks to power lines and electronic switches. The energy routing process is controlled by a special entity called the *energy router* [73]. Following this architecture, a local area packetized power network consisting of a group of energy subscribers and a core energy router is presented in [74], where a strategy to match energy suppliers and consumers is devised.

Within this setting, the allocation and transfer of energy among BSs is performed through the PPG infrastructure, where a centralized energy router is responsible for deciding the power allocation and transfer among the BSs over time (Fig. 4.1). This energy allocation and transfer problem is solved devising an online framework combining: 1) pattern learning (time series forecasting), 2) adaptive control (through MPC), 3) energy allocation and 4) energy routing, see Fig. 4.2. **Pattern learning** is performed via Gaussian Processes (GPs), to learn the BS energy harvesting and consumption (load) patterns over time. This knowledge is utilized within the multi-step ahead **MPC** block, that is in charge of determining the role of each BS, i.e., whether it should act as an energy *source* or *consumer*, and the maximum energy amount that it can either supply (if acting as a source) or demand (consumer), in order to keep the BS system as much as possible energetically self-sufficient over time. The **energy allocation** block computes the actual amount of energy to transfer from energy sources to consumers: two schemes are proposed, one based on convex optimization and one, used as a benchmark, based on an optimal assignment problem, that is solved via the Hungarian method. Finally, once the energy allocations are computed, the **energy transfer**

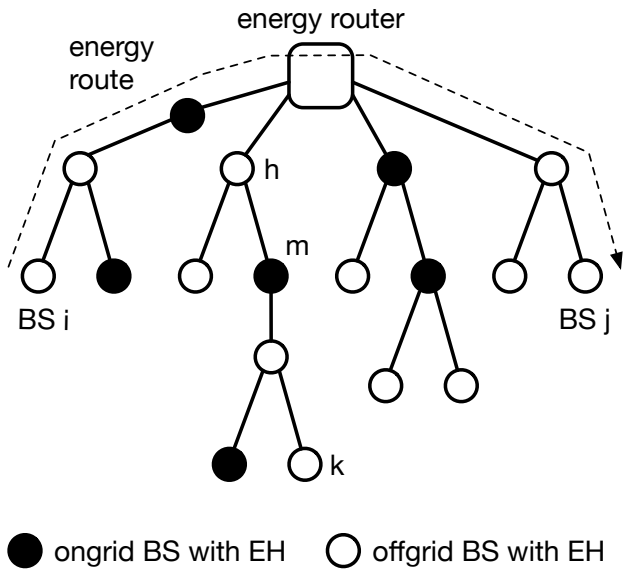

Figure 4.1: Power packet grid topology.

block schedules in time the energy routes, by transferring the energy among nodes. Since the PPG is operated in a Time Division Multiplexing (TDM) fashion, each power link can only be used for a single energy transfer operation at a time. An optimal algorithm to allocate routing schedules is put forward, ensuring that routes between energy sources and consumers do not interfere in time and space, while minimizing the total time needed to complete the energy transfers. Further details are provided in Section 4.4.

Although the considered online optimization problem can be solved with other tools, such as a monolithic formulation or dynamic programming, the presented decomposition into four sub-problems makes it possible to deal with low-complexity convex problems, without introducing significant approximations and/or quantization to the involved variables. The resulting approach is practical and appealing for real-world applications.

Numerical results, obtained with real-world harvested energy traces and traffic load patterns, show that the proposed approach effectively keeps the outage probability[1] to nearly zero for a wide range of traffic load and system configurations. Also, the amount of energy purchased from the power grid to operate the mobile network is reduced by more than 50% with respect to computing energy schedules solely based on the present network status [75], i.e., disregarding future energy arrivals and load conditions. As we elaborate in Section 4.2, we have not identified previous works coping with distributed BS deployments with energy harvesting, storage and transfer capabilities (via PPG), and proposing an energy management solution based on statistical learning and predictive control.

[1]Computed as the ratio between the number of BSs that are unable to serve the users within range due to energy scarcity, and the total number of BSs.

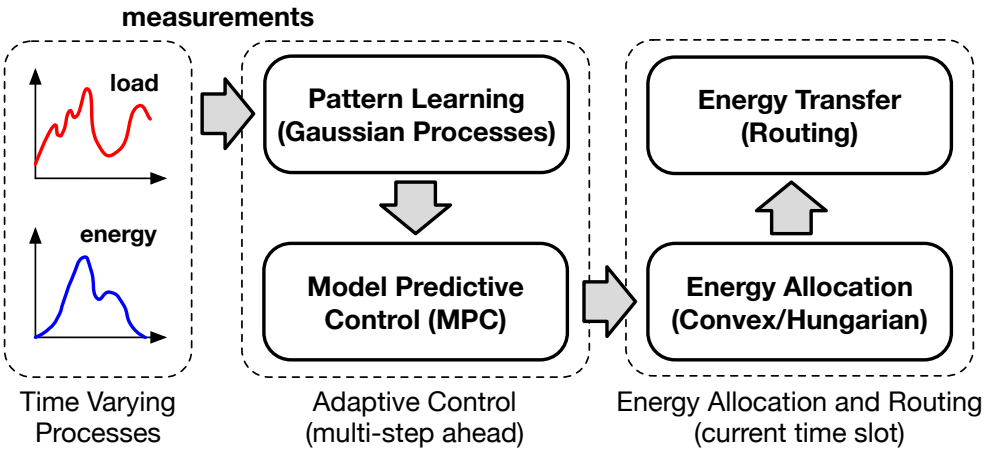

Figure 4.2: Overview of the optimization framework.

4.1.1. Contributions

The main contributions of the present chapter are:

- We present an online statistical learning framework based on Gaussian Processes, which is customized to learn the EH and consumption (load) patterns over time. Specifically, a specific composite kernel is designed and tuned with optimal hyperparameters to cope with local quasi-periodic structures in the data, with noise operating at different scales. GPs are then utilized to predict these processes in future time slots, in an online and adaptive fashion (based on the most recent samples).
- We formulate an online and predictive optimization problem for the energy transfer across EH BSs with the goal of making the mobile network energetically self-sustainable.
- We provide numerical results, quantifying the effectiveness of the proposed solution with real-world harvested energy and load traces. An important finding is that the combination of forecasting and predictive control can substantially reduce the total amount of energy that the BS system drains from the power grid, halving it in most cases. This descends from a more intelligent redistribution of the harvested energy.

4.1.2. Chapter Outline

The chapter is organized as follows. In Section 4.2, we present the literature on energy cooperation, the mathematical tools used in this work and highlight the novel aspects of our design. The network scenario is described in Section 4.3. Our optimization framework is detailed in Section 4.4. The numerical results are presented in Section 4.5, and final remarks are provided in Section 4.6.

4.2. Related Work

In this section, we present some specific literature on energy cooperation, the mathematical tools used in this chapter, namely MPC and GPs, and highlight the novel aspects of the proposed design.

4.2.1. Energy Transfer in Mobile Cellular Networks

The concept of *energy transfer*, also referred to as *energy cooperation* [22, 24, 29] or *energy exchange* [53], is motivated by the fact that the distributed renewable energy generated at the BSs can be leveraged upon through a microgrid connecting them [56], with the aim of improving the network self-sustainability, while reducing the cost entailed in purchasing the energy from the power grid. Energy sharing among BSs is investigated in [24] through the analysis of several multiuser network structures. A two-dimensional and directional water-filling-based offline algorithm is proposed to control the harvested energy flows in time and space, with the objective of maximizing the system sum-rate throughput. In [29], the authors introduce a new entity called the *aggregator*, which mediates between the grid operator and a group of BSs to redistribute the energy flows, reusing the existing power grid infrastructure: one BS injects power into the aggregator and, simultaneously, another one draws power from it. This scheme does not consider the use of *energy storage devices*, and for this reason some of the harvested energy can be lost if none of the base stations drains it when it is injected. The authors of [76] consider BSs with energy harvesting capabilities connected to the power grid as a means to carry out the energy trading. A joint optimization tackling BS operation and power distribution is performed to minimize the on-grid power consumption of the BSs. Wired energy transfer to/from the power grid, and a user-BS association scheme based on cell zooming are investigated. The problem is solved using heuristics. A similar approach is considered in [77], where two problems are addressed: the first one consists of optimizing the energy allocation at individual BSs to accommodate for the temporal dynamics of harvested energy and mobile traffic. Considering the spatial diversity of mobile traffic patterns, the second problem amounts to balancing the energy consumption among BSs, by adapting the cell size (radio coverage) to reduce the on-grid energy consumption of the cellular network. Again, the solutions are obtained through heuristic algorithms. Also, in these works, differently to what we propose here, *BSs do not perform any actual energy transfer among them.*

A two-cell renewable-energy-powered system is studied in [78], where the sum-rate over all users is maximized while determining the direction and amount of energy to be transferred between the two BSs. Energy can be transferred across the network either through power lines or wireless transfer and the energy transfer efficiency is taken into account. This resource allocation problem is formulated under a Frequency Division Multiple Access (FDMA) setup and is solved numerically. A low-complexity heuristic approach is also proposed as a practical near-optimal strategy when the transfer efficiency is sufficiently high and the channel gains are similar for all users. A similar two-BS scenario is considered in [22], where BSs gather energy from the power grid and from renewable energy sources, have a limited energy storage capability, and are connected through power lines. The authors study the case where renewable energy and energy demand profiles are deterministically known ahead of time, and find the optimal energy cooperation policy by solving a linear program. They then consider a more realistic case where the profiles are stochastic and

propose an online greedy algorithm. Finally, an intermediate scenario is addressed, where the energy profiles are obtained from a deterministic pattern, adding a small amount of random noise at each time step.

The authors of [53] consider a setup similar to ours, i.e., multiple BSs, energy harvesting with local storage devices and energy exchange among BSs through the power grid. The main differences are that *perfect knowledge* of hourly varying energy demand profile (BS load) and hourly harvested energy is assumed, and energy routing is not studied. An optimal constrained problem is formulated, assessing its performance via simulation. Other relevant papers are [56, 79]. There, energy sharing takes place either via physical power lines or through the power grid (virtual energy exchange). Interestingly, the authors investigate the impact of the power line infrastructure topology: agglomerative and divisive hierarchical clustering algorithms are utilized to determine it. Upon establishing the physical connections among BSs, an optimization framework for day-to-day cost optimization is developed for the cases of 1) zero knowledge, 2) perfect knowledge, and 3) partial future knowledge of the harvested energy process. The main differences with respect to our work are: for the partial future knowledge case, a static model is adopted, where the amount of energy harvested through the day is given by an average value for each time slot, plus a random displacement. Average values are obtained from historical data, but *are kept fixed* during the day. In contrast to this, we devise an *online* estimation algorithm through which future harvested energy incomes are estimated based on those measured in the most recent time slots, providing *online adaptation and tracking* capabilities. Also, in [56] perfect knowledge of the BS consumption pattern across a whole day is assumed, whereas we estimate and track it at runtime. Online predictive control takes these estimates into account for the computation of optimal energy transfers, making our solution applicable to real settings.

Techniques exploiting energy trading / sharing through, e.g., spectrum sharing or Coordinated MultiPoint (CoMP), are combined for energy cost reduction in EH BS networks and a power grid in [28]. While the authors discuss interesting future research directions, their system model does not consider time dynamics. The joint energy purchase and wireless load sharing among mobile network operators is exploited in [80] to reduce energy costs. The authors of this paper propose a scheme named *energy group buying with load sharing*, where the two operators are aggregated into a single group to implement a day-ahead and real-time energy purchase, and their BSs share the wireless traffic to maximally put lightly-loaded BSs into sleep mode. This scenario is tackled using two-stage stochastic programming. The scenario that we consider here is different, as we focus on actual energy exchange among BSs belonging to the same operator. The authors of [81] consider a delay minimization problem in an energy harvesting communication network with energy cooperation. Their study considers fixed data and energy routing topologies, determining optimum data rates, transmit powers, and energy transfers through an iterative algorithm, subject to flow and energy conservation constraints, to minimize the network delay. Two last papers are [82, 83]. The authors of [82] consider multiple EH transmitters communicating with multiple receivers, with the goal of maximizing the weighted throughput within a data broadcasting setup. They put forward an iterative algorithm that solves the energy and bandwidth allocation sub-problems optimally. [83] presents an energy-bandwidth allocation problem for a multiuser network where each node is powered with renewable and grid energy and the aim is to maximize the weighted sum throughput for transmitter-receiver pairs, while minimizing the use of grid energy. Differently from our present work, in this prior paper energy harvesting flows are considered to be deterministically known be-

forehand, and the energy transfer between nodes is not explicitly modeled in terms of architecture, physical layer technology and (possibly multi-hop) energy routing.

4.2.2. Pattern Learning along with Multi-step Optimization Techniques

Model Predictive Control has its roots in optimal control theory. The main idea is to use a dynamic model to forecast the system behavior, and exploit the forecast state sequence to obtain the *control* at the current time. The system usually evolves in slotted time, the control action is obtained by solving, at each time slot, a finite horizon optimal control problem where the initial state is the current state of the system. The optimization yields a finite control sequence, and the first control action in this sequence is applied [84]. MPC has the ability to anticipate future events and makes control decisions accordingly. It has been widely used in industrial processes, including chemical plants [85–87] and oil refineries [88, 89] and, recently, to balance energy consumption in smart energy grids [90–92]. Moreover, it has been applied to supply chain management problems, with promising results [93–96].

It is known that using time-series forecasting within an MPC framework can improve the quality of the control actions by providing insight into the future [97]. Over the last decades, numerous forecasting approaches have been developed, including Autoregressive Integrated Moving Average (ARIMA) processes and ANNs. ARIMA models (introduced by Box and Jenkins in [98]) are known for their prediction accuracy, but their main limitation lies in the assumption that the data follows a linear model. Conversely, ANNs capture non-linear models and, in turn, can be a good alternative to ARIMA [99]. Nonetheless, ANNs give rise to mixed results for purely linear correlation structures. In [100, 101], hybrid schemes that combine them are put forward to take advantage of their unique strengths. Experimental results with real-world data indicate that their combined use can improve the prediction accuracy achieved by either of the techniques when used in isolation.

Several authors have proposed the use of non-linear models to build non-linear adaptive controllers. In most applications, however, these non-linearities are unknown, and non-linear parameterization must be used instead. In time-series analysis, where the underlying structure is largely unknown, one of the main challenges is to define an appropriate form of non-linear parameterization for the forecasting model. Some implementations claim to be non-parametric, such as GPs, which can be considered (in some sense) as equivalent to models based on an infinite set of non-linear basis functions [102]. The basic idea of GPs is to place a *prior distribution* directly on the space of functions, without finding an appropriate form of non-linear parameterization for the forecasting model. This can be thought of as a generalization of a Gaussian distribution over functions. Moreover, a GP is completely specified by the mean function and the *covariance function* or *kernel*, which has a particular (but simple) parametric structure, defined through a small number of *hyperparameters*. The term non-parametric does not mean that there are no parameters, but that the parameters can be conveniently adapted from data. While GPs have been used in time-series forecasting [103], to the best of the authors' knowledge, [104] is the first application of GPs to electrical load forecasting [105–108].

The electricity supply is mainly influenced by meteorological conditions and daily seasonality. Nevertheless, forecasting for short-term horizons of about a day is often performed using univariate

prediction models, which are considered to be sufficient because the weather tends to change in a smooth fashion, which is reflected in the electricity demand itself. Also, in a real-world online forecasting scenario, multivariate modeling is usually considered impractical [106]. Due to daily seasonality, we can say that the electrical load data bears some similarities with the time series that we consider in this chapter, i.e., the harvested energy profile of Section 4.3.2 and the traffic load of Section 4.3.3.

The idea of combining MPC and GPs was first proposed in [109], where the framework is evaluated by means of a simple (simulated) first order non-linear process. Other practical implementations can be found in application domains such as greenhouse temperature control systems [110], gas-liquid separation plant control systems [111], combustion power plants control systems [112] and in a number of other cases [113–116]. To the best of our knowledge, the present work is the first where MPC and GPs are combined to control an energy harvesting mobile network. Our purpose is thus to demonstrate the feasibility of application and realization of a GP based control algorithm for online power management, highlighting its potentials for the development of greener technologies, with the aim of improving the network self-sustainability.

4.2.3. Novelty of the Present Work

Despite the existence of previous works on energy cooperation, here we consider a more complete setup, where: (i) EH BSs are equipped with storage capabilities, (ii) the harvesting process and traffic load in the system are unknown and *fully stochastic*, (iii) the harvested energy and traffic load in BSs that we use for GP training and for our numerical results come from real-world traces, and (iv) the physical power grid is based on the novel concept of PPG. The combination of MPC and GPs has already been considered in the literature. However, to the best of our knowledge, this is the first time where this tool chain is used in an energy-aware mobile network scenario. Also, in the proposed optimization architecture, the overall problem is split into sub-blocks, where optimization problems are convex, can be solved at runtime and have low-complexity. This makes it possible to implement the presented solution in real systems.

4.3. System Model

We consider a mobile network comprising a set $\mathcal{S}$ of $n_s = |\mathcal{S}|$ BSs, each with energy harvesting capabilities, i.e., a solar panel, an energy conversion module and an energy storage device. Some of the BSs are ongrid (termed *ongrid* BSs, being part of set $\mathcal{S}_{\text{on}}$) and, in turn, can obtain energy from the power grid. The remaining BSs are *offgrid* (set $\mathcal{S}_{\text{off}}$). The proposed optimization process evolves in slotted time $t = 1, 2, \ldots$, where the slot duration corresponds to the time granularity of the control and can be changed without requiring any modifications to the following algorithms.

4.3.1. Power Packet Grids

A PPG is utilized to distribute energy among the BSs. The grid architecture is similar to that of a multi-hop network, see Fig. 4.1, where circles are BSs and the square is the energy router, which is in charge of energy routing decisions and power allocation. As assumed in [74], BSs are connected

through DC power links (electric wires) and the transmission of energy over them is operated in a TDM fashion. Energy transfer occurs by first establishing an *energy route*, which corresponds to a sequence of power links between the energy source and the destination. Each power link can only be used for a single transfer operation at a time. Power distribution losses along the power links follow a linear function of the distance between the source and the destination [74]. They depend on the resistance of the considered transmission medium and are defined by [117]: $R = \rho\ell/A$, where ρ is the resistivity of the wire in $\Omega\text{mm}^2/\text{m}$, ℓ is the length of the power link in meters, and A is the cross-sectional area of the cable in mm^2. Here, we consider a PPG with a single energy router in the center of the topology. A number of sub-trees originates from the router and, without loss of generality, each hop is assumed to have the same length ℓ, i.e., the same power loss.

4.3.2. Harvested Energy Profiles

Solar energy generation traces have been obtained using the SolarStat tool [35]. For the solar modules, the commercially available Panasonic N235B photovoltaic technology is considered. Each solar panel has 25 solar cells, leading to a panel area of $0.44\,\text{m}^2$, which is deemed practical for installation in a urban environment, e.g., on light-poles. As discussed in [31, 35], the EH inflow is generally bell-shaped with a peak around mid-day, whereas the energy harvested during the night is negligible. Here, the framework in [35] is utilized to obtain the amount of energy harvested for each BS $n \in \{1, \ldots, n_s\}$ in time slot t, which is denoted by $H_n(t)$.

4.3.3. Traffic Load and Power Consumption

Traffic load traces have been obtained using real mobile data from the Big Data Challenge organized by Telecom Italia Mobile (TIM) [118]. The dataset is the result of a computation over Call Detail Records (CDRs), logging the user activity within the TIM cellular network for the city of Milan during the months of November and December 2013. For the traffic load traces we use the CDRs related to SMS, calls and Internet activities, performing spatial and temporal aggregation. In this way, we obtain a daily traffic load profile for each BS.

Clustering techniques have been applied to the dataset to understand the behavior of the mobile data. To this end, we use DBSCAN unsupervised clustering [119] to classify the load profiles into several categories. In Fig. 4.3, we show the typical traffic behavior of two clusters, corresponding to the heaviest (cluster 1) and lightest (cluster 2) daily load. As noted in previous works, the traffic is time-correlated (and daily periodic) [31, 120]. In our numerical results, each BS has an associated load profile, which is picked at random as one of the two clusters in Fig. 4.3. Depending on the cluster association probabilities, there is some imbalance in the load distribution across BSs that, as we shall see, plays a key role in the performance of energy transfer algorithms. Given the traffic load profile $L_n(t)$, intended as the percentage of the total bandwidth that a BS n allocates to serve the users in its radio cell, the BS energy consumption (energy outflow), referred to in the following as $O_n(t)$, is computed through the linear model in [31] (see Eq. (1) in that paper).

4.3.4. Energy Storage Units

Energy storage units are interchangeably referred to as Energy Buffers (EBs). The EB level for BS $n \in \{1, \ldots, n_s\}$ is denoted by $B_n(t)$ and three thresholds are defined: B_{up}, B_{ref} and B_{low},

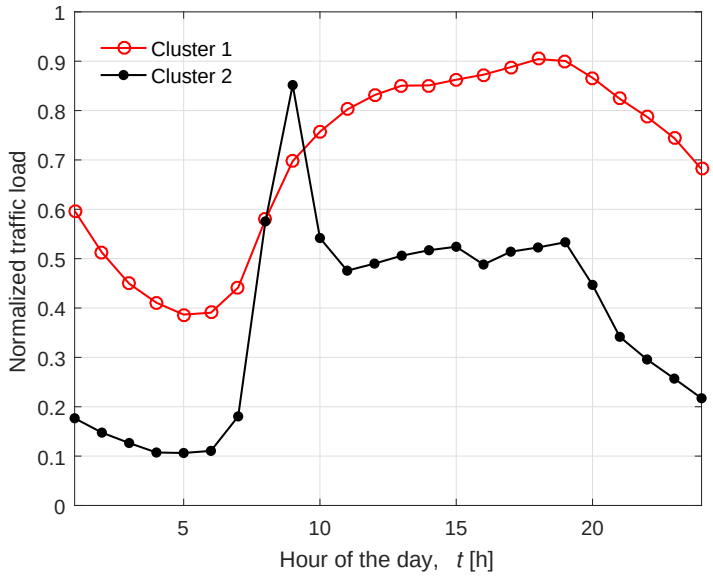

Figure 4.3: Load pattern profiles (two classes).

respectively termed the *upper*, *reference* and *lower* energy threshold, with $0 < B_{\text{low}} < B_{\text{ref}} < B_{\text{up}} < B_{\max}$. $B_{\max}$ is the EB capacity, B_{ref} is the desired (reference) EB level and B_{low} is the lowest energy level that any BS should ever reach. B_{up} is used in the energy purchase process from the power grid, as detailed shortly below. For an *offgrid* BS, i.e., $n \in \mathcal{S}_{\text{off}}$, if t is the current time slot, $B_n(t)$ is the EB level at the beginning of time slot t, which is updated at the beginning of the next time slot $t+1$ as:

$$B_n(t+1) = \xi_n(t)(B_n(t) + H_n(t) - O_n(t) + T_n(t)) \,, \tag{4.1}$$

where $T_n(t)$ is the amount of energy transferred to/from BS n in time slot t, which is positive if BS n is a consumer or negative if BS n acts as an energy source. In fact, for a source we have $T_n(t) < 0$, as this models the outflow energy, i.e., the energy that the BS transfers, which is drained from its energy buffer, while for a consumer we use $T_n(t) > 0$, as this models inflow energy, i.e., the new energy that is injected into the buffer. $H_n(t)$, $O_n(t)$ are the amount of energy harvested and the energy that is locally drained (to support the local data traffic), respectively. Finally, $\xi_n(t)$ represents the losses in the EB due to charging and discharging. It depends upon the current state of charge of the EB, which is a realistic assumption. For example, using the model in [121], we have:

$$\xi_n(t) = 1 - \frac{(B_n(t) - B_{\max}/2)^2}{\beta_{\text{loss}}(B_{\max}/2)^2} \,, \tag{4.2}$$

where $\beta_{\text{loss}} > 1$ is a constant depending upon the technology in use. Note that, as β_{loss} increases, the storage losses decrease, whereas $\beta_{\text{loss}} \to \infty$ models an ideal battery.

The EB level of an *ongrid* BS $n \in \mathcal{S}_{\text{on}}$ is updated as:

$$B_n(t+1) = \xi_n(t)(B_n(t) + H_n(t) - O_n(t) + T_n(t) + \theta_n(t)) \,, \tag{4.3}$$

where $\theta_n(t) \geq 0$ represents the energy purchased by BS n from the power grid during time slot t. The behavior of a BS (i.e., $T_n(t)$ and $\theta_n(t)$) depends on its EB level. If the BS behaves as an *energy source*, it is eligible for transferring a certain amount of energy $T_n(t)$ to other BSs. In this work, we assume that if the total energy in the buffer at the beginning of the current time slot t is $B_n(t) < B_{\text{up}}$ and the BS n is ongrid, then the difference $\theta_n(t) = B_{\text{up}} - B_n(t)$ is purchased from the power grid in slot t, as an ongrid BS should always be a source, i.e., in the position of transferring energy to other BSs. If instead the BS behaves as an *energy consumer*, it demands energy from the sources. For example, the energy demand in time slot t may be set to $B_{\text{ref}} - B_n(t)$, so that the EB level would ideally become no smaller than the reference threshold B_{ref} by the end of the current time slot t. Note that, this can only be strictly guaranteed if $H_n(t) - O_n(t) \geq 0$. However, $B_n(t)$ is updated at the beginning of time slot t, whereas $H_n(t)$ and $O_n(t)$ are only known by the end of it. To cope with this, the theory of Sections 4.4.2 and 4.4.3 computes $T_n(t)$ accounting for the expected behavior $\mathbb{E}[H_n(t) - O_n(t)]$, where $\mathbb{E}[\cdot]$ is the expectation operator.

4.4. Optimization Framework

An optimal energy transfer is sought as follows. At time t, let i and j respectively be an energy source ($T_i(t) < 0$) and a consumer ($T_j(t) > 0$). $|T_i(t)|$ is the amount of energy that source i offers to the other BSs and with $T_i^j(t) > 0$ we indicate the amount of energy that i transfers to j in time slot t, we must have $T_i(t) + \sum_{j \neq i} T_i^j(t) = 0$, $\forall i$, where $T_i^j(t) = -T_j^i(t)$, $\forall i, j$, and $T_i^i(t) = 0$, $\forall i$. Once i and j are selected, the energy routing path is unique, which descends from the PPG network model, and we refer to $a_{ij} \in [0, 1]$ as the energy loss coefficient between i and j, which depends on the routing path (number of hops and their length). Due to routing losses, the energy received at node j is $T_i^j(t)a_{ij}$. A first objective function $f_1(t)$ weighs the energy losses incurred in the energy exchange:

$$f_1(t) = \sum_{i,j \in \mathcal{S}} (T_i^j(t) - T_i^j(t)a_{ij})^2 \,. \tag{4.4}$$

The second objective is to transfer energy among BSs such that all EB levels are kept as close as possible to B_{ref}, at all times. This is evaluated through a second objective function [2]:

$$f_2(t) = \sum_{n \in \mathcal{S}} (B_n(t) - B_{\text{ref}})^2 \,. \tag{4.5}$$

With π we indicate an energy transfer policy, which specifies $T_i^j(t)$, $\forall\, i, j \in \mathcal{S}$, $t \geq 0$. An optimal

[2] B_{ref} can be made BS specific without requiring any changes in the following analysis.

policy π^* is found as:

$$\begin{aligned}
&\pi^* = \underset{\pi}{\operatorname{argmin}} \left\{ \lim_{\tau \to +\infty} \frac{1}{\tau} E \left[\sum_{t=0}^{\tau-1} (\zeta f_1(t) + (1-\zeta) f_2(t)) \right] \right\} , \\
&\textbf{Subject to:} \\
&T_i^j(t) = -T_j^i(t) \,, \forall i, j \in \mathcal{S} \,, \forall t \,, \\
&B_i(t) - B_{\max} \leq \sum_{j \in \mathcal{S}} T_i^j(t) \leq B_i(t) \,, \forall i \in \mathcal{S} \,, \forall t \,, \\
&\text{if } i \in \mathcal{S}_{\text{on}}, B_i(t) \text{ obeys Eq. (4.1)}, \forall t \,, \\
&\text{if } i \in \mathcal{S}_{\text{off}}, B_i(t) \text{ obeys Eq. (4.3)}, \forall t \,.
\end{aligned} \tag{4.6}$$

In Eq. (4.6), the two objectives are combined through weight $\zeta \in [0, 1]$ and the expectation is needed as harvested energy and traffic load are random processes. $\sum_{j \in \mathcal{S}} T_i^j(t)$ is the net flow for node i, which can either be positive or negative and the corresponding bounds have to be enforced accordingly. In real settings, optimally solving Eq. (4.6) is difficult, as energy and load statistics are non-stationary. A possible approach consists of modeling the problem as a sequence of stationary dynamics of the environment, using a dedicate Markov Decision Process (MDP) for each, and detecting the change points [122]. While of theoretical value, such approaches are still preliminary and impractical. Next, we develop an online approach based on MPC, with tracking capabilities over a finite time horizon, whose objective is to approximate π^*.

4.4.1. Overview of the Online Optimization Framework

A diagram of the optimization process is shown in Fig. 4.2, involving the following steps:

1. **Pattern learning (Section 4.4.2):** The harvested energy and traffic load processes are statistically modeled through Bayesian non-parametric tools. This allows each BS to *independently* track its own harvested energy and load processes, capturing their statistical behavior and obtaining multi-step ahead forecasts. These forecasts are then fed into the MPC optimization approach of Section 4.4.3.

2. **Model predictive control (Section 4.4.3):** The goal of the MPC block is to determine the BS role (source/consumer) and obtain $T_n(t)$, for all BSs n and t. The MPC block considers the current system state, i.e., traffic load, harvested energy and EB levels, but also future ones (based on the forecasts from MPC).

3. **Energy allocation (Section 4.4.4):** A convex optimization problem is formulated to assess how the available energy $|T_i(t)|$ from the sources i is to be split among the consumers j in time slot t, these energy shares are referred to as $T_i^j(t)$.

4. **Energy routing (Section 4.4.5):** For every time t, once the energy allocations $T_i^j(t)$ are obtained, this block finds a feasible and optimal schedule implementing the required energy transfers (energy routing) from sources to consumers. Since the PPG is operated in a TDM fashion, each power link can only be used for a single energy transfer operation at a time. Thus, routes must be allocated so that they do not overlap in time.

We remark that, solving MPC (step 2) and the following energy allocation (step 3) as two separate steps provides an approximation to the combined objective $\zeta f_1(t) + (1-\zeta) f_2(t)$. On the other hand, energy allocation (step 3) and routing (step 4) can be executed as two separate optimization problems without incurring any inter-dependency as long as, for any optimal solution for the first problem, the number of slots needed to schedule the involved energy routing paths is smaller than the maximum number of slots that the system can devote to the energy transfer. In this case, separability holds for the energy allocation and routing problems. With the system parameters that we use in this chapter (see Table 4.2), this holds when the number of BSs is $n_s \leq 48$.

4.4.2. Pattern Learning

In this section, we present statistical models to automatically capture the hidden structure in harvested energy and load processes. GPs have become popular for regression and classification, often showing impressive performance [123]. Hereinafter, we will focus on GPs for regression, according to the function-space view applied to the Bayesian linear model [123]. The Bayesian linear model for regression is defined as:

$$f(\boldsymbol{x}) = \phi(\boldsymbol{x})^\top \boldsymbol{w}, \quad r = f(\boldsymbol{x}) + \epsilon, \tag{4.7}$$

where $\boldsymbol{w}$ is a vector of weights, also known as model parameters, $f(\boldsymbol{x})$ is the function value, which is linear in the weights $\boldsymbol{w}$, r is the observed real value, and $\phi(\cdot) : \mathbb{R}^D \to \mathbb{R}^F$ maps the D-dimensional input column vector $\boldsymbol{x}$ into an F-dimensional feature vector $\phi(\boldsymbol{x}) = \boldsymbol{\phi}$. Assume we are given with a training dataset with N observations, $\mathcal{D} = \{(\boldsymbol{x}_i, r_i)\}_{i=1}^N$, where each pair $(\boldsymbol{x}_i, r_i)$ consists of the D-dimensional input column vector $\boldsymbol{x}_i$ and the scalar target r_i. We can aggregate inputs and targets in a $D \times N$ matrix $\boldsymbol{X}$ and an N-dimensional column vector $\boldsymbol{r}$, so that $\mathcal{D} = (\boldsymbol{X}, \boldsymbol{r})$, and $\phi(\boldsymbol{X}) = \boldsymbol{\Phi}$ becomes an $F \times N$ matrix in the feature space. We are interested in the conditional distribution of the targets, given the inputs in the feature space and the model parameters. We further assume that r differs from $f(\boldsymbol{x})$ by additive noise, which follows an independent identically distributed (i.i.d.) Gaussian distribution with zero mean and variance σ_n^2, i.e., $\epsilon \sim \mathcal{N}(0, \sigma_n^2)$. From the i.i.d. assumption, it follows that the *likelihood* (i.e., the conditional distribution of the targets given the inputs in the feature space and the model parameters) is factorized over cases for the N observations, i.e., $\boldsymbol{r}|\boldsymbol{X}, \boldsymbol{w} \sim \mathcal{N}(\boldsymbol{\Phi}^\top \boldsymbol{w}, \sigma_n^2 \boldsymbol{I}_N)$.

We can perform regression in the function-space view by using a Gaussian Process (GP), modeling a distribution over functions. Formally: a GP is a collection of random variables, any finite number of which have a joint Gaussian distribution. Moreover, it is completely specified by the mean function and the *covariance function* (or *kernel*). We define the mean function and the *covariance function* of process $f(\cdot) \sim \mathcal{GP}(m(\boldsymbol{x}), k(\boldsymbol{x}, \widehat{\boldsymbol{x}}))$ as

$$\begin{aligned} m(\boldsymbol{x}) &= \mathbb{E}[f(\boldsymbol{x})] \\ k(\boldsymbol{x}, \widehat{\boldsymbol{x}}) &= \mathbb{E}[(f(\boldsymbol{x}) - m(\boldsymbol{x}))(f(\widehat{\boldsymbol{x}}) - m(\widehat{\boldsymbol{x}}))^\top]. \end{aligned} \tag{4.8}$$

Next, we consider the zero mean function, i.e., $m(\boldsymbol{x}) = 0$, which is a very typical choice [123]. In the Bayesian linear model of Eq. (4.7), the *prior* distribution is set to be Gaussian with zero

mean and covariance matrix $\boldsymbol{\Sigma}_w$, i.e., $\boldsymbol{w} \sim \mathcal{N}(\mathbf{0}, \boldsymbol{\Sigma}_w)$. Thus, we can derive an example GP as:

$$\begin{aligned} m(\boldsymbol{x}) &= \phi(\boldsymbol{x})^\top \mathbb{E}[\boldsymbol{w}] = \mathbf{0} \\ k(\boldsymbol{x}, \widehat{\boldsymbol{x}}) &= \phi(\boldsymbol{x})^\top \mathbb{E}[\boldsymbol{w}\boldsymbol{w}^\top]\phi(\widehat{\boldsymbol{x}}) = \phi(\boldsymbol{x})^\top \boldsymbol{\Sigma}_w \phi(\widehat{\boldsymbol{x}}). \end{aligned} \tag{4.9}$$

Assume the training dataset has N observations, then vector $\boldsymbol{f} = [f(\boldsymbol{x}_1), \ldots, f(\boldsymbol{x}_N)]^\top$ has a joint Gaussian distribution, i.e., $\boldsymbol{f}|\boldsymbol{X} \sim \mathcal{N}(\mathbf{0}, \boldsymbol{K})$, where the $N \times N$ covariance matrix $\boldsymbol{K}$ can be computed evaluating the *covariance function* or *kernel* for the N observations, i.e., $\boldsymbol{K}_{ij} = \phi(\boldsymbol{x}_i)^\top \boldsymbol{\Sigma}_w \phi(\boldsymbol{x}_j)$ for $i, j = 1, \ldots, N$. Given the noise $\epsilon \sim \mathcal{N}(0, \sigma_n^2)$, it follows from the i.i.d. assumption that a diagonal matrix $\sigma_n^2 \boldsymbol{I}_N$ must be added to $\boldsymbol{K}$, as compared to the noise-free model in the GP literature [123]. To make prediction for the test case $f(\boldsymbol{x}_*) = f_*$ given $\phi(\boldsymbol{x}_*) = \boldsymbol{\phi}_*$, we consider the joint Gaussian *prior* distribution over functions

$$\begin{bmatrix} \boldsymbol{r} \\ f_* \end{bmatrix} = \mathcal{N}\left(\mathbf{0}, \begin{bmatrix} \boldsymbol{K} + \sigma_n^2 \boldsymbol{I}_N & \boldsymbol{k}_* \\ \boldsymbol{k}_*^\top & k(\boldsymbol{x}_*, \boldsymbol{x}_*) \end{bmatrix}\right), \tag{4.10}$$

where we define the N-dimensional column vector $\boldsymbol{k}_*$ such that the i-th element equals $\phi(\boldsymbol{x}_i)^\top \boldsymbol{\Sigma}_w \phi(\boldsymbol{x}_*)$. To derive the *posterior* distribution over functions we need to condition the joint Gaussian *prior* distribution over functions on the data, so that we get the key predictive equations of GPs for regression:

$$\begin{aligned} & f_* | \boldsymbol{x}_*, \boldsymbol{X}, \boldsymbol{r} \sim \mathcal{N}(\mu, \Sigma) \\ & \mu = \boldsymbol{k}_*^\top [\boldsymbol{K} + \sigma_n^2 \boldsymbol{I}_N]^{-1} \boldsymbol{r} \\ & \Sigma = k(\boldsymbol{x}_*, \boldsymbol{x}_*) - \boldsymbol{k}_*^\top [\boldsymbol{K} + \sigma_n^2 \boldsymbol{I}_N]^{-1} \boldsymbol{k}_*. \end{aligned} \tag{4.11}$$

In practice, the predictive mean μ is used as a point estimate for the function output, while the variance Σ can be translated into uncertainty bounds (predictive error-bars) on this point estimate, thus making GPs for regression very appealing for MPC applications (see [109, 124, 125]).

For any set of basis functions in the feature space, we can compute the corresponding *covariance function* or *kernel*; conversely, for every (positive definite) *covariance function* or *kernel*, there exists a (possibly infinite) expansion in terms of basis functions in the feature space. As we show shortly, the choice of the kernel deeply affects the performance of a GP for a given task, as much as the choice of the parameters (architecture, activation functions, learning rate, etc.) does for a neural network. Specifically, the *hyperparameters* of the kernel must be set in order to optimize the *marginal likelihood*,

$$p(\boldsymbol{r}|\boldsymbol{X}) = \int p(\boldsymbol{r}|\boldsymbol{f}, \boldsymbol{X}) p(\boldsymbol{f}|\boldsymbol{X}) d\boldsymbol{f}. \tag{4.12}$$

Under the Gaussian assumption, the *prior* distribution is Gaussian, $\boldsymbol{f}|\boldsymbol{X} \sim \mathcal{N}(\mathbf{0}, \boldsymbol{K})$, and the *likelihood* is a factorized Gaussian, $\boldsymbol{r}|\boldsymbol{f}, \boldsymbol{X} \sim \mathcal{N}(\boldsymbol{f}, \sigma_n^2 \boldsymbol{I}_N)$, thus $\boldsymbol{r}|\boldsymbol{X} \sim \mathcal{N}(\mathbf{0}, \boldsymbol{K} + \sigma_n^2 \boldsymbol{I}_N)$. Extensive derivation for the formulation of $f_*|\boldsymbol{x}_*, \boldsymbol{X}, \boldsymbol{r}$ and generalization to more that one test case can be found in [123].

Suppose we have N_* observations in the test set, i.e., $(\boldsymbol{X}_*, \boldsymbol{r}_*)$, to make prediction for the test cases $f(\boldsymbol{X}_*) = \boldsymbol{f}_*$ given $\phi(\boldsymbol{X}_*) = \boldsymbol{\Phi}_*$, we consider the joint Gaussian *prior* distribution over functions

$$\begin{bmatrix} \boldsymbol{r} \\ \boldsymbol{f}_* \end{bmatrix} = \mathcal{N}\left(\mathbf{0}, \begin{bmatrix} \boldsymbol{K} + \sigma_n^2 \boldsymbol{I}_N & \boldsymbol{K}_* \\ \boldsymbol{K}_*^\top & \boldsymbol{K}_{**} \end{bmatrix}\right), \tag{4.13}$$

where we define the $N \times N_*$ matrix $\boldsymbol{K}_*$ similarly to $\boldsymbol{k}_*$, such that $\boldsymbol{K}_{*,ij} = \phi(\boldsymbol{x}_i)^\top \boldsymbol{\Sigma}_w \phi(\boldsymbol{x}_{*,j})$ for $i = 1, \ldots, N$, $j = 1, \ldots, N_*$, and $\boldsymbol{x}_{*,j}$ is a column vector in $\boldsymbol{X}_*$. Finally, we define the $N_* \times N_*$ matrix $\boldsymbol{K}_{**}$ similarly to $k(\boldsymbol{x}_*, \boldsymbol{x}_*)$, such that $\boldsymbol{K}_{**,ij} = \phi(\boldsymbol{x}_{*,i})^\top \boldsymbol{\Sigma}_w \phi(\boldsymbol{x}_{*,j})$ for $i, j = 1, \ldots, N_*$, thus we get the key predictive equations of GPs for regression:

$$\begin{aligned} \boldsymbol{f}_* | \boldsymbol{X}_*, \boldsymbol{X}, \boldsymbol{r} &\sim \mathcal{N}(\boldsymbol{\mu}, \boldsymbol{\Sigma}) \\ \boldsymbol{\mu} &= \boldsymbol{K}_*^\top [\boldsymbol{K} + \sigma_n^2 \boldsymbol{I}_I]^{-1} \boldsymbol{r} \\ \boldsymbol{\Sigma} &= \boldsymbol{K}_{**} - \boldsymbol{K}_*^\top [\boldsymbol{K} + \sigma_n^2 \boldsymbol{I}_I]^{-1} \boldsymbol{K}_*. \end{aligned} \tag{4.14}$$

The choice of the kernel: This choice deeply affects the performance of a GP for a given task, as it encodes the similarity between pairs of outputs in the function domain. There has been significant work on constructing base and composite kernels [126]. Common base kernels include the Squared Exponential (SE) kernel, the Rational Quadratic (RQ) kernel, and the Standard Periodic (SP) kernel, defined as:

$$\begin{aligned} k_{\text{SE}}(\boldsymbol{x}, \widehat{\boldsymbol{x}}) &= \sigma_{\text{SE}}^2 \exp(-||\boldsymbol{x} - \widehat{\boldsymbol{x}}||^2/(2\ell_{\text{SE}}^2)) \\ k_{\text{RQ}}(\boldsymbol{x}, \widehat{\boldsymbol{x}}) &= \sigma_{\text{RQ}}^2 (1 + ||\boldsymbol{x} - \widehat{\boldsymbol{x}}||^2/(2\alpha_{\text{RQ}}\ell_{\text{RQ}}^2))^{-\alpha_{\text{RQ}}} \\ k_{\text{SP}}(\boldsymbol{x}, \widehat{\boldsymbol{x}}) &= \sigma_{\text{SP}}^2 \exp(-2\sin^2(\pi||\boldsymbol{x} - \widehat{\boldsymbol{x}}||\text{p}_{\text{SP}})/\ell_{\text{SP}}^2). \end{aligned} \tag{4.15}$$

The properties of the functions under a GP with a SE kernel can display long range trends, where the length-scale ℓ_{SE} determines how quickly a process varies with the inputs. The RQ kernel is derived as a scale mixture of SE kernels with different length-scales. The SP kernel is derived by mapping the two dimensional variable $(\cos(\boldsymbol{x}); \sin(\boldsymbol{x}))$ through the SE kernel. Derivations for the RQ and SP kernels are in [123].

Note that valid kernels (i.e., those having a positive-definite covariance function) are closed under the operators $+$ and $\times$. This allows one to create more representative (and composite) kernels from well-understood basic components, according to the following key rules [126]:

- Any subexpression[3] $\mathcal{P}$ can be replaced with $\mathcal{P} + \mathcal{B}$, where $\mathcal{B}$ is any base kernel family.
- Any subexpression $\mathcal{P}$ can be replaced with $\mathcal{P} \times \mathcal{B}$, where $\mathcal{B}$ is any base kernel family.
- Any base kernel $\mathcal{B}$ can be replaced with any other base kernel family $\mathcal{B}'$.

In time series, summing kernels can express superpositions of different processes, operating at different scales, whereas multiplying kernels may be a way of converting global data properties onto local data properties. From here on, we will use one-dimensional kernels in the form RQ $\times$ SP with period p_{SP}, which correspond to a local quasi-periodic structure in the data, with noise operating at different scales. Note that kernels over multidimensional inputs can be constructed via the operators $+$ and $\times$ over individual dimensions. Next, we consider models based on zero-mean GPs for the runtime multi-step ahead forecasting of time series, with application to a) Harvested Energy Profile $H_n(t)$ (defined in Section 4.3.2) and b) Traffic Load $L_n(t)$ (Section 4.3.3).

[3]Subexpression refers to any valid kernel family, either basic or composite.

The basic routine for prediction: We use models based on zero-mean GPs for the runtime forecasting of time series, with application to $H_n(t)$ and $L_n(t)$, $n \in \{1, \ldots, n_s\}$, $t = 1, \ldots, T$. The strong daily seasonality of the data is evident for both time series, as well as the presence of noise at different scales. Therefore, we define composite kernels for $H_n(t)$ and $L_n(t)$ in the form RQ $\times$ SP with period $\mathrm{p_{SP}}$, i.e.,

$$\begin{aligned} k(x, \widehat{x}) =& \sigma^2 \exp(-2 \sin^2(\pi d \mathrm{p_{SP}})/\ell_{\mathrm{SP}}^2) \\ & \times (1 + d^2/(2\alpha_{\mathrm{RQ}} \ell_{\mathrm{RQ}}^2))^{-\alpha_{\mathrm{RQ}}} \end{aligned} \tag{4.16}$$

where $\sigma = \sigma_{\mathrm{RQ}} \sigma_{\mathrm{SP}}$ and $d = |x - \widehat{x}|$ is the Euclidean distance between inputs. At this point, the *hyperparameters* of the kernel must be set in order to optimize the *marginal likelihood*, which is defined in Eq. (4.12), and here implemented using the toolbox of [127]. For compactness, we aggregate the *hyperparameters* of the kernel in the initialization set $\boldsymbol{\theta}^{(s)} = \{\sigma, \mathrm{p_{SP}}, \ell_{\mathrm{SP}}, \alpha_{\mathrm{RQ}}, \ell_{\mathrm{RQ}}\}$. Here, we opt for $\sigma = 1$, $\mathrm{p_{SP}} = 24$, and select the free parameters (ℓ_{SP}, α_{RQ}, ℓ_{RQ}) via a grid search, scanning combinations in the range $[10^{-2}, 10^2]$. To model the strong daily seasonality in the data, we also opt for a prior distribution on the period $\mathrm{p_{SP}}$, which is a delta function, i.e., $\delta(\mathrm{p_{SP}} - 24) = 1$ if and only if $\mathrm{p_{SP}} = 24$, so that we treat the period $\mathrm{p_{SP}}$ as a constant, excluding it from the optimization (see [127]).[4]

Algorithm 1 Pseudo-code for the basic routine

1: Pre-training phase: find the optimal *hyperparameters* $\boldsymbol{\theta}^{(0)}$ for the kernel $k(\cdot, \cdot)$, starting from $\boldsymbol{\theta}^{(s)}$ and minimizing the *marginal likelihood* on the training dataset $\{(\boldsymbol{x}_i, r_i)\}_{i=1}^{N}$
2: Set $t = 1$
3: **while** $t \leq T - (N + N_*)$ **do**
4: Set $\mathcal{D}^{(t)} = (\boldsymbol{X}^{(t)}, \boldsymbol{r}^{(t)}) = \{(\boldsymbol{x}_i, r_i)\}_{i=t-1+1}^{t-1+N}$
5: Set $\mathcal{D}_*^{(t)} = (\boldsymbol{X}_*^{(t)}, \boldsymbol{r}_*^{(t)}) = \{(\boldsymbol{x}_i, r_i)\}_{i=t-1+N+1}^{t-1+N+N_*}$
6: **if** $(t - 1 \mod S) = 0$ **then** % $t - 1$ is a multiple of S
7: Training phase: find the optimal *hyperparameters* $\boldsymbol{\theta}^{(t)}$ for the kernel $k(\cdot, \cdot)$, starting from $\boldsymbol{\theta}^{(0)}$ and minimizing the *marginal likelihood* on the training dataset $(\boldsymbol{X}^{(t)}, \boldsymbol{r}^{(t)})$
8: **end if**
9: Forecasting phase: get $(\boldsymbol{\mu}, \boldsymbol{\Sigma})$ with test set $(\boldsymbol{X}_*^{(t)}, \boldsymbol{r}_*^{(t)})$ and using the key predictive equations of GPs in Eq. (4.14)
10: Compute $\mathrm{RMSE}_*^{(t)} = \sqrt{(\sum_{i=1}^{N_*} e_i^2)/N_*}$, $\boldsymbol{e} = \boldsymbol{r}_*^{(t)} - \boldsymbol{\mu}$
11: Set $t = t + 1$
12: **end while**

Algorithm 1 describes the basic routine for the pre-training phase (line 1), training phase (line 7), and forecasting phase (line 9) for both zero-mean GPs, i.e., the same basic reasoning holds for $H_n(t)$ and $L_n(t)$, where $\boldsymbol{x}_t$ contains the time indices (in either the training or test dataset) and r_t refers to either process $H_n(t)$ or $L_n(t)$, at time t and BS n. Also, we assume that we can access the N values in the training dataset, and we wish to predict the N_* values in the

[4] In our numerical results, we have considered a time step duration of one hour, so setting $\mathrm{p_{SP}} = 24$ entails a periodicity of one day.

test set, where $\mathcal{D}^{(t)} = (\boldsymbol{X}^{(t)}, \boldsymbol{r}^{(t)})$ refers to the training dataset and $\mathcal{D}_*^{(t)} = (\boldsymbol{X}_*^{(t)}, \boldsymbol{r}_*^{(t)})$ refers to the test set, at time t, respectively. According to the pre-training phase, we first have to find the optimal *hyperparameters* $\boldsymbol{\theta}^{(0)}$ for the kernel $k(\cdot,\cdot)$, starting from $\boldsymbol{\theta}^{(s)}$ and minimizing the *marginal likelihood* on the training dataset $\{(\boldsymbol{x}_i, r_i)\}_{i=1}^N$. Note that $\boldsymbol{\theta}^{(0)}$ will serve as initialization for the optimal *hyperparameters* $\boldsymbol{\theta}^{(t)}$ at each step of the online forecasting routine, as the optimal *hyperparameters* $\boldsymbol{\theta}^{(t)}$ are found over the training dataset $(\boldsymbol{X}^{(t)}, \boldsymbol{r}^{(t)})$, which changes at each step of the online forecasting routine. Assuming Gaussian noise with variance σ_n^2, thus Gaussian likelihood, it follows that we can perform exact inference. To do it, we use the Conjugate Gradients (CG) optimization tool implemented in toolbox [127]. We get $(\boldsymbol{\mu}, \boldsymbol{\Sigma})$ via Eq. (4.14) given the test set $(\boldsymbol{X}_*^{(t)}, \boldsymbol{r}_*^{(t)})$ with N_* test cases, at time t. Finally, we derive the Root Mean Square Error (RMSE) $\text{RMSE}_*^{(t)}$ over the N_* test cases, starting from residuals $\boldsymbol{e}$, at time t, and iterating the procedure (except for the pre-training phase) up to time $T-(N+N_*)$. For the numerical results, the training phase (line 7) is performed once every S steps: in Algorithm 1, we write $(t-1 \mod S) = 0$, i.e., $t-1$ is a multiple of S. Thus, the training phase (line 7) is performed when $t = 1$.

4.4.3. Model Predictive Control

The system to be controlled is described by means of a discrete-time model:

$$\boldsymbol{B}(t+1) = \boldsymbol{\xi}(t) \circ (\boldsymbol{B}(t) + \boldsymbol{T}(t) + \boldsymbol{W}(t) + \boldsymbol{\theta}(t)), \tag{4.17}$$

where t is the current time slot and $\circ$ is the element-wise matrix product. All matrices $\boldsymbol{\xi}, \boldsymbol{B}, \boldsymbol{T}, \boldsymbol{W}, \boldsymbol{\theta}$ have size $M \times n_s$. $\boldsymbol{B}(t)$ has elements $[\boldsymbol{B}(t)]_{k,n} = B_n(k)$ (the *system state*), representing the energy buffer level for BS n in time slot k, with $k = t, t+1, \ldots, t+M-1$, were M is the *optimization horizon*. $\boldsymbol{\xi}$ accounts for EB losses, whose n-th column is $[\xi_n(t), \xi_n(t+1), \ldots, \xi_n(t+M-1)]^T$. Note that the system state in the first time slot t is known, whereas those in the following $M-1$ time slots have to be estimated. Referring to Section 4.4.2, we thus have $M = N_*+1$. Matrix $\boldsymbol{T}(t)$ with elements $[\boldsymbol{T}(t)]_{k,n} = T_n(k)$ denotes the *control* matrix, representing the amount of energy that each BS n shall either transfer (if $T_n(k) < 0$) or receive ($T_n(k) > 0$) in time slot $k = t, \ldots, t+M-1$. $\boldsymbol{\theta}$ has elements $[\boldsymbol{\theta}(t)]_{k,n} = \theta_n(k)$, which can be greater than zero only for ongrid BSs. Matrix $\boldsymbol{W}(t)$, with elements $[\boldsymbol{W}(t)]_{k,n} = H_n(k) - O_n(k)$, models the effective energy income, i.e., the stochastic behavior of the forecast profiles (harvested and consumed energy), with:

$$\boldsymbol{W}(t) \sim \mathcal{N}(\overline{\boldsymbol{W}}(t), \Sigma_{\boldsymbol{W}(t)}), \tag{4.18}$$

where $\overline{\boldsymbol{W}}(t)$ and $\Sigma_{\boldsymbol{W}(t)}$ contain the mean and variance of the forecast estimates, respectively. Note that processes $H_n(k)$ and $O_n(k)$ are statistically characterized through the prediction framework of Section 4.4.2, and their difference is still a Gaussian r.v. (in fact, $O_n(k)$ is derived from $L_n(k)$ through a linear model, and as such is still Gaussian distributed). Following [128], due to the stochastic nature of Eq. (4.18), the system state $\boldsymbol{B}(t)$ can also be written in a probabilistic way:

$$\boldsymbol{B}(t) \sim \mathcal{N}(\bar{\boldsymbol{B}}(t), \Sigma_{\boldsymbol{B}(t)}), \tag{4.19}$$

where $\bar{\boldsymbol{B}}(t)$ and $\Sigma_{\boldsymbol{B}(t)}$ are the mean and the variance of $\boldsymbol{B}(t)$, respectively.

Objective functions: The goal of the MPC controller is to determine the amount $T_n(k)$ that each BS n should either transfer or receive in time slots $k = t, \ldots, t+M-1$, so that all the energy buffers remain as close as possible to the reference value B_{ref}. A first quadratic cost function tracks the total amount of energy that is to be exchanged among BSs in time slot k, with $k = t, \ldots, t+M-1$:

$$f_1^{\text{MPC}}(\boldsymbol{T}(k)) = \sum_{n \in \mathcal{S}} T_n(k)^2. \tag{4.20}$$

Through a second objective function, $f_2^{\text{MPC}}(\cdot)$, the MPC controller seeks to equalize the BS energy buffer levels as close as possible to the reference threshold B_{ref} (see Section 4.3.4):

$$f_2^{\text{MPC}}(\boldsymbol{B}(k)) = \sum_{n \in \mathcal{S}} (B_n(k) - B_{\text{ref}})^2. \tag{4.21}$$

Control problem: The following finite-horizon and multi-objective optimization problem is formulated:

$$\min_{\boldsymbol{T}(t)} \quad \frac{1}{M}\mathbb{E}\left[\sum_{k=t}^{t+M-1}\left(\alpha f_1^{\text{MPC}}(\boldsymbol{T}(k)) + \alpha^c f_2^{\text{MPC}}(\boldsymbol{B}(k))\right)\right] \tag{4.22a}$$

$$\text{subject to:} \quad \boldsymbol{B}(t) \sim \mathcal{N}(\bar{\boldsymbol{B}}(t), \Sigma_{\boldsymbol{B}(t)}), \tag{4.22b}$$

$$\boldsymbol{W}(t) \sim \mathcal{N}(\overline{\boldsymbol{W}}(t), \Sigma_{\boldsymbol{W}(t)}), \tag{4.22c}$$

$$B_{\text{low}} \leq B_n(k) \leq B_{\text{max}}, \tag{4.22d}$$

$$T_n(k)_{\text{min}} \leq T_n(k) \leq T_n(k)_{\text{max}}, \tag{4.22e}$$

$$\text{with: } k = t, t+1, \ldots, t+M-1$$

where $\alpha \in [0, 1]$ is a weight to balance the relative importance of the two cost functions and $\alpha^c = 1 - \alpha$. B_{low} and B_{max} are the energy buffer limitations defined in Section 4.3.4, constraint Eq. (4.22e) defines the amount of energy that each BS $n \in \mathcal{S}$ can exchange in slot k and depends on the system state, i.e., the energy buffer level $B_n(k)$, the expected harvested energy and expected traffic load: the system state defines the limits of the control action for each k. Note that $f_1^{\text{MPC}}(\cdot)$ (Eq. (4.20)) differs from Eq. (4.4) in that the energy losses due to the routing are not considered; this makes it possible to decouple energy allocation and routing problems. Instead, $f_2^{\text{MPC}}(\cdot)$ (Eq. (4.21)) and Eq. (4.5) track the same exact cost, with the only difference that the time horizon M in Eq. (4.22) is finite. Hence, Eq. (4.22) departs from a global optimal solution in two respects: **1)** the number of optimization steps M is finite (the optimality gap is expected to be small for increasing M), **2)** $f_1(\cdot)$ is upper bounded by neglecting the energy routing losses, which allows for a fast and efficient solution through a decomposition of energy allocation and routing.

For any fixed value of α, and since the optimization problem must be solved at runtime, it is strongly preferable to choose a convex optimization formulation such as Eq. (4.22), which can be solved through standard techniques. Here, we have used the `CVX` tool [129] to obtain the optimal solution $\boldsymbol{T}(t)^* = [T_n(k)^*]$, which represents the amount of energy that BS $n \in \mathcal{S}$ shall either offer or demand in time slot $k = t, \ldots, t+M-1$.

Optimization algorithm: The MPC controller performs as follows [130]:

1. **Step 1:** At the beginning of time slot k, the system state is obtained, that is energy buffer levels for all BSs, the harvested energy and traffic load forecasts for the next M time slots (the optimization horizon).
2. **Step 2:** The control problem in Eq. (4.22) is solved yielding a sequence of control actions over the horizon M.
3. **Step 3:** Only the first control action is performed and the system state is updated upon implementing the required energy transfers.
4. **Step 4:** Forecasts are updated and the optimization cycle is repeated from **Step 1**.

4.4.4. Energy Allocation

Solving Eq. (4.22), we obtain $T_n(t)$ for each BS n in any given slot t. In this section, we solve the energy allocation problem, i.e., we compute for each source n, how to split $T_n(t)$ among the consumers. Note that this also depends on the distribution losses between sources and consumers and, in turn, on the electrical PPG topology.

Notation: At time t, we use indices i and j to respectively denote an arbitrary BS source (set $\mathcal{Y}_s$) and an arbitrary BS consumer (set $\mathcal{Y}_c$). g_{ij} is the number of hops in the PPG topology between source $i \in \mathcal{Y}_s$ and consumer $j \in \mathcal{Y}_c$, in matrix notation $\boldsymbol{G} = [g_{ij}]$. We assume that all hops have the same physical length and $a_{ij} = \varphi(g_{ij}) \in [0, 1]$ is the energy loss attenuation coefficient between i and j and $\varphi(\cdot)$ is a suitable loss function (depending on the number of hops, i.e., on the physical distance that the energy has to travel, see Section 4.3.1). Let i be a source, the maximum amount of energy that a consumer j can receive from i is defined as $e_{ij} \triangleq |T_i(t)|a_{ij}$, $i \in \mathcal{Y}_s, j \in \mathcal{Y}_c$. In matrix notation $\boldsymbol{E} = [e_{ij}]$. For notation compactness, we collect the energy demands from all consumers j into a demand vector $\boldsymbol{d} = [d_1, d_2, \ldots, d_{|\mathcal{Y}_c|}]$, where element $d_j \triangleq T_j(t)$ is the energy demand from consumer j.

Objective functions: As a first objective, we seek to minimize the difference between the amount of energy that the BS sources $i \in \mathcal{Y}_s$ deliver to the BS consumers $j \in \mathcal{Y}_c$ and the consumers' energy demand. The energy amount $|T_i(t)|$ can possibly be distributed among multiple consumers and we denote by $y_{ij} \in [0, 1]$ the fraction of $|T_i(t)|$ that is allocated from source i to consumer j, in matrix notation $\boldsymbol{Y} = [y_{ij}]$. The actual amount of energy that consumer j receives from i is $y_{ij}e_{ij} = y_{ij}|T_i(t)|a_{ij}$. We write a first cost function as:

$$f_1(\boldsymbol{Y}, \boldsymbol{E}, \boldsymbol{d}) = \sum_{i \in \mathcal{Y}_s} \left(\sum_{j \in \mathcal{Y}_c} y_{ij}e_{ij} - d_j \right)^2 . \tag{4.23}$$

Due to the existence of a single path between any source and consumer pair and due to the fact that each power link can only be used for a single transfer operation at a time, a desirable solution shall: i) pick source and consumer pairs (i, j) in such a way that the physical distance (g_{ij}) between them is minimized and ii) achieve the best possible match between sources and consumers, i.e.,

use source i, whose available energy is the closest to that required by consumer j, for all (i, j) pairs. Ideally, for each i we would like y_{ij} to be equal to 1 for a single value of j and zero for any other consumer (i.e., 1-of-$|\mathcal{Y}_c|$ coding scheme, where $|\mathcal{Y}_c|$ gives the number of consumers). If this is infeasible, multiple sources will supply the consumer, leading to $y_{ij} > 0$ for multiple values of j and $\sum_j y_{ij} \leq 1$. Minimizing the following cost function, amounts to minimizing the number of hops g_{ij} between sources and consumers and favoring solutions with 1-of-$|\mathcal{Y}_c|$ coding for y:

$$f_2(\boldsymbol{Y}, \boldsymbol{G}) = \sum_{i \in \mathcal{Y}_s} \left(\sum_{j \in \mathcal{Y}_c} -\exp\left(\frac{y_{ij}}{g_{ij}}\right) \right). \tag{4.24}$$

With this cost function we are looking for a sparse solution (i.e., a small number of sources with y_{ij} close to 1). Note that when $y_{ij} \to 1$ and g_{ij} is minimized, the argument y_{ij}/g_{ij} is maximized and the negative exponential is minimized. Also, the exponential function was picked as it is convex, but any increasing and convex function would do.

Solution through convex optimization: At each time slot t, each BS n updates its buffer level $B_n(t)$, using either Eq. (4.1) or Eq. (4.3) (note that $B_n(t-1)$, $H_n(t-1)$, $O_n(t-1)$, $T_n(t-1)$ and $\theta_n(t-1)$ are all known in slot t, see Section 4.3). The MPC problem of Section 4.4.3 is solved. Each source i evaluates e_{ij} for all $j \in \mathcal{Y}_c$ through $e_{ij} = |T_i(t)|a_{ij}$, and each consumer j sets its energy demand as $d_j = T_j(t)$. Hence, using Eq. (4.23) and Eq. (4.24), the following *convex* optimization problem is formulated:

$$\min_{\boldsymbol{Y}} \quad \beta f_1(\boldsymbol{Y}, \boldsymbol{E}, \boldsymbol{d}) + (1-\beta) f_2(\boldsymbol{Y}, \boldsymbol{G}) \tag{4.25a}$$

$$\text{subject to:} \quad 0 \leq y_{ij} \leq 1, \qquad \forall i \in \mathcal{Y}_s, \forall j \in \mathcal{Y}_c, \tag{4.25b}$$

$$\sum_{j \in \mathcal{Y}_c} y_{ij} \leq 1, \qquad \forall i \in \mathcal{X}_s, \tag{4.25c}$$

where $\beta \in [0, 1]$ is a weight used to balance the relative importance of the two cost functions. The first constraint represents the fact that y_{ij} is a fraction of the available energy from source i, and the second constraint encodes the fact that the total energy i that each source transfers cannot exceed its offer $|T_i(t)|$. For any fixed value of β, Eq. (4.25) is a convex minimization problem which can be solved through standard techniques. The optimal solution $\boldsymbol{Y}^* = [y^*_{ij}]$ specifies the energy fraction tat any source i must send to consumer j.

Solution as an assignment problem: At any time t, the energy distribution problem from sources to consumers can alternatively be modeled as an assignment problem, where each source $i \in \mathcal{Y}_s$ has to be *matched* with a consumer $j \in \mathcal{Y}_c$. This approach can be solved through the *Hungarian method* [131], an algorithm capable of finding an optimal assignment for a given square $m \times m$ cost matrix, where $m = \max(|\mathcal{Y}_s|, |\mathcal{Y}_c|)$. An assignment is a set of m entry positions in the cost matrix, no two of which lie in the same row or column. The sum of the m entries of an assignment is its cost. An assignment with the smallest possible cost is referred to as *optimal*. Let $\boldsymbol{C} = [c_{ij}]$ be the cost matrix, where rows and columns respectively correspond to sources i and consumers j. Hence, c_{ij} is the cost of assigning the i-th source to the j-th consumer and is obtained

as follows:

$$c_{ij} = \beta(e_{ij} - d_j)^2 + (1-\beta)\left(-\exp\left(\frac{1}{g_{ij}}\right)\right), \tag{4.26}$$

where $\beta \in [0,1]$, the first term weighs the quality of the match (d_j should be as close as possible to e_{ij}) and the second the quality of the route. To ensure the cost matrix is a square matrix, additional rows or columns are to be added when the number of sources and consumers differs. As typically assumed, each element in the added row or column is set equal to the largest number in the matrix.

The main difference between the optimal solution found by solving the convex optimization problem (Eq. (4.25)) and that found by the Hungarian method is that the latter *always* returns a one-to-one match between sources and consumers, i.e., each consumer can only be served by a single source (1-of-$|\mathcal{Y}_c|$ coding). While this is desirable to diminish losses, it is not always optimal and can lead to inefficient allocations in some cases, as we shall see shortly.

4.4.5. Energy Routing

Next, we present an optimal sequential allocation algorithm to implement the energy transfers from sources $i \in \mathcal{Y}_s$ to consumers $j \in \mathcal{Y}_c$, in time slot t. Through the previous analysis, the allocation matrix $\boldsymbol{Y}^* = [y^*_{ij}]$ is known and an energy transfer is to be implemented for each entry y^*_{ij} for which $y^*_{ij} > 0$. Note that, in the considered topology each energy transfer y^*_{ij} has a single associated routing path r, connecting the energy source i to the energy consumer j. Such *energy route* consists of the collection of: source node i, destination node j and the intermediate nodes (if any) connecting i to j in the considered topology (Fig. 4.1). Let R be the number of such routing paths, which are collected through the set of indices $\mathcal{R} = \{1, 2, \ldots, R\}$ (see the example in Fig. 4.4a). The problem to be solved is to schedule in time these energy transfers so that:

- The time needed to complete the R energy transfers is minimized.
- The destinations j are prioritized according to the residual energy in their local buffers B_j, i.e., the smaller B_j, the higher the priority. This induces a corresponding priority mechanism on the routes in $\mathcal{R}$.

This problem bears similarities with the literature on optimal airplane landing schedules, e.g., [132]. Specifically, a parallel may be drawn between the runaways of [132] and our routing classes (see below). The main difference is that in our case routing classes may contain common (and thus interfering) routes: this makes the analysis more involved, requiring major modifications in the definition of the system state, in the calculation of route serving and completion times and single-stage costs. Below, we report the optimal and original analysis addressing our technical scenario.

Mini-slots: Each time slot is further split into a number of mini-slots of equal duration, where $e_{\max}$ is the maximum transmission energy capacity (system parameter) for a power link in a mini slot. Given an energy route $r \in \mathcal{R}$ with source node i and consumer node j, the required number of mini slots to transfer the amount of energy $y_{ij}e_{ij}$ from i to j is $\Delta_r = \lceil y_{ij}e_{ij}/e_{\max} \rceil$.

System model for sequential allocation: We refer to the example network of Fig. 4.4a. There, we have three source nodes i_1, i_2, i_3 and two destination nodes j_1, j_2. $R = 3$ energy routing paths are to be allocated, with $\mathcal{R} = \{1, 2, 3\}$, where route 1 connects i_1 to j_1, route 2 connects i_2 to j_1 and route 3 connects i_3 to j_2. The dependencies among routes are modeled through the bipartite graph of Fig. 4.4b: the nodes in the left hand side represent the three routes and the nodes in the right hand side represent the *routing classes*. A routing class contains the routes that have at least one link in common, and that for this reason cannot be allocated in overlapping time intervals, i.e., only one route can be active in any mini-slot for each routing class. The routes within a routing class are referred to as *interfering*. In our analysis, variable Q represents the number of routing classes. Routing classes q_1, q_2 ($Q = 2$) suffice to track the dependencies in Fig. 4.4a and they have route 2 in common. The following properties are key to our analysis. P1) Disjoint routes from different classes can be allocated concurrently: this is the case for paths 1 and 3. P2) Common routes, i.e., route 2, can also be allocated, but this entails that both classes will be busy for the whole serving time of route 2: during this serving period both classes will be prevented from any further allocation.

In the following analysis, a generic route is indicated by variable r, i and j are the corresponding source and destination nodes, $\mathcal{R}_r$ is the set collecting all routing classes that contain route r. $\tilde{t}_r$ and t_r respectively denote the mini-slot at the end of which route r is allocated and the completion time, i.e., the mini-slot at the end of which the energy transfer for route r is complete. All time variables are expressed in terms of number of mini-slots and we assume that energy transfers occur from allocation to completion, without interruption.

State space and transitions: We define an allocation vector $\boldsymbol{v} = [v_1, v_2, \ldots, v_R]$ with R binary entries $v_r \in \{0, 1\}$, $r = 1, \ldots, R$, where $v_r = 1$ if route r has been already allocated, and $v_r = 0$ otherwise. The state space is defined as the tuple $\boldsymbol{s} = (\boldsymbol{v}, (n_1, t_1), (n_2, t_2), \ldots, (n_Q, t_Q))$, where (n_q, t_q) indicates the index n_q of the route that is currently allocated for routing class q, with associated energy transfer completion time t_q. Let $\boldsymbol{s}$ be the current system state, a system transition due to the *allocation* of any route $r = 1, \ldots, R$ is *feasible* if:

1. If r belongs to a single routing class $\dot{q}$, we have $\mathcal{R}_r = \{\dot{q}\}$, and its allocation is feasible if $v_r = 0$ and its serving time is $\tilde{t}_r = t_{\dot{q}}$, i.e., we need to wait for the current transfer for class $\dot{q}$ to finish before we can allocate the new one for route r.

2. If r belongs to multiple routing classes, collected through set $\mathcal{R}_r$, then its allocation is feasible if $v_r = 0$ and it serving time is $\tilde{t}_r = \max_{q \in \mathcal{R}_r} t_q$, i.e., in this case we need the transfers for all the classes in $\mathcal{R}_r$ to finish.

This leads to a transition from state $\boldsymbol{s}$ to state $\boldsymbol{s}'$:

$$\boldsymbol{s} \Rightarrow \boldsymbol{s}' = (\boldsymbol{v}', (n'_1, t'_1), (n'_2, t'_2), \ldots, (n'_Q, t'_Q)) \tag{4.27}$$

where,

- $v'_k = v_k$, for $k = 1, \ldots, R$, $k \neq r$,
- $v'_k = 1$, if $k = r$,

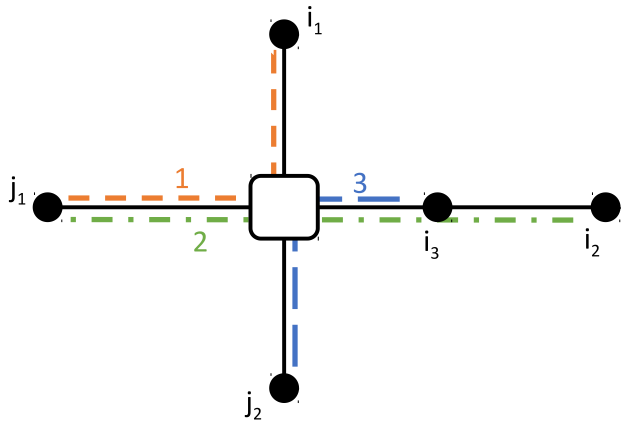

(a) Example of energy routing network: each i_x is a source node and each j_x is a consumer node. Three routes $\{1, 2, 3\}$ are present.

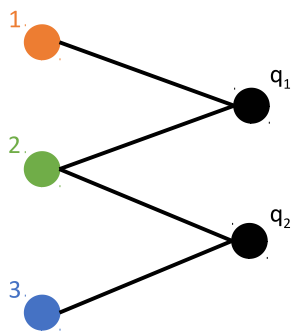

(b) Bipartite graph encoding the dependencies among routes. Route 1 ($i_1 \to j_1$) and 2 ($i_2 \to j_1$) interfere, as well as routes 2 and 3 ($i_3 \to j_2$). Interfering routes are collected in routing classes q_1, q_2.

Figure 4.4: Example for the allocation of energy routes.

- $(n'_q, t'_q) = (n_q, t_q)$, $q = 1, \ldots, Q$ and $q \notin \mathcal{R}_r$,
- $(n'_q, t'_q) = (r, \tilde{t}_r + \Delta_r)$, $q = 1, \ldots, Q$ and $q \in \mathcal{R}_r$.

Note that if route r is contained in multiple routing classes, the completion time for all such classes must be $\tilde{t}_r + \Delta_r$, as the transfer will concurrently involve all of them. The feasibility set encoding these conditions for any state $\boldsymbol{s}$ is denoted by $\mathcal{F}(\boldsymbol{s})$. Transition $\boldsymbol{s} \Rightarrow \boldsymbol{s}' \in \mathcal{F}(\boldsymbol{s})$ has an entangled single-stage cost:

$$\omega(\boldsymbol{s}') = \left(1 - \frac{B_j}{B_{\max}}\right) \sum_{q \in \mathcal{R}_r} \left(\tilde{t}_r - t_q + \Delta_r\right) , \tag{4.28}$$

where j is the destination node of the current route r and B_j is its residual battery. The term $(1 - B_j/B_{\max})$ prioritizes the destination (consumer) j according to B_j. The term $\tilde{t}_r - t_q + \Delta_r$ is the amount of time during which routing class q will be busy to serve route r. Note that, when r is in multiple classes, i.e., $|\mathcal{R}_r| > 1$, there may be a temporal inefficiency due to waiting for the class with the longest completion time ($\tilde{t}_r = \max_{q \in \mathcal{R}_r} t_q$). This inefficiency is weighed through the term $\tilde{t}_r - t_q$,

	$N_* = 1$	$N_* = 2$	$N_* = 12$	$N_* = 24$
$S = 1$	0.0119	0.0170	0.0385	0.0512
$S = T$	0.0116	0.0166	0.0383	0.0511

(a) Average $\text{RMSE}_*^{(t)}$ for $H(t)$.

	$N_* = 1$	$N_* = 2$	$N_* = 12$	$N_* = 24$
$S = 1$	0.0389	0.0464	0.0670	0.0740
$S = T$	0.0415	0.0483	0.0671	0.0743

(b) Average $\text{RMSE}_*^{(t)}$ for $L(t)$.

Table 4.1: Average $\text{RMSE}_*^{(t)}$.

which is *greater than zero* in case class $q \in \mathcal{R}_r$ is freed before the serving time $\tilde{t}_r$, i.e., $t_q < \tilde{t}_r$. The optimal policy in the next paragraph minimizes these inefficiencies, achieving the fastest allocation.

Optimal policy: The accumulated cost from a state $\boldsymbol{s}$ can be obtained through the following Bellman equation:

$$\Omega(\boldsymbol{s}) = \min_{\boldsymbol{s}' \in \mathcal{F}(\boldsymbol{s})} \{\omega(\boldsymbol{s}') + \Omega(\boldsymbol{s}')\} \tag{4.29}$$

The initial state $\boldsymbol{s}_0 = (\boldsymbol{v}_0, (0,0)^Q)$ contains $\boldsymbol{v}_0 = (0, 0, \ldots, 0)$ (all-zeros), and the routing classes terms $(n_q, t_q) = (0, 0)$ for $q = 1, \ldots, Q$ and has cost $\Omega(\boldsymbol{s}_0) = 0$. The optimal schedule is found by finding:

$$\boldsymbol{s}^* = \underset{\boldsymbol{s} \in \Pi}{\text{argmin}} \{\Omega(\boldsymbol{s})\}\,, \tag{4.30}$$

where Π is the set of final states, a final state being any state with $\boldsymbol{v}_{\text{end}} = (1, 1, \ldots, 1)$ (all-ones) and the remaining terms (n_q, t_q) depending on the outcome of the Bellman recursion. The optimal schedule is derived by tracking the sequence of transitions that transform the initial state $\boldsymbol{s}_0$ into all possible and feasible final states $\boldsymbol{s} \in \Pi$ which are recursively evaluated through Eq. (4.29), inducing $\boldsymbol{s}^*$ through Eq. (4.30).

4.5. Numerical Results

The forecasting approach based on GPs is evaluated in Section 4.5.1, whereas results of the proposed optimization framework are provided in Section 4.5.2, using the algorithm of [75] as a benchmark.

4.5.1. Performance Evaluation of the Pattern Learning Scheme

The proposed GP-based forecasting method proposed in Section 4.4.2 is here assessed for the runtime multi-step ahead forecasting of time series $H(t)$ and $L(t)$. The time slot duration is set to one hour, $N = 24 \times 14 = 336$ hours (i.e., two weeks of data), $T = 24 \times 60 = 1,440$ hours (i.e., two months of data), and $\sigma_n = 10^{-5}$. This choice of parameters is valid for both time series, as well as the use of the kernel $k(\cdot, \cdot)$ in Eq. (4.16), whereas the *hyperparameters* differ, depending on the nature of data.

In Table 4.1a and Table 4.1b we show the average RMSE for $H(t)$ and $L(t)$, computed evaluating the mean of the RMSE measures up to time $T-(N+N_*)$, where we track $\text{RMSE}_*^{(t)}$ over the N_* test cases, given $N_* = 1, 2, 12, 24$. Also, as we perform the training phase once every S steps, comparing the numerical results when $S = 1$ and $S = T$, i.e., when we update the free GP parameters at each step of the online forecasting routine ($S = 1$), or just once every T steps ($S = T$), at time $t = 1$. In general, the average $\text{RMSE}_*^{(t)}$ increases as we increase the N_* test cases up to 24, which corresponds to predicting the time series one day into the future. However, the worst performance is 0.0743, which is still rather small if we consider that both time series are normalized in $[0, 1]$ prior to processing. Also, predictions for $H(t)$ (Fig. 4.5a) are more precise than predictions for $L(t)$ (Fig. 4.5b), and this is due to the nature of the data, given that we use the same kernel for both time series. In fact, values in $H(t)$ (Fig. 4.5a) follow a more regular behavior than those in $L(t)$ (Fig. 4.5b), with quasi-periodic streams of zero values corresponding to zero solar energy income during the night. These quasi-periodic streams of zero values help reinforcing prediction, while allowing for a higher confidence at nighttime (see Fig. 4.6a). Finally, tuning parameter S explains the impact of re-optimizing the *hyperparameters* according to the most recent history (i.e., two weeks of data), but with a longer execution time. Numerical results suggest that tuning parameter S could be reasonable when data exhibit multiple strong local behaviors rather than just a strong daily seasonality, and the kernel has to adapt to these. However, $S = 1$ could not be the obvious optimal choice (see Table 4.1a).

In Fig. 4.5a and Fig. 4.5b we show real values and predictions for two weeks of data, where we track the one-step (i.e., $N_* = 1$) predictive mean value at each time slot of the online forecasting routine. The strong daily seasonality is evident, as well as the quasi-periodic structure in data with noise operating at different scales. Note that predictions for $H(t)$ (Fig. 4.5a) are more accurate than those for $L(t)$ (Fig. 4.5b), and this result can be confirmed by comparing the average $\text{RMSE}_*^{(t)}$ in Tables 4.1a and 4.1b for $N_* = 1$. As expected, predictions may be far from real values when some unusual events occur, see, for example, the low solar energy income within hours 456 and 480 (sixth peak from the left), in Fig. 4.5a, or the sudden peaks in the traffic load profile of Fig. 4.5b, which are very day-specific.

In Figs. 4.6a and 4.6b we show real and predicted values for three days of data, i.e., the last two days of the training dataset, and 24 hours for the test set, plotting the multi-step predictive mean value with $N_* = 24$. Here, we compare the use of the kernel $k(\cdot, \cdot)$ in Eq. (4.16) with common base kernels from the literature, such as the popular Squared Exponential (SE) kernel, the Rational Quadratic (RQ) kernel, and the Standard Periodic (SP) kernel, see Eq. (4.16). Also, we compare the use of the kernel $k(\cdot, \cdot)$ in Eq. (4.16) in terms of generalization capabilities over the training dataset and the test set, i.e., we perform forecasting over the training dataset and the test set, after the optimization of the *hyperparameters* given the observations. Note that the proposed kernel (solid line) shows the best performance in terms of forecasting, since composite kernels are more representative than base ones. Specifically, the RMSE is close to zero over the training dataset (due to the fact that we set $\sigma_n = 10^{-5}$, i.e., $\sigma_n \neq 0$), and this result also holds for both the SE and RQ cases. However, the generalization capabilities over the test set are quite limited for SE and RQ. In fact, these base kernels have limited expressive power, and simply act like smoothers. Finally, the SP kernel succeeds in recovering the strong daily seasonality in the data, but it fails to model noise at different scales. Again, its expressive power is quite limited, with respect to our

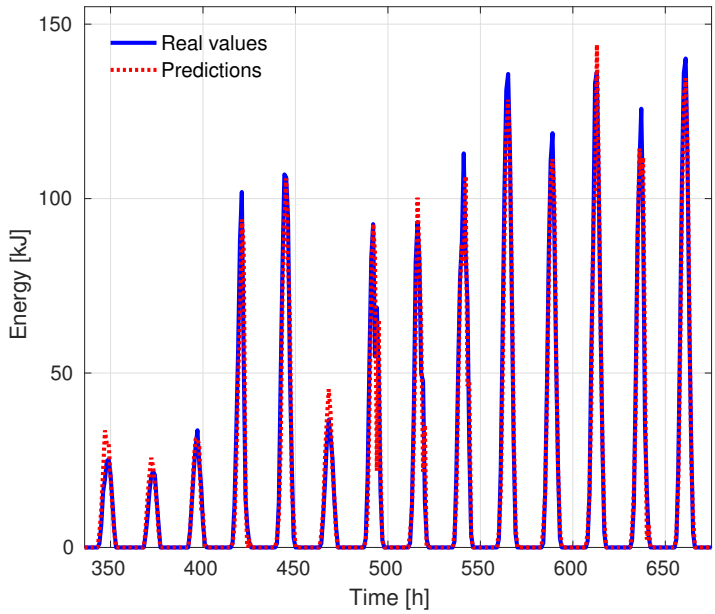

(a) One-step predictive mean value for $H(t)$.

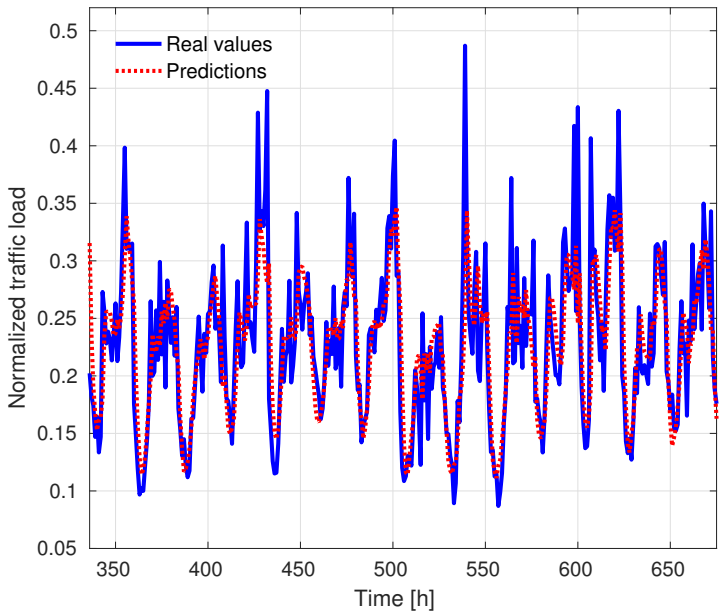

(b) One-step predictive mean value for $L(t)$.

Figure 4.5: One-step online forecasting for two weeks of data.

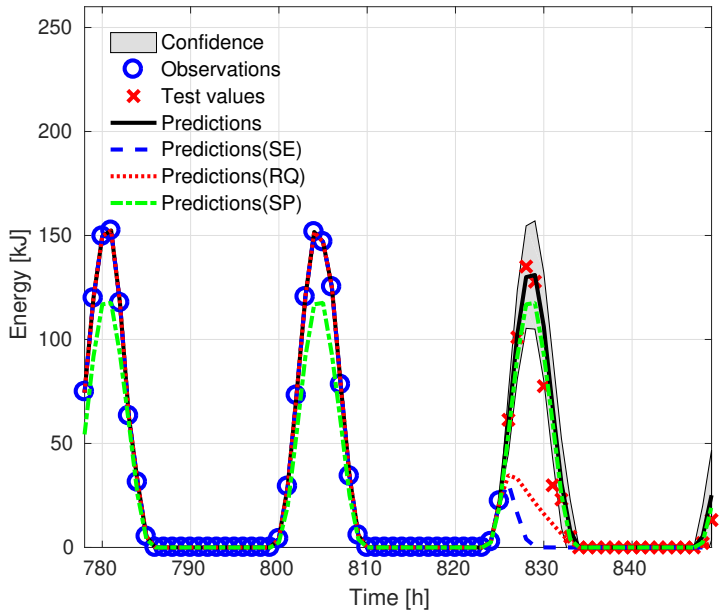

(a) Multi-step predictive mean value for $H(t)$.

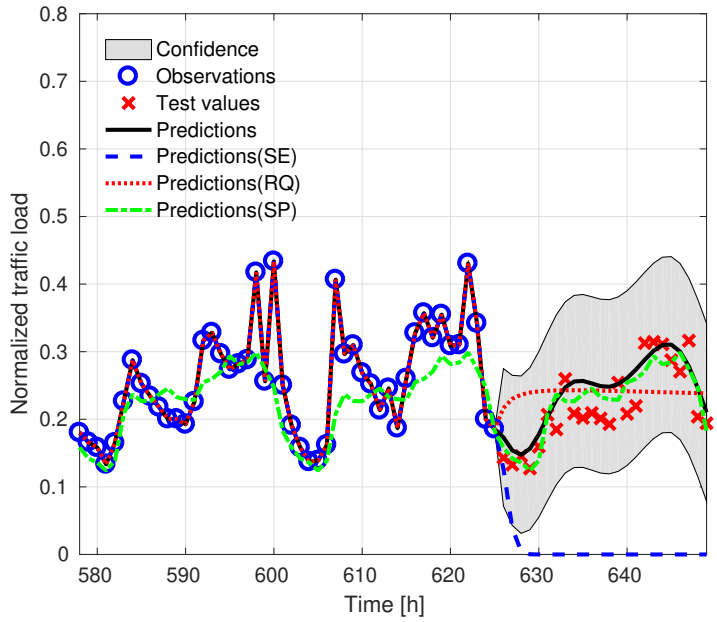

(b) Multi-step predictive mean value for $L(t)$.

Figure 4.6: Multi-step prediction with different kernels.

Table 4.2: System parameters used in the numerical results.

Parameter	Value
Number of BSs, n_s (set $\mathcal{S}$)	18
Number of ongrid BSs (set $\mathcal{S}_{\text{on}}$)	6
Cable resistivity, ρ	$0.023\,\Omega\text{mm}^2/\text{m}$
Cable cross-section, A	$10\,\text{mm}^2$
Length of a power link, ℓ	100 m
Energy buffer capacity, $B_{\max}$	360 kJ
Upper energy threshold, B_{up}	$0.7B_{\max}$ (70%)
Reference energy threshold, B_{ref}	$0.5B_{\max}$ (50%)
Lower energy threshold, B_{low}	$0.1B_{\max}$ (10%)
Time slot duration	1 h
Mini slot duration	60 s
Maximum transmission energy capacity, $e_{\max}$	90 kJ/mini-slot
MPC optimization horizon M	24 h
MPC weight parameter α	0.5
Energy allocation weight parameter β	0.5

proposed kernel in Eq. (4.16).

4.5.2. Performance Evaluation of the Optimization Framework

In this section, the following schemes are compared: i) no energy exchange **(NOEE)**, i.e., the offline BSs only have to rely on the locally harvested energy, ii) convex solution **(CONV)**: this is the scheme of [75], which computes energy allocations solely based on the system configuration in the current time slot. This approach is *myopic*, as no knowledge into the future behavior of the system is exploited. iii) Hungarian solution **(HUNG)**: the energy allocation is found through the Hungarian method of Section 4.4.4; this is also a myopic approach. iv) Convex solution with model predictive control **(GPs+MPC+CONV)**: this is the combined optimization approach of Sections 4.4.2, 4.4.3 and 4.4.4, and v) Hungarian solution with model predictive control **(GPs+MPC+HUNG)**. ii) and iii) carry out energy allocation and routing only considering the current time slot, while iv) and v) also take into account the future system evolution, exploiting pattern learning and multi-step ahead adaptive control.

Before discussing the numerical results, some considerations are in order. All the algorithms purchase some energy from the power grid, although the way in which they use it differs. With NOEE, the energy purchased is exclusively used to power the base stations that are ongrid, whereas those being offgrid have to uniquely rely on the harvested energy. Convex and Hungarian solutions allow some energy redistribution among the base stations. With these schemes, an energy rich BS

can transfer energy to other BSs whose energy buffer is depleted. Note that an energy rich base station may belong to either the ongrid set or to the offgrid one. The latter case occurs when, for instance, a BS experiences no traffic during the day and all the energy it harvests is stored locally. In this case, this BS is likely to be "energy rich", and energy transfer schemes consider it as an energy source for other BSs. Looking at the whole BS network, it can gather energy in two ways: i) harvesting it from the environment and ii) purchasing it from the power grid. The harvested energy is basically free of charge and shall be utilized to the best extent: energy transfer among BSs makes this possible. The energy bought by the ongrid BSs is costly and shall also be utilized as efficiently as possible. Below, we shall evaluate both aspects.

For the numerical results, we consider the scenario of Section 4.3. For the EBs, we set $B_{\max} = 360\,\text{kJ}$, which corresponds to a battery capacity of $100\,\text{W h}$ (e.g., a small size Li-Ion battery). The slot time is set to one hour, solar EH traces are obtained using SolarStat [35] for the city of Chicago, and the BS topology is that of Fig. 4.1, with 6 ongrid BSs and a total of $n_s = 18$ BSs. The other simulation parameters are listed in Table 4.2. The curves plotted in Figs. 4.7a, 4.7b, 4.9a and 4.9b are obtained averaging over $1,000$ simulation instances. Each simulation instance accounts for 168 hours, i.e., one week. The harvested energy profile for each BS is set at the beginning of each simulation instance starting from a specific date, which is picked at random from the real-trace dataset. For the traffic load, each BS picks one of the two available load clusters at random, with probability p (in the abscissa). Moreover, Figs. 4.7a, 4.7b and 4.8 are obtained with ideal EBs, i.e., $\beta_{\text{loss}} \to \infty$. This changes in Figs. 4.9a and 4.9b where both cases, ideal and non-ideal ($\beta_{\text{loss}} = 3$), are shown. Finally, the location of the ongrid BSs within the topology of Fig. 4.1 changes randomly at every simulation instance.

In Fig. 4.7a, we show the average BS energy buffer level over different traffic load configurations. For the load assignment, each BS independently picks one of the two traffic clusters in Section 4.3.3: cluster 2 (low traffic load) is picked with probability p and cluster 1 (high load) is picked with probability $1-p$. p is then varied as a free parameter along the abscissa. As expected, the average energy buffer level when $p = 0$ is lower than that with $p = 1$, as the traffic load in cluster 1 is higher. Regarding the approaches, the highest difference in the energy buffer levels is found between NOEE and GPs+MPC+HUNG, with an increment of around 60% (on average) when MPC is adopted. Moreover, the Hungarian methods outperform convex solutions because, with their assignment policy, any consumer is matched to a single source and this reduces the amount of energy that is distributed, leaving more energy in the energy rich buffers. As we show shortly, this behavior is not really desirable as, e.g., it leads to higher outage probabilities.

As a proxy to the network QoS, the outage probability at time t, $\gamma(t)$, is here defined as the ratio between the number of BSs whose energy buffer level gets completely depleted, and the total number of BSs in the system n_s. The outage probability $\gamma(t)$ as a function of the traffic load is plotted in Fig. 4.7b. For all schemes, $\gamma(t)$ is an increasing function of the load. The probability that a BS runs out of service due to energy scarcity is higher when energy cannot be transferred among BSs (NOEE) and is in general very high across the whole day for HUNG-based solutions. However, applying MPC to the Hungarian method leads to a reduction in the average outage probability of about 54%. Moreover, from Fig. 4.8 we see that with the Hungarian method, $\gamma(t)$ increases when the amount of energy harvested is very little (i.e., nighttime). The problem is that the Hungarian allocation technique returns a matching of source-consumer pairs, where each source is allocated to a single consumer and, in turn, some of the BSs may not be allocated in some time slots (due

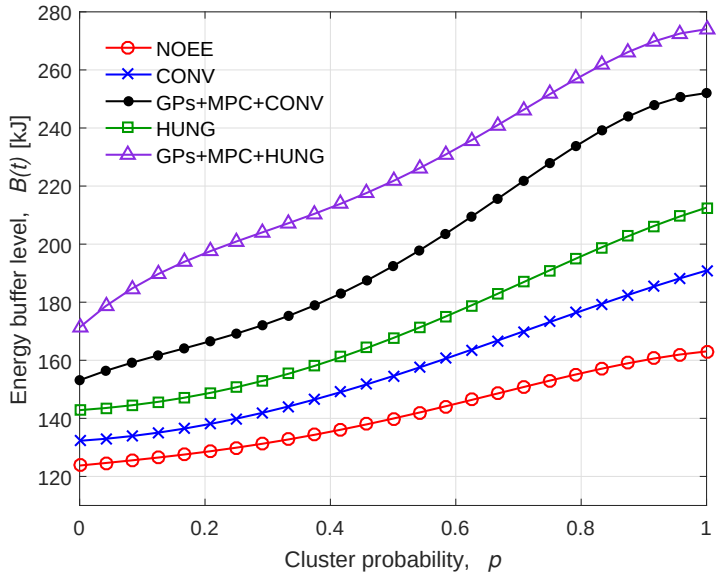

(a) Energy buffer level *vs* cluster probability p.

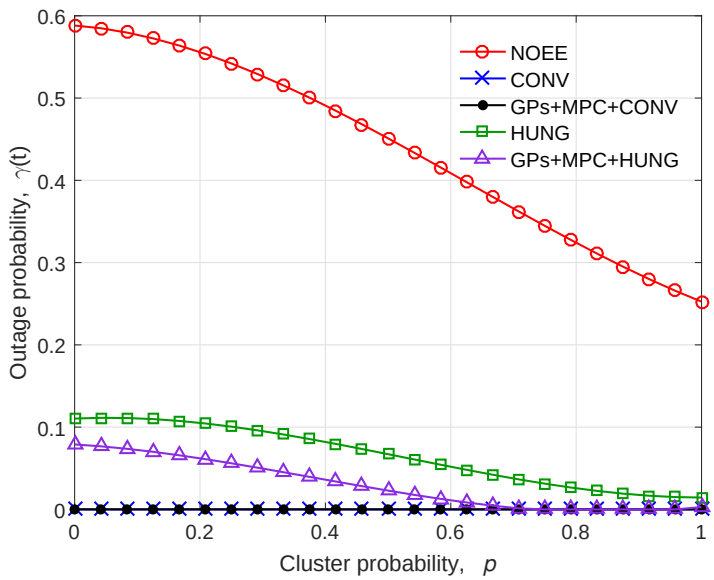

(b) Outage probability $\gamma(t)$ *vs* cluster probability p.

Figure 4.7: Numerical results over the cluster probability p.

to the imbalance between number of sources and number of consumers). This leads to high outage probabilities for the considered scenario. CONV-based techniques are more flexible in this respect, as they allow energy transfer from multiple BSs and in different amounts. This translates into a zero outage probability in both cases, with and without MPC.

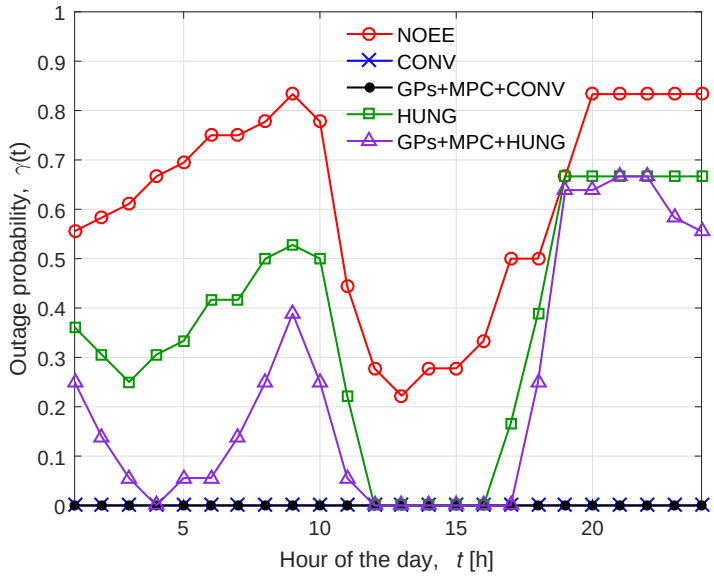

Figure 4.8: Outage probability $\gamma(t)$ over a day.

From the previous graphs, one may conclude that CONV and GPs+MPC+CONV (foresighted optimization) provide the same benefits, being both capable of lowering the outage probability down to zero. However, looking at additional metrics reveals that the two approaches show important differences. For example, in Fig. 4.9a we compare these solutions in terms of amount of energy that ongrid BSs purchase from the power grid. A big gap can be observed between the two schemes, proving that the application of pattern learning and MPC is indeed highly beneficial, leading to a reduction of more that 55% in the amount of energy purchased from the power grid.

Along these lines, we perform another set of simulations by putting a cap on the maximum amount of energy that can be bought during a full day by the ongrid BSs. Specifically, we define a *purchased energy threshold* η as the ratio between the amount of energy that each ongrid BS is allowed to purchase and the total amount of energy it would require to serve a fully loaded scenario across an entire day, i.e., the BS purchases energy up to $B_{\max}$ every time slot. A plot of $\gamma(t)$ against threshold η is shown in Fig. 4.9b. From this graph, we see that predictive control (GPs+MPC+CONV) leads to a much smaller outage probability than CONV. Moreover, as η increases beyond 0.5 the outage probability drops to zero, which is a big improvement with respect to CONV, for which γ is about 10%. Similar results are obtained for GPs+MPC+HUNG when compared with HUNG, although in this case the gain is slightly smaller.

The use of non-ideal energy buffers is evaluated in Figs. 4.9a and 4.9b, using $\beta_{\text{loss}} = 3$. In this case, the energy losses incurred in the charging and discharging processes lead to an increase in the energy purchased from the power grid ($\approx 10\%$) and in the outage probability ($\approx 15\%$) over time, due to the smaller EB levels with respect to the ideal EB scenario.

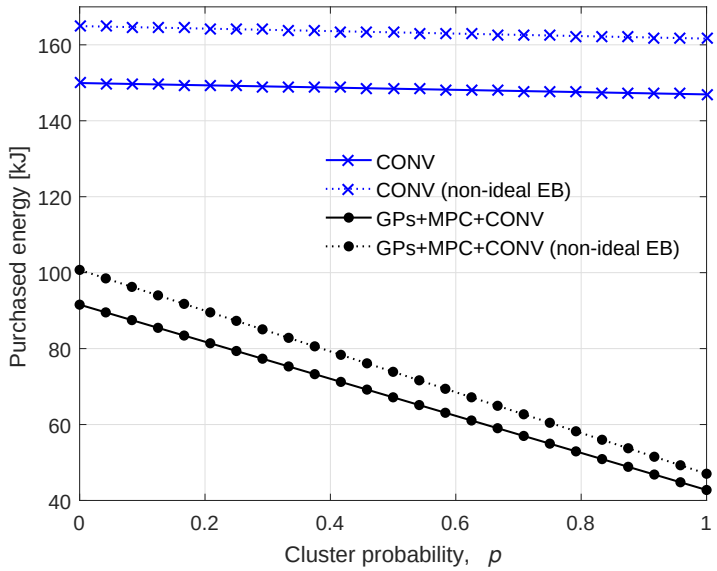

(a) Purchased energy *vs* cluster probability p.

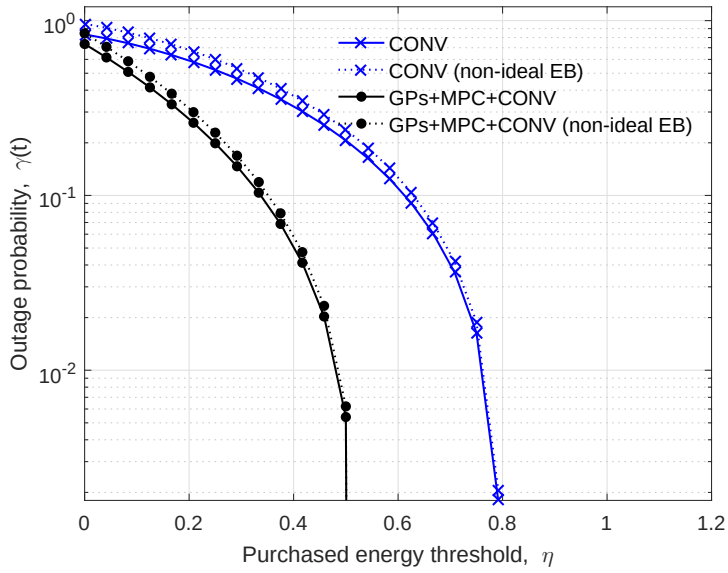

(b) Outage probability $\gamma(t)$ *vs* purchased energy threshold.

Figure 4.9: Numerical results regarding purchased energy.

4.6. Conclusions

In this chapter, we have considered small cell deployments where energy harvesting and packet power networks are combined to provide energy self-sustainability through the use of own-generated

energy and carefully planned power transfers among network elements. This amounts to a combined learning and optimization problem (resource scheduling), where learning is carried out on energy arrival (harvested ambient energy) and traffic load traces and this knowledge is exploited, at runtime, for the computation of optimal energy transfer policies among the distributed energy buffers. This foresighted optimization is performed combining model predictive control and convex optimization techniques. Numerical results reveal great advantages over the case where energy transfer schedules are optimized disregarding future energy and load forecasts: the amount of energy purchased from the power grid is reduced by more than 50% and the outage probability is lowered to zero in nearly all scenarios.

The energy transfer scenario posed in this chapter could be extended to the case where *edge computing* servers are located close to the base stations. In this way, the energy cooperation approach could be improved by considering not only the traffic load in the base station, but also the computational tasks dynamically assigned to the edge servers. This entails a new research paradigm that will be studied in the following chapter.

5

Energy Harvesting and Edge Computing Resource Management

5.1. Introduction

The full potential of 5G radio access technology can be realized through the use of distributed intelligence, whereby content, control, and computation are moved closer to mobile users, hereby referred to as the *network edge*. This evolution has lead to the emergence of the MEC paradigm, which allows network functions to be virtualized and deployed at the network edge to guarantee the low latency required by some applications. The convergence of communication and computing within the mobile network poses new challenges related to energy consumption, as BSs are densely-deployed to maximize capacity and also empowered with computing capabilities to minimize latency. In addition, energy savings within the virtualized computing platform are of great importance, as virtualization can also lead to energy overheads. Therefore, precise knowledge about the edge energy usage is key in this aspect. Experimental results in [133] and [134] show that the locus of energy consumption for the Virtualized Network Function (VNF) components is the Virtual Machine (VM) where the VNF is instantiated and executed. Thus, the energy consumption can be minimized by launching an optimal number of VMs (technique referred to as VM *soft-scaling*) with efficient resource allocation policies [135].

To cope with these challenges, energy efficiency and self-sufficiency are key considerations where the adoption of EH hardware within the network can provide a feasible solution. However, the deployment of EH farms and MEC capabilities comes at a big investment cost and needs an optimized planning for each network operator. Hence, *multi-operator sharing* techniques, such as infrastructure sharing, can be exploited to diminish these costs.

In this chapter, EH and MEC paradigms are combined towards sustainable mobile networks. We consider an edge shared infrastructure equipped with a solar EH farm for energy efficiency purposes together with a MEC server for low-latency computation where we propose an energy and computation resource management framework with two main goals: (i) maximize the exploitation of the available resources at the edge in a fair fashion among BSs belonging to different operators; and (ii) decreasing the monetary cost incurred by energy purchases from the power grid. These two problems are solved devising an online framework combining: (i) pattern forecasting via a specific type of Recurrent Neural Network (RNN) [136], that learns energy harvesting and traffic load profiles over time, and (ii) adaptive control via foresighted optimization performed through MPC theory [84].

Numerical results, obtained with real-world harvested energy, traffic load, and energy price traces, show that the use of adaptive control schemes provides important benefits in decreasing energy costs within the mobile network. Specifically, our proposal is able to reduce the amount of purchased energy from the electrical grid of more than 50% with respect to the case where no EH is considered, and about 30% with respect to the case where no foresighted optimization is applied,

i.e., the optimization is performed disregarding future energy and traffic load forecasts. Moreover, it is capable of reducing the computational load in the edge server about 20% with respect to two benchmarks.

5.1.1. Contributions

The main contributions of the present chapter are:

- We present a novel scenario where EH and MEC paradigms are combined within a multi-operator infrastructure-sharing mobile network, discussing new possibilities towards energy cooperation.
- We propose an online forecasting framework based on RNNs, customized to learn the EH and consumption patterns over time. Specifically, a Long Short-Term Memory (LSTM) architecture is designed in this respect.
- We formulate two online and predictive optimization problems based on MPC theory for energy purchases from the power grid and MEC resources allocation, with the goal of diminishing energy costs to mobile operators.
- We provide numerical results, quantifying the effectiveness of the proposed solution with real-world traces. An important finding is that the combination of forecasting and predictive control can substantially reduce the total amount of energy that the system drains from the power grid and decrease the computational load in a MEC server, minimizing the related energy consumption while maximizing the low-latency edge computation. See Section 5.5 for more details.

5.1.2. Chapter Outline

The chapter is organized as follows. In Section 5.2, we present the related literature and highlight the novel aspects of our work. The network scenario is described in Section 5.3. The optimization framework is detailed in Section 5.4. Numerical results are presented in Section 5.5, and final remarks are provided in Section 5.6.

5.2. Related Work

Some literature related to multi-operator sharing techniques in mobile networks is discussed here. Then, some works dealing with MEC resource allocation and VM soft-scaling for energy savings are presented. Lastly, the novelties of this work regarding existing literature are detailed.

Multi-operator sharing techniques: network operators sharing looks a promising viable solution towards the reduction of both capital and operational costs. This new paradigm, promoted by legal regulations that obligate the operators to install their antennas on the same buildings, embraces a set of strategies that enable a joint use of resources to reach a common goal, i.e., to guarantee customer service while achieving energy and cost reductions [7]. The joint energy

purchase and wireless load sharing among mobile network operators is exploited in [80] to reduce energy costs. The authors propose a scheme where two operators are aggregated into a single group to implement a day-ahead and real-time energy purchase, and their BSs share the wireless traffic to maximally put lightly-loaded BSs into sleep mode. This scenario is tackled using two-stage stochastic programming. The scenario that we consider here is different, as we focus on energy sharing infrastructure where energy and computation capabilities are allocated to BSs.

A distributed game theoretic intra-cell roaming-based infrastructure sharing scheme, where mobile operators may switch off their BSs and roam their traffic to active BSs operated by other operators in the same cell is presented in [7]. Moreover, they discuss possible network deployments and architectures in current and future cellular scenarios motivated by the coexistence of multiple operators in the same area.

Technological, regulatory, and business landscape from the perspective of sharing network resources is investigated in [137], where different approaches and technical solutions are presented. The authors introduce a model for estimating savings on capital and operating expenses, and evaluate it through simulation for various scenarios. Moreover, they assess the benefits of *Managed Services* for the shared network case, a potentially highly attractive model to overcome some of the challenges posed by infrastructure sharing. The authors in [138] discuss the business model implications of different multi-operator solutions for indoor deployment. The key findings are in the areas of: (i) how multi-operator small cell solutions can fit into existing market practices when it comes to operator business, (ii) how local network operators, i.e., third parties, and outsourcing can play a role in the business landscape, and (iii) how different spectrum allocation and access strategies can play a role for indoor network deployments.

Radio Access Network (RAN) sharing where multiple mobile operators with a consolidated network infrastructure coexist in a given set of geographical areas is investigated in [139]. The operators have then to decide whether it is profitable to upgrade their RAN technology by deploying additional small-cell BSs and if to share the investment (and the deployed infrastructure) with other operators. They address these strategic problems by proposing a mathematical framework that returns optimal infrastructure sharing strategies for operators (coalitions and network configuration) when varying techno-economic parameters such as achievable throughput and pricing models for the service offered to the users. Fair sharing possibilities of stored renewable energy in densely populated areas among multiple mobile network operators is addressed in [30]. To this end, a bankruptcy game is designed so as to capture the energy sharing interactions among operators. Furthermore, Shapley Value is employed to fairly determine the amounts of energy to be allocated to each mobile operator.

MEC resource allocation and VM soft-scaling schemes: the distribution of resources within a MEC server has been extensively studied in the literature from different perspectives and scenarios. Some examples are in order.

In [140], a fair resource allocation approach to maximize the overall network throughput, under the constraint of each mobile user's minimum transmission rate is proposed. They formulate the problem as a fair Nash bargaining resource allocation game, where they obtain the near optimal bargaining resource allocation strategy for the mixed integer nonlinear programming optimization.

MEC computation resource allocation is tackled along with offloading decision making and Internet content caching within heterogeneous mobile networks in [141]. The authors formulate

a convex problem and then decompose it in order to solve it in a distributed way using an Alternating Direction Method of Multipliers-based algorithm. Along the same lines, a distributed joint computation offloading and resource allocation optimization scheme in heterogeneous networks within MEC is presented in [142]. An optimization problem is formulated to provide the optimal computation offloading strategy policy, uplink subchannel allocation, uplink transmission power allocation, and computation resource scheduling. The optimization problem is decomposed into two sub-problems due to the NP-hard property and solved through mutual iteration of two proposed algorithms.

MEC can leverage on the Network Function Virtualization (NFV) benefits to significantly reduce the energy consumption of network infrastructures. In virtualized computing environments, the VMs running in the server(s) are the main elements contributing to the energy consumption. Thus, energy saving studies within the virtualized computing environment have involved: (i) *autoscaling* [143], i.e., scaling down of the number of running computing nodes, (ii) *VM migration* [144], i.e., movement of a VM from one host to another, and (iii) *soft resource scaling* [145], i.e., shortening of the access time to physical resources, all hereby referred to as VM *soft-scaling*, i.e., the reduction of computing resources per time instance.

Algorithms for the dynamic on/off switching of servers have been proposed as a way of minimizing energy consumption in computing platforms. In [143], at the beginning of each time slot computing resources are provisioned depending on the expected server workloads via a reinforcement learning-based resource management algorithm, which learns on-the-fly the optimal policy for dynamic workload offloading and the autoscaling of servers. In [144], the Central Processing Unit (CPU) utilization thresholds are used to identify over-utilized servers. Hence, migration policies, enabled by the live VM migration method [146], are applied for moving the VMs between physical nodes (servers). The VMs are only moved to hosts that will accept them without incurring high energy cost, i.e., without any increase in the CPU utilization. Subsequently, the idle servers are switched off.

Power management is also of interest in virtualized computing platforms, i.e., data centers using virtualization technologies. In [145], a power management approach called *VirtualPower* is presented. The algorithm exploits hardware power scaling, i.e., the dynamic power management strategies using Dynamic Voltage and Frequency Scaling (DVFS) [147] [148], and software-based methods, i.e., scaling the allocation of physical resources to VMs using the hypervisor scheduler, for controlling the power consumption of underlying platforms. Due to the low power management benefits obtained from hardware scaling, a *soft resource scaling* mechanism is proposed whereby the scheduler shortens the maximum resource usage time for each VM, i.e., the time slice allocated for using the underlying physical resources.

Novelty of the present work: despite the existence of previous works on energy cooperation (see Section 2.3 and 4.2), sharing among operators and MEC resource allocation, here we consider an original scenario where: (i) we put together EH and MEC topics within a shared infrastructure among multiple operators; (ii) we consider only one EH farm within each macro cell, instead of EH hardware for every BS, to reduce deployment costs; and (iii) harvesting process, traffic load, and energy prices come from real-world traces. Apart from these novelties regarding the scenario, more contributions are discussed in Section 5.1.1.

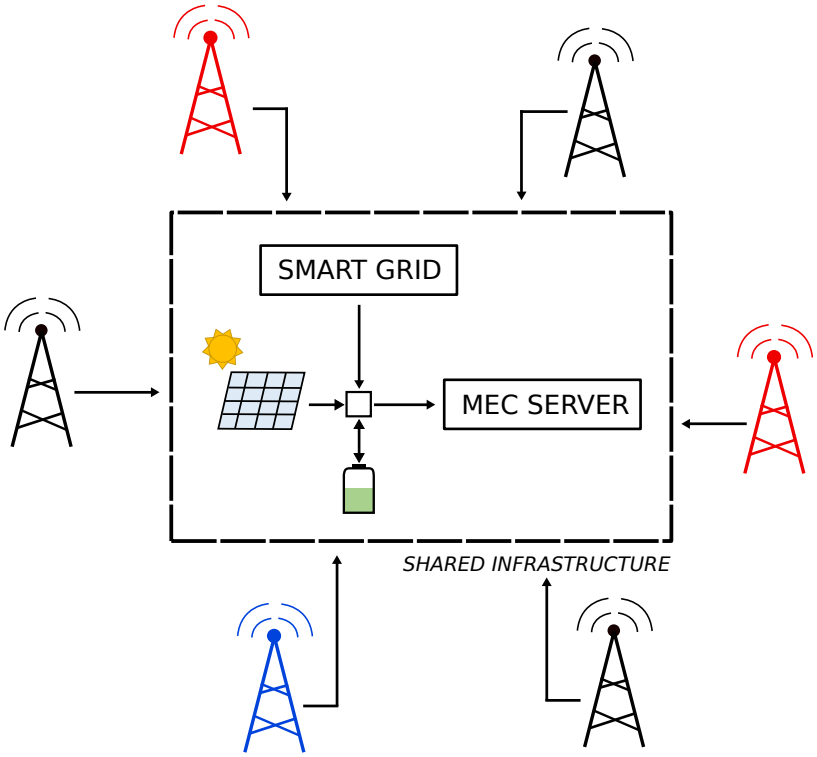

Figure 5.1: Example of the considered scenario where three operators (black, red and blue) share the EH and MEC infrastructure.

5.3. System Model

We consider a densely-deployed macro cell comprising a set $\mathcal{N}$ of $N = |\mathcal{N}|$ BSs. Each BS n belongs to a certain mobile operator $s \in \mathcal{S}$ with a total number of S operators. N_s defines the total number of BSs within operator s. As a major deployment of MEC in line with current trends for future mobile networks as suggested by big network operators (e.g., Huawei Technologies [149]), each macro cell provides a cache-enabled MEC server for computation capabilities. Each MEC server hosts M VMs. Moreover, an EH farm, i.e., one or more solar panels, an energy conversion module and an energy storage device, is co-located with the MEC server for sustainability purposes. Energy supply from the power grid is also available in case is needed. The whole infrastructure, the MEC server along with the EH farm, is to be shared among all the BSs within the same cell, regardless if they belong to different mobile operators. The overall scenario is depicted in Fig. 5.1. Finally, the proposed optimization evolves in slotted time $t = 1, 2, \ldots,$ where the slot duration corresponds to the time granularity of the control and can be changed without requiring any modifications to the following algorithms.

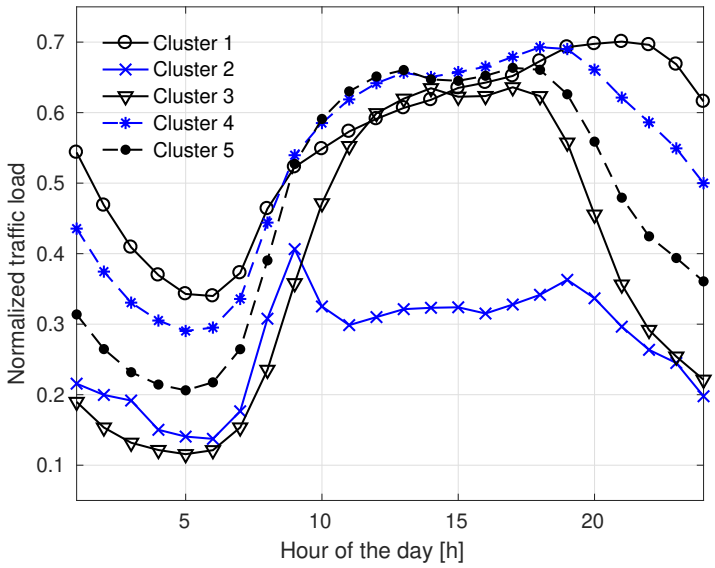

Figure 5.2: Traffic load patterns.

5.3.1. Harvested Energy Profiles

Solar energy generation traces have been obtained using the SolarStat tool [35]. For the solar modules, the commercially available Panasonic N235B photovoltaic technology is considered. Each solar panel has 25 solar cells, leading to a panel area of $0.44\,\mathrm{m}^2$, which is deemed practical for installation in a urban environment. As discussed in [31,35], the EH inflow is generally bell-shaped with a peak around mid-day, whereas the energy harvested during the night is negligible. Here, the framework in [35] is utilized to obtain the amount of energy harvested for each EH farm in time slot t, which is denoted by $h(t)$.

5.3.2. Traffic Load Profiles

Traffic load traces have been obtained using real mobile data from the Big Data Challenge organized by TIM [118]. The dataset is the result of a computation over Call Detail Records (CDRs), logging the user activity within the TIM cellular network for the city of Milan during the months of November and December 2013. For the traffic load traces we use the CDRs related to SMS, calls and Internet activities, performing spatial and temporal aggregation. In this way, we obtain a daily traffic load profile for each BS.

Clustering techniques have been applied to the dataset to understand the behavior of the mobile data. To this end, we use the X-means clustering algorithm [150] to classify the load profiles into several categories. In Fig. 5.2, we show the traffic behavior of five clusters, being cluster 1 the heaviest and cluster 2 the lightest on average daily load. In our numerical results, each BS n has an associated normalized load profile $c_n(t) \in [0, 1]$, which is picked at random as one of the five clusters in Fig. 5.2. We assume the computational load is given by $\Gamma_n(t) = \eta_{comp} c_n(t)$, where η_{comp}

is a parameter depending on the specific network scenario. The aim is to compute $\Gamma_n(t)$ at the edge for each BS whenever possible, i.e., if there are enough computation resources (VMs) available in the MEC server. If not, the remaining load is transferred to a network processor in a cloud server.

5.3.3. Energy Consumption

Given a certain macro cell, the overall energy consumption is formulated as follows for a certain time slot t:

$$o_{\text{tot}}(t) = \sum_{n=1}^{N} o_n(t) + o_{\text{MEC}}(t)\,, \tag{5.1}$$

where $o_n(t)$ is the energy consumption related to BS n, and $o_{\text{MEC}}(t)$ is the MEC server one. Given $c_n(t)$, the BS energy consumption $o_n(t)$ is computed through the linear model in [31] (Eq. (1) in that paper) with $o_n(t) = o_{ind} + \alpha c_n(t)$, where o_{ind} is a load independent value that represents the operation energy, including baseband processing, cooling, etc. $\alpha > 0$ is a system parameter which depends on the BS type, and in product with $c_n(t)$, provides the load dependent component.

Moreover, $o_{\text{MEC}}(t)$ is defined as follows [151]: $o_{\text{MEC}}(t) = o_{\text{idle}} + \gamma(t) o_{\text{dyn}}(t)$, where o_{idle} is the server load-independent operational component, and o_{dyn} is the maximum energy amount that is consumed by the server when it operates at full power. Moreover, o_{dyn} is linearly scaled with respect to the actual computational load $\gamma(t) \in [0, 1]$ processed in time slot t, providing the load-dependent component. This model represents the number of VMs running in time slot t, and on the CPU frequency that is allotted to each virtual machine. Specifically, VMs are instantiated on top of the physical CPU cores, and each VM is given a share of the MEC server CPU, memory and network input/output interfaces. The CPU is thus the main consumer of energy in the MEC server [144] due to the VM-to-CPU share mapping. We also note that, in practical application scenarios, the maximum per-VM computation load to be computed is generally limited up to an assigned value in bytes, named Γ_{max} [135]. Hence, in a given time slot t, each BS n will require $r_n(t) = \lceil \Gamma_n(t)/\Gamma_{max} \rceil$ VMs (with $\Gamma_n(t)$ in bytes, i.e., without normalization) to allocate its total computational load at the edge. The $N \times \tau$ matrix $\boldsymbol{R(t)}$ with elements $r_n(t)$, specifies the VMs needs per BS n over the time horizon τ. However, due to limited resources in the MEC server, the needed $r_n(t)$ VMs may not be allocated to BS n, being $m_n(t) \leq r_n(t)$ the actual number of VMs allocated to BS n in time slot t. $m_n(t)$ is an objective variable found in the optimization problem of Section 5.4. Therefore, it holds that the computational load in the MEC server at time t is given by:

$$\gamma(t) = \frac{\sum_{n=1}^{N} m_n(t)}{M}. \tag{5.2}$$

where M denotes the maximum number of VMs that can be allocated, i.e., the server capacity. Finally, with $f_s(t)$ we indicate the total number of VMs that are assigned to operator $s \in \mathcal{S}$ in time slot t, where $f_s(t) = \sum_{n \in \mathcal{N}_s} m_n(t)$.

5.3.4. Energy Storage Units

Every EH farm within the network provides an energy storage unit, referred also as EB. The EB level for a certain macro cell is denoted by $b(t)$. $B_{\max}$ is the EB capacity. For a certain EB in

current time slot t, $b(t)$ is the EB level at the beginning of time slot t, updated at the beginning of the next time slot $t+1$ as:

$$b(t+1) = b(t) + h(t) - o_{tot}(t) + \theta(t) - l(t)\,, \tag{5.3}$$

where $o_{tot}(t)$ corresponds to the overall energy consumption and thus the amount of energy that is transferred to all BSs within the cell in time slot t to cover the energy demand. $h(t)$ is the amount of energy harvested. $\theta(t)$ represents the energy purchased from the power grid during time slot t. Finally, $l(t)$ represents the losses in the EB due to battery deficiency and charging/discharging processes, and is calculated as $l(t) = \eta_{EB} b(t)$ for a certain time slot t, with η_{EB} being the energy losses factor [30]. The goal is to maximize the use of $h(t)$ to cover the energy demand $o_{tot}(t)$ while minimizing the energy purchase $\theta(t)$ from the electrical grid. Note that $b(t)$ is updated at the beginning of time slot t, whereas $h(t)$ and $o_{tot}(t)$ are only known at the end of it. The expected behavior $\mathbb{E}[h(t) - o_{tot}(t)]$ is obtained through the theory in Section 5.4.1 to make foresighted decisions, where $\mathbb{E}[\cdot]$ is the expectation operator.

5.3.5. Electric Retail Pricing

Hourly electric supply charges have been taken from the US National Grid database [152], considering the energy cost for the state of New York between January 2015 and August 2017. The price that the shared infrastructure within each cell has to pay to purchase energy at a certain time slot t is denoted by $p(t)$.

5.4. Optimization Framework

In this section, we propose an energy and computation resource management framework with two main objectives: (i) maximize the exploitation of the available resources in a fair fashion among BSs belonging to different operators; and (ii) decreasing the monetary cost incurred by energy purchases from the power grid. These two objectives pose two coupled problems, i.e., (i) refers to **P1**, and (ii) to **P2**, that have to be solved sequentially due to the impact of **P1** over the MEC server energy consumption, and therefore in the overall energy consumption used in **P2** (see Eq. (5.1) and (5.3)). The section is organized as follows: first, notation and the two coupled problems are formulated; details about the pattern forecasting are given in Section 5.4.1; the MPC adaptive controller is discussed in Section 5.4.2; lastly, the algorithm steps of the optimization framework are detailed in Section 5.4.3.

Notation: in what follows, boldface symbols, such as $\boldsymbol{b}(t)$, are used to denote variables across multiple time slots, whereas $b(t)$ indicates the corresponding variable at time t. The system to be controlled is described through the following discrete-time model:

$$\boldsymbol{b}(t+1) = \boldsymbol{b}(t) + \boldsymbol{\theta}(t) + \boldsymbol{w}(t) - \boldsymbol{\ell}(t), \tag{5.4}$$

where t is the current time slot. The vector $\boldsymbol{b(t)}$ with elements $b(t)$ denotes the *system state*, representing the energy buffer level for time slots $t, t+1, \ldots, t+\tau-1$, were τ is the optimization horizon. $\boldsymbol{\theta(t)}$ with elements $\theta(t)$ denotes the *control* vector, specifying the amount of energy $\theta(t)$

purchased in every time slot within τ. The vector $\boldsymbol{w(t)}$ with elements $w(t)$ models the *system disturbance*, i.e., the stochastic behavior of the forecast profiles (harvested and consumed energy) and corresponds to $w(t) = h(t) - o_{tot}(t)$. In addition, an energy demand vector $\boldsymbol{d(t)}$ with elements $d(t)$ is defined to represent the minimum energy needed to cover the expected energy consumption within τ. It is calculated for a certain time slot t as follows:

$$\begin{cases} d(t) = 0 \quad if \quad w(t) \geq 0, \\ d(t) = |w(t)| \quad if \quad w(t) < 0. \end{cases} \tag{5.5}$$

Moreover, the $N \times \tau$ matrix $\boldsymbol{M(t)}$ with elements $m_n(t)$, specifies the VMs allocation per BS n over the time horizon τ.

P1 - MEC resources allocation: an equal distribution of MEC resources over time among the different operators is pursued by controlling the VMs allocation per BS regarding the expected traffic load. It should be noted that a maximization on the use of the available resources located in the edge is seeked, i.e., $\gamma(t) \to 1$, assuming that the computation load required from BS is in general higher than the computation capacity of the MEC server, and thus some of this load may be transferred to the core network. Specifically, we want to minimize the difference between the actual computational load processed at the edge $m_n(t)$ per BS n, and the total computational load $r_n(t)$ that BS n has to compute in time slot t in terms of VMs. With π_{VM} we denote a VMs allocation policy, which specifies $\boldsymbol{M(t)} = [m_n(t)], \forall n \in \mathcal{N}$. An optimal policy π^*_{VM} is found as:

$$\begin{aligned} &\pi^*_{VM} = \underset{\pi_{VM}}{\operatorname{argmin}} \left\{ \lim_{\tau \to +\infty} \frac{1}{\tau} \mathbb{E} \left[\sum_{t=0}^{\tau-1} \sum_{n=1}^{N} (r_n(t) - m_n(t))^2 \right] \right\}, \\ &\quad \text{Subject to:} \\ &\quad 0 \leq m_n(t) \leq M, \quad \forall n, \\ &\quad \sum_{n=1}^{N} m_n(t) \leq M, \quad \forall t, \\ &\quad \beta_s \sum_{t=0}^{\tau-1} f_s(t) = \beta_i \sum_{t=0}^{\tau-1} f_i(t), \\ &\quad \text{with: } s = 1, \ldots, S; \quad i = 1, \ldots, S; \quad \text{and } s \neq i\,. \end{aligned} \tag{5.6}$$

The first and second constraints define the bounds with respect to the MEC server capacity. The third constraint guarantees that the VMs allocation over time among the different operators will be fair, where $\beta_s \in [0, 1]$ is a weighted factor defined as $\beta_s = 1 - N_s/N$. This allows the system to distribute proportionally the available MEC resources, designating more VMs to those mobile operators that own more BSs within a cell.

P2 - Grid energy purchase: cost decrease related to energy purchases from the grid is achieved by controlling the amount of energy that the shared infrastructure buys from the electrical grid over time considering harvested energy, traffic load, energy price and stored energy. With π_e

we denote an energy purchase policy, which specifies $\boldsymbol{\theta(t)}$. An optimal policy π_e^* is found as:

$$\begin{aligned}
&\pi_e^* = \underset{\pi_e}{\operatorname{argmin}} \left\{ \lim_{\tau \to +\infty} \frac{1}{\tau} \mathbb{E} \left[\sum_{t=0}^{\tau-1} \left(p(t)\theta(t) + \varepsilon l(t) \right) \right] \right\} , \\
&\quad \text{Subject to:} \\
&\quad \mathbb{E}\left[b(t+1) = b(t) + \theta(t) + w(t) \right] , \\
&\quad d(t) \leq b(t) \leq B_{\max}, \\
&\quad 0 \leq \theta(t) \leq B_{\max} \, .
\end{aligned} \tag{5.7}$$

The goal is to minimize the energy cost over time, i.e., $p(t)\theta(t)$, subject to certain constraints: the first holds the discrete-time model used; the second defines the energy buffer limitations, ensuring through $d(t)$ that the energy buffer contains enough energy to fulfill the expected demand; the third determines the limits in the energy purchasing process. Moreover, the addition of $l(t)$ in the formulation acts as a regularization factor that takes into account the energy losses in the whole process. $\varepsilon > 0$ is a normalizing constant used to equalize both terms in the objective function.

In both Eq. (5.6) and (5.7), the expectation is needed as harvested energy and traffic load are random processes. In real settings, optimally solving both problems is difficult, as energy and load statistics are non-stationary. Therefore, we propose an online approach based on MPC with tracking capabilities over a finite time horizon H, whose objective is to approximate π^* for each one of the two problems.

The framework consists of two main blocks: (i) ***pattern forecasting*** **(Section 5.4.1)** and (ii) ***adaptive control*** **(Section 5.4.2)**. In the first block, the harvested energy and traffic load processes are predicted through a ML approach, specifically using a type of RNN [136]. More details are provided in Section 5.4.1. This allows to track energy and traffic load over time, capturing their statistical behavior and obtaining forecasts for the corresponding time series. Note that energy prices are available one-day ahead, thus their forecasting is not needed. Energy and load forecasts are then fed into the second block where foresighted optimization is performed using MPC. In **P1**, the controller decides the number of VMs allocated to BS n in time slot t, i.e., $m_n(t)$. As for **P2**, this block determines the amount of energy $\theta(t)$ that has to be purchased from the electrical grid at each time slot t. The adaptive control block takes online actions, considering not only the current system state, i.e., harvested energy, traffic load, energy price and EB levels, but also future ones (based on the forecasts from the forecasting block), anticipating events and acting accordingly. More details are given in Section 5.4.2.

5.4.1. Pattern Forecasting

RNN are a generalization of feed-forward neural networks (the input signal goes only one way within the network), that have been devised for handling temporal and predictive problems. LSTM networks are a particular kind of RNN, introduced in [153]. They have been explicitly designed to avoid the long-term dependency issue, which is the cause of the vanishing-gradient problem in normal RNNs [154].

The capability of learning long-term dependencies is due to the structure of the LSTM units, which incorporates gates that regulate the learning process. The neurons in the hidden layers of

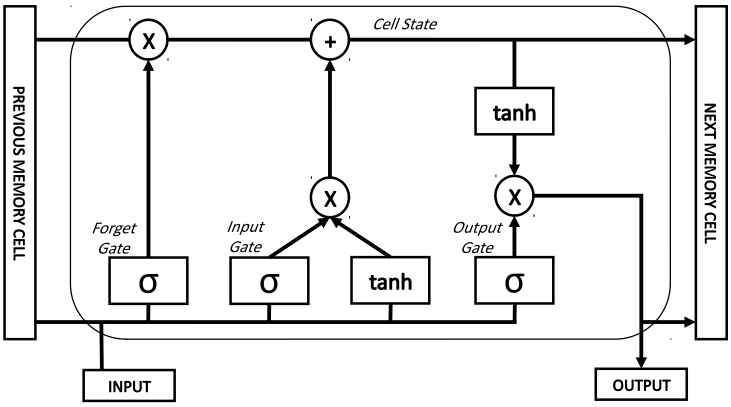

Figure 5.3: LSTM memory cell diagram.

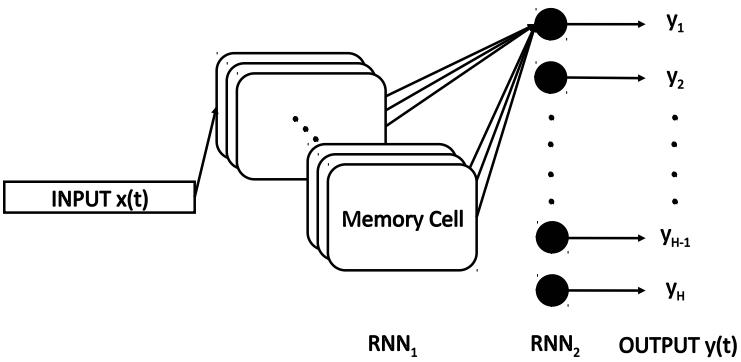

Figure 5.4: LSTM network architecture.

an LSTM are Memory Cells (MCs). A MC has the ability to store or forget information about past network states by using structures called *gates*, which consist of a cascade of a neuron with sigmoidal activation function and a pointwise multiplication block. Thanks to this architecture, the output of each memory cell possibly depends on the entire sequence of past states, making LSTM networks suitable for processing time series with long time dependencies [153]. An LSTM memory cell diagram is presented in Fig. 5.3. The input gate is a neuron with sigmoidal activation function (σ). Its output determines the fraction of the MC input that is fed to the cell state block. Similarly, the forget gate processes the information that is recurrently fed back into the cell state block. The output gate, instead, determines the fraction of the cell state output that is to be used as output of the MC at each time step. Gate neurons usually have sigmoidal activation functions (σ), while the input and cell state use the hyperbolic tangent (tanh) activation function. All the internal connections of the MC have unitary weight [153].

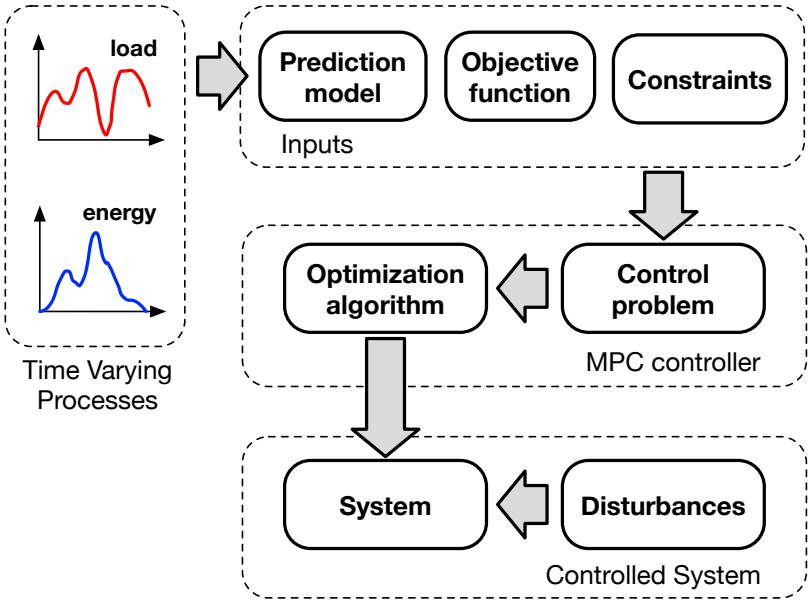

Figure 5.5: Model predictive control framework.

An LSTM neural network [136] has been used to forecast the harvested energy $h(t)$ and the traffic load $c_n(t)$ profiles for each BS n at each time slot t. The proposed architecture for the traffic classification is depicted in Fig. 5.4. In our design, we consider two stacked layers combining one LSTM layer with a final output fully connected layer, i.e., each output neuron from the previous layer is connected to all input neurons of this layer (weights are not shared). Let $\boldsymbol{x(t)}$ be the input vector to the network where it can be $\boldsymbol{x(t)} = \boldsymbol{h(t)}$ or $\boldsymbol{x(t)} = \boldsymbol{c(t)}$ ($\boldsymbol{h(t)}$ corresponds to the energy harvesting dataset and $\boldsymbol{c(t)}$ to the traffic load one). More details about the input datasets are given in Section 5.3 (5.3.1 and 5.3.2 respectively) and Section 5.5.1. The first layer RNN_1 is composed by $N_{RNN_1} = 32$ MCs. The final fully connected layer RNN_2 performs the actual regression where the output vector $\boldsymbol{y(t)}$ with elements $y(t)$ contains the forecast values in the corresponding time series with size $1 \times \tau$, where τ is the finite time horizon. The network is trained using the ADAM optimizer [155] and the Mean Squared Error (MSE) as the objective function. This function is utilized in order to measure the performance of the estimated forecast where the error is obtained as the difference between the real known value $y(t)$ and the estimation $\hat{y}(t)$. It is defined as follows:

$$MSE = \frac{1}{\tau} \sum_{t=1}^{\tau} \left(\hat{y}(t) - y(t)\right)^2 \tag{5.8}$$

During training, Eq. 5.8 is iteratively minimized, by rotating training examples in the batch set so as to span the entire input $\boldsymbol{x(t)}$. Performance evaluation is discussed in Section 5.5.1.

5.4.2. Adaptive Control

A general MPC framework is composed of (i) an input section, (ii) an MPC controller and (iii) a real system [115]. The first block contains the prediction model (see Section 5.4.1). The MPC

solves a control problem at runtime (see below). Finally, the real system block receives the optimal actions from the MPC controller and behaves accordingly. An overall diagram is shown in Fig. 5.5. More details about MPC are given in Section 4.2.2.

The application of MPC theory within **P1** and **P2**, presented in Eq. (5.6) and (5.7), poses new finite-horizon formulations over τ at time k as follows:

P1:

$$\min_{\boldsymbol{M}(k)} \quad \frac{1}{\tau}\mathbb{E}\left[\sum_{k=t}^{t+\tau-1}\sum_{n=1}^{N}(r_n(t)-m_n(t))^2\right] \tag{5.9a}$$

$$\text{subject to:} \quad 0 \leq m_n(t) \leq M, \quad \forall n, \tag{5.9b}$$

$$\sum_{n=1}^{N} m_n(t) \leq M, \quad \forall t, \tag{5.9c}$$

$$\beta_s \sum_{k=t}^{t+\tau-1} f_s(k) = \beta_i \sum_{k=t}^{t+\tau-1} f_i(k), \tag{5.9d}$$

$$\text{with: } s = 1,\ldots,S; i = 1,\ldots,S; s \neq i, \tag{5.9e}$$

$$\text{with: } k = t, t+1, \ldots, t+\tau-1\,.$$

P2:

$$\min_{\boldsymbol{\theta(k)}} \quad \frac{1}{\tau}\mathbb{E}\left[\sum_{k=t}^{t+\tau-1}(p(k)\theta(k)+\varepsilon l(k))\right] \tag{5.10a}$$

$$\text{subject to:} \quad \mathbb{E}\left[b(k+1) = b(k)+\theta(k)+w(k)-\ell(t)\right], \tag{5.10b}$$

$$d(k) \leq b(k) \leq B_{\max}, \tag{5.10c}$$

$$0 \leq \theta(k) \leq B_{\max}, \tag{5.10d}$$

$$\text{with: } k = t, t+1, \ldots, t+\tau-1\,.$$

Since the optimization problem must be solved at runtime, it is strongly preferable to choose a convex optimization formulation such as Eq. (5.10) and (5.9). Here, we have used the `CVX` tool [129] to obtain the optimal solutions $\boldsymbol{\theta(t)}^* = [\theta(t)^*]$ and $\boldsymbol{M(t)}^* = [m_n(t)^*]$.

5.4.3. Algorithm Steps:

The optimization framework performs as follows [130]:

1. at the beginning of time slot t, the system state is obtained: energy buffer level $b(t)$, harvested energy $h(t)$ and traffic load forecasts $c_n(t)$, and energy price within the optimization horizon τ.

2. **P1** is solved by using the traffic load forecasts $c_n(t)$, finding $\boldsymbol{M(t)}^* = [m_n(t)^*]$ and yielding a sequence of control actions over the time horizon (τ slots). By doing this, the expected total energy consumption $o_{\text{tot}}(t)$ over τ is obtained (see Eq. (5.1)) thanks to Eq. (5.2) and the found solution $\boldsymbol{M(t)}^*$.

Parameter	**Value**
Number of BSs per macro cell, N	10
Number of operators per macro cell, S	3
Computational load parameter, η_{comp}	0.2
BS operation energy consumption, o_{ind}	13.6 W
BS type parameter, α	1.1
MEC server static consumption, o_{idle}	3 W
MEC server dynamic consumption, $o_{\text{dyn}}(t)$	6 W
Maximum per-VM computation load, Γ_{max}	100 MB
Energy buffer capacity, $B_{\max}$	1 kW h
Energy losses factor, η_{EB}	0.15
Time slot duration	1 h
Normalizing constant, ε	1
MPC optimization horizon τ	24 h

Table 5.1: System parameters used in the numerical results.

3. the **P2** solution $\boldsymbol{\theta(t)}^* = [\theta(t)^*]$ is found thanks to **P1** solution, yielding a sequence of control actions over the time horizon τ.
4. Only the first action is carried out and the system state is updated upon implementing the required actions, i.e., MEC resource allocation and energy purchase.
5. at next time slot $t+1$, predictions are updated and the optimization cycle is repeated from step 1.

5.5. Numerical Results

In this section, we evaluate the performance of the proposed optimization framework through some numerical results, considering the scenario of Section 5.3. For the EB, we set $B_{\max} = 1\,\text{kW h}$, and we consider Li-Ion battery technology with non-ideal features, i.e., energy losses are contemplated through the parameter η_{EB}. The rest of parameters used for the simulations are listed in Table 5.1. The pattern forecasting block is assessed in Section 5.5.1, whereas results of the overall framework are provided in Section 5.5.2.

5.5.1. Performance Evaluation of the Pattern Forecasting

To assess the performance of the proposed forecasting approach, we utilize the datasets introduced in Sections 5.3.1 and 5.3.2. The solar generation dataset contains 175, 200 samples taken every hour during a period of 20 years in the city of Los Angeles, US. The traffic load dataset has

$1,440$ samples taken every hour for a period of two months in the city of Milan, Italy. For both datasets, we perform τ-steps ahead forecasts, where τ is the optimization horizon (we use $\tau =$ 24 hours), using sequences of 24 past time samples. 80% of the dataset is used for training, while the remaining samples are used to evaluate the accuracy of the obtained forecasts. The setup has been implemented in Python using the high-level neural-networks-API Keras [156], running on top of Tensorflow [157].

An example of forecasting is shown in Fig. 5.6. Harvested energy forecasts ($h(t)$ in Fig. 5.6a) are more precise than load forecasts ($c_n(t)$ in Fig. 5.6b), as solar energy traces follow quite regular bell-shape patterns, which are easier to predict. This fact is confirmed by the average RMSE over the test samples: in the case of $h(t)$ we obtain RMSE $= 0.033$, whereas for $c_n(t)$ we get RMSE $= 0.08$.

5.5.2. Performance Evaluation of the Optimization Framework

This section is split into two subsections discussing the performance of the propose online optimization framework regarding the two tackled problems **P1** and **P2** separately.

P1 - MEC resources allocation: we compare our scheme, named **MPC-P1** against two benchmarks. **B1-P1** distributes the resources equally among the operators. This means each operator gets the same amount of VMs in every time slot t. Hence, no foresighted optimization is performed in this benchmark, but however, it provides fairness. On the other hand, MEC resources are shared proportionally to the BS load in **B2-P1**, i.e., the higher the load, more resources the BS gets. Again, no adaptive control is applied here and also there is no fairness. This benchmark prioritizes to cover the load over the equality among operators.

The curves plotted in Figs. 5.7 and 5.8 are obtained averaging over 500 simulation instances. Each simulation instance accounts for 168 hours, i.e., one week. The harvested energy profile is set at the beginning of each simulation instance starting from a specific date, which is picked at random from the real-trace dataset. For the traffic load, each BS picks one of the five available load clusters at random (see Fig. 5.2). Moreover, the optimization horizon has been set at $\tau = 24$. The number of operators and BSs within a cell are listed in Table 5.1. Regarding the distribution of BSs among operators within a cell, operator 1 owns $N_1 = 2$ BSs, operator 2 has $N_2 = 3$, and the third one owns the rest up to $N = 10$, i.e., it controls $N_3 = 5$ BSs.

In Fig. 5.7, the average computational load over the MEC server capacity, in terms of available number of VMs, is evaluated. The goal is to maximize the amount of load that is computed in the edge, while minimizing the computational load whenever is possible to reduce the energy consumption related to the MEC server (see Eq. 5.1). The average computation load achieved by **B1-P1** and **B2-P1** is always 1, due to the fact that these benchmarks distribute the overall resources among all BSs without dynamic allocation over time. Nonetheless, our scheme **MPC-P1** is able to reduce the computational load while the available resources increase up to the 50% when $M = 50$. On average, it reduces the computation about 20% with respect to the two benchmarks. This result confirms the benefits of the adaptive control in this problem.

Fig. 5.8 shows the average difference between the amount of VMs needed $\boldsymbol{R(t)}$ to cover the load at time slot t and the actual allocated $\boldsymbol{M(t)}$ over the MEC server capacity. If $\boldsymbol{R(t)} - \boldsymbol{M(t)} > 0$, the respective amount of load is sent to the core network to be processed (see Section 5.3.3 for more

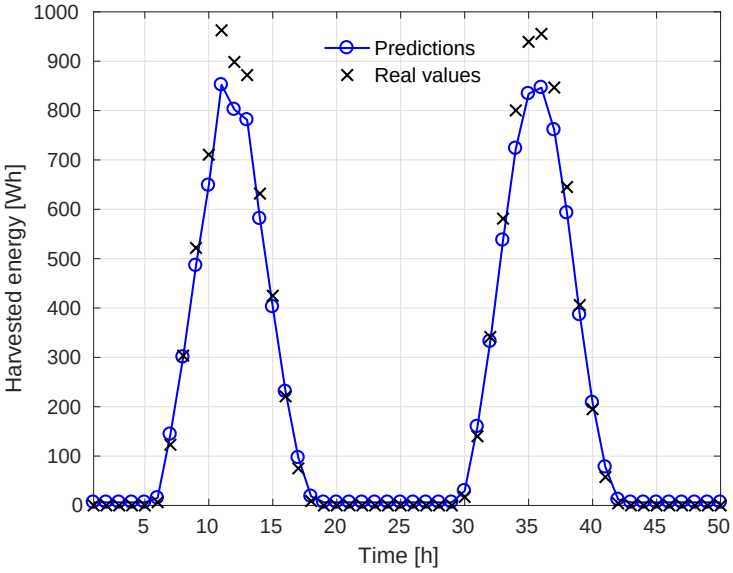

(a) Example of harvested energy $h(t)$ forecast.

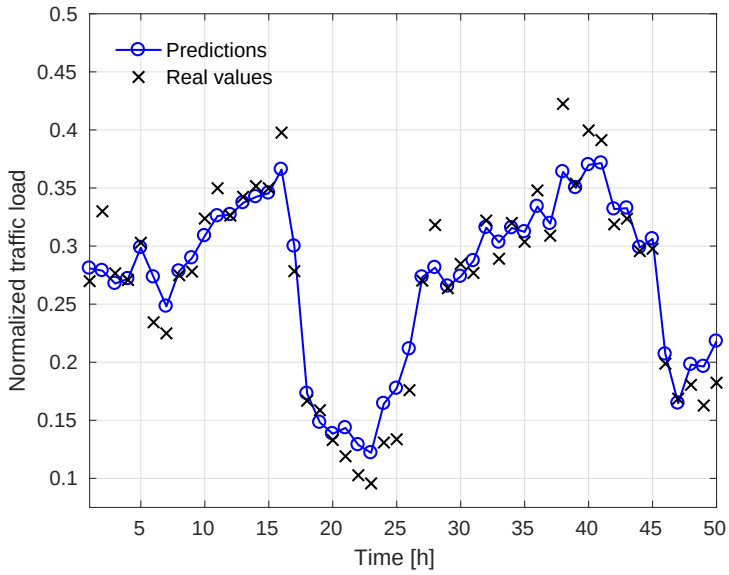

(b) Example of traffic load $c_n(t)$ forecast.

Figure 5.6: LSTM forecasting examples.

details). This happens when the MEC server capacity is not high enough to cover the demand, it can be observed for all the approaches when $M < 30$. If $\boldsymbol{R(t)} - \boldsymbol{M(t)} < 0$, it means that the number of allocated VMs is higher than needed, and then some resources are underutilization. This happens in **B1-P1** and **B2-P1** when the MEC server capacity goes beyond 30 VMs, i.e., these

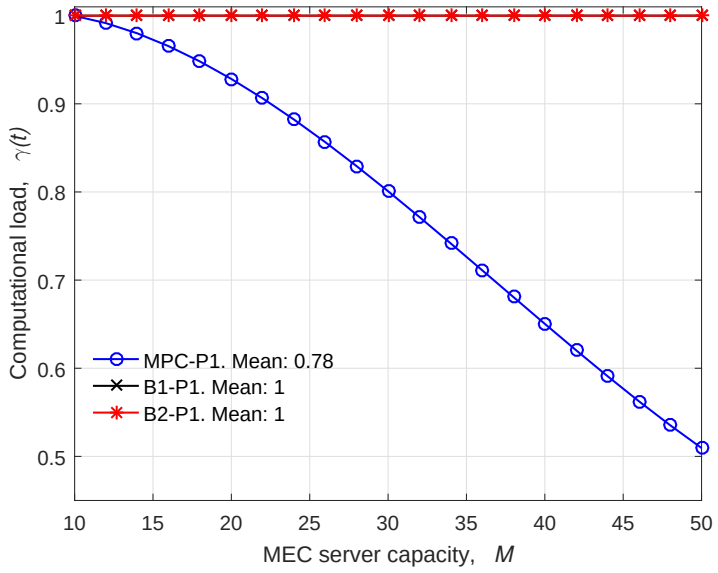

Figure 5.7: Average computational load *vs* capacity in the MEC server.

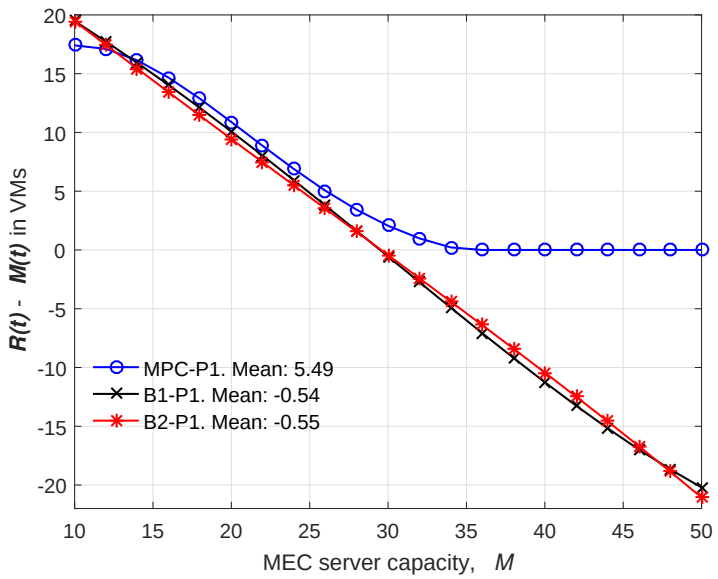

Figure 5.8: Average difference between needed $\boldsymbol{R(t)}$ and allocated $\boldsymbol{M(t)}$ VMs *vs* capacity in the MEC server.

approaches allocate more resources than required to some BSs, increasing the energy consumption of the MEC server without need. In this case, the **MPC-P1** proposal outperforms the benchmarks since it allocates the exact amount of needed VMs to cover the load, without incurring in under

	MPC-P2	**B1-P2**	**B2-P2**
Energy cost [cents/Wh]	0.348	0.791	0.514
Energy buffer level [Wh]	438.33	443.14	90.74

(a) Traffic load probability, ρ

	MPC-P2	**B1-P2**	**B2-P2**
Energy cost [cents/Wh]	0.434	0.891	0.622
Energy buffer level [Wh]	394.52	399.78	22.92

(b) EB losses factor, η_{EB}

	MPC-P2	**B1-P2**	**B2-P2**
Energy cost [cents/Wh]	0.298	0.823	0.457
Energy buffer level [Wh]	526.28	427.11	201.03

(c) EH farm capacity

Table 5.2: Average values of the performance evaluation regarding **P2**.

usage, reflected as $\boldsymbol{R(t)} - \boldsymbol{M(t)} = 0$.

P2 - Grid energy purchase: our proposed scheme, in this case **MPC-P2**, is again compared versus two benchmarks: **B1-P2** performs similarly as **MPC-P2** but however does not consider the use of EH within the system. This is addressed to understand the impact of the integration of renewable energy sources within the mobile network and its capability to create self-sustainable networks. The second benchmark **B2-P2** is *myopic*, as no knowledge into the future behavior of the system is exploited. This approach does not perform any pattern prediction neither foresighted optimization, and the system purchases energy from the grid to cover the current energy demand, i.e., $\theta(t) = d(t)$ for each time slot t. It would refer to a real case where no intelligence has been applied to the system and works following the planned deployment, thus no dynamic control has been configured. We choose these two benchmarks due to the impossibility to compare our scheme against others from the literature since, to the best of out knowledge, the considered scenario here is novel and has not been investigated yet.

In Fig. 5.9, we show the system operation of the **MPC-P2** approach over a day. Based on the energy price $p(t)$ and on the expected behavior of $\mathbb{E}[h(t) - o_{tot}(t)]$, the adaptive control scheme purchases energy over time. One peak in the purchase process (blue curve) can be observed around six in the morning ($t = 6$), due to the low energy price at that time. Another increasing purchase time is noticed from $t = 16$ (4 pm) when the disturbance, i.e., $w(t) = h(t) - o_{tot}(t)$ (green curve) decreases, which corresponds to an increase in the expected traffic load and a decrease in the expected harvested energy due to the approaching sunset.

The results plotted in Figs. 5.10, 5.11 and 5.12 are obtained averaging over 500 simulation instances. Each simulation instance accounts for 168 hours, i.e., one week. The harvested energy

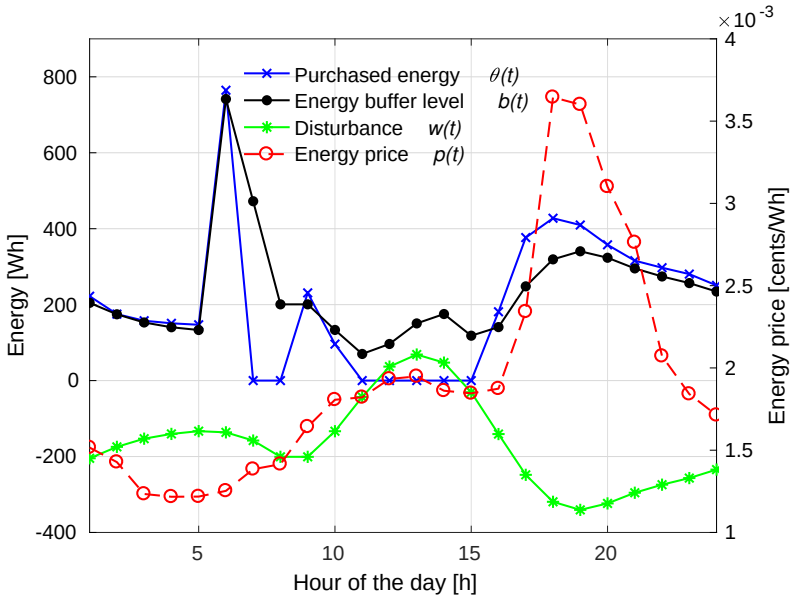

Figure 5.9: MPC behavior over one day.

profile is set at the beginning of each simulation instance starting from a specific date, which is picked at random from the real-trace dataset. For the traffic load in Figs. 5.11 and 5.12, each BS picks one of the five available load clusters at random (see Fig. 5.2).

For the traffic load in Fig. 5.10, each BS picks between cluster 1 and cluster 2 (see Fig. 5.2) with probability ρ. Cluster 1 refers to the traffic load profile with the highest average load ($\rho = 1$), and cluster 2 to the lowest ($\rho = 0$). The sweep over ρ allows to evaluate the performance of the framework from high to load network load conditions. The energy buffer capacity $B_{\max}$ and the EB losses factor η_{EB} are set with the values from Table 5.1. In Fig. 5.10, we show the average purchased energy comparison across different traffic load configurations. As expected, the higher the traffic load, i.e., $\rho = 1$, the higher the amount of energy that is purchased from the power grid. However, our approach **MPC-P2** leads to a reduction in the purchased energy of more than 50% with respect to **B1-P2** and about 26% for **B2-P2** on average.

In Fig. 5.11, the energy buffer capacity $B_{\max}$ is set as the value from Table 5.1. In this case, a sweep over the EB losses factor η_{EB} is performed to understand how important are the non-ideal processes in the energy storage for the optimization. The average purchased energy against η_{EB} is shown where it can be observed that more energy is needed to be purchased when higher losses. Again, our scheme **MPC-P2** outperforms the two benchmarks: there is a reduction of about 52% with respect to **B1-P2** and close to 32% for **B2-P2**. It is worth to mention that for the ideal EB case, i.e., $\eta_{EB} = 0$, the best performance is achieved by **B2**. However, a non-ideal EB has been considered for the rest of results to adequate for a real scenario. Moreover, it should be noted that the increasing slope of **MPC-P2** is much less pronounced than the others. This is a remarkable result, meaning that our approach is able to dynamically adapt to higher losses but however without incurring in higher energy purchases and related costs. This can be confirmed

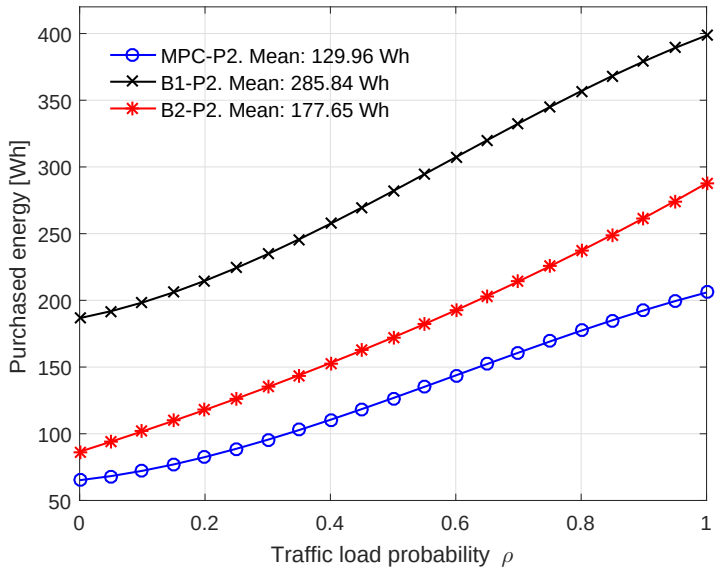

Figure 5.10: Average purchased energy *vs* traffic load.

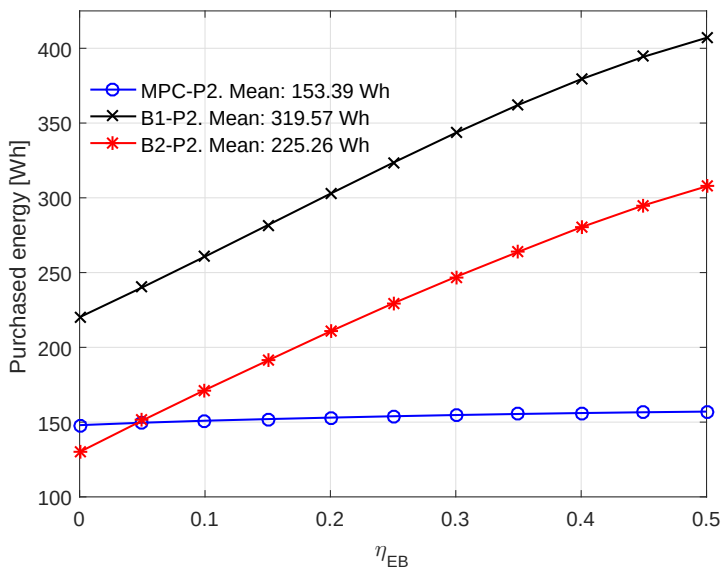

Figure 5.11: Average purchased energy *vs* EB losses factor.

with the results shown in Table 5.2b.

In Fig. 5.12, the energy buffer losses factor η_{EB} is set as the value from Table 5.1. In this figure, the average purchased energy over several EH farm capacities is shown. The EH farm capacity refers to the number or size of solar panels equipped within the shared infrastructure and also refers

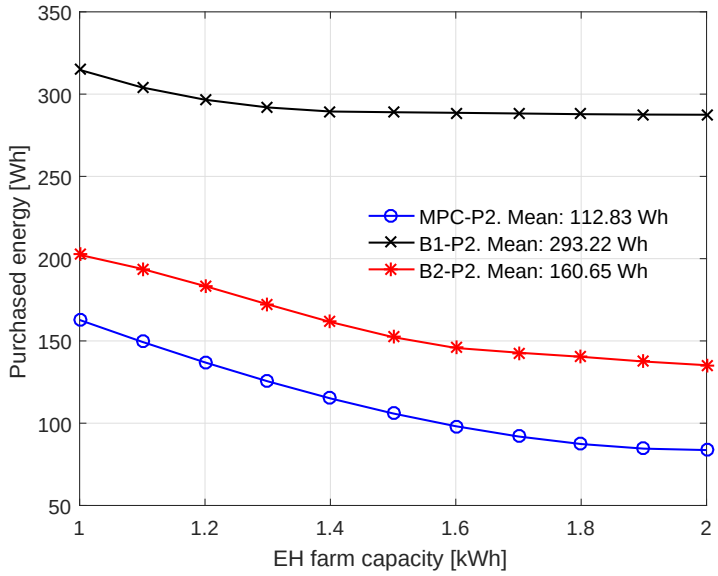

Figure 5.12: Average purchased energy *vs* EH farm capacity.

to the energy storage capacity. Actually, in this graph, both parameters are linearly dependent. Hence, the abscissa axis of Fig. 5.12 shows the maximum EB capacity. As expected, an increase in the EH capabilities translates into a decrease in the energy purchase needs. In this case, **MPC-P2** and **B2-P2** behave with a similar slope, however **MPC-P2** is able to purchase less energy than **B2-P2** in about 30%. This reduction is more than 60% with respect to **B1-P2**.

Lastly, more numerical results regarding average energy costs and EB levels are presented in Table 5.2. Conclusions about energy costs are the same as those aforementioned for energy purchases, i.e., **MPC-P2** outperforms both benchmarks with notable results. As for the average EB level, **MPC-P2** and **B1-P2** perform with similar results: they are able to maintain an average medium level with respect to $B_{\max}$, although **B1-P2** requires to purchase much more energy, as we have discussed before, due to the lack of renewable energy sources to power the network. **B2-P2** provides a much lower EB level over time due to its own nature, i.e., the benchmark purchases energy to cover the current demand, preventing the EB to be filled up with surplus energy. It should be noted that **MPC-P2** allows the possibility to set a certain desired EB level, named B_{ref}. This could be done by introducing another objective function in **P2**, Eq. 5.7, as follows: $f_{B_{\text{ref}}} = (b(t) - B_{\text{ref}})^2$. By doing so, the system can be configured to save as much energy as possible by setting B_{ref} close to 0. In this way, **MPC-P2** would reduce even more the energy purchased over time. However, this configuration may entail some risks due to the possible sudden rise in traffic demand or drop in harvested energy, which would compromise the network service and could produce an outage. Therefore, a more balanced B_{ref} is desirable dealing with the tradeoff between saving energy but ensuring the service.

Finally, we evaluate the impact of the optimization horizon τ in the foresighted optimization

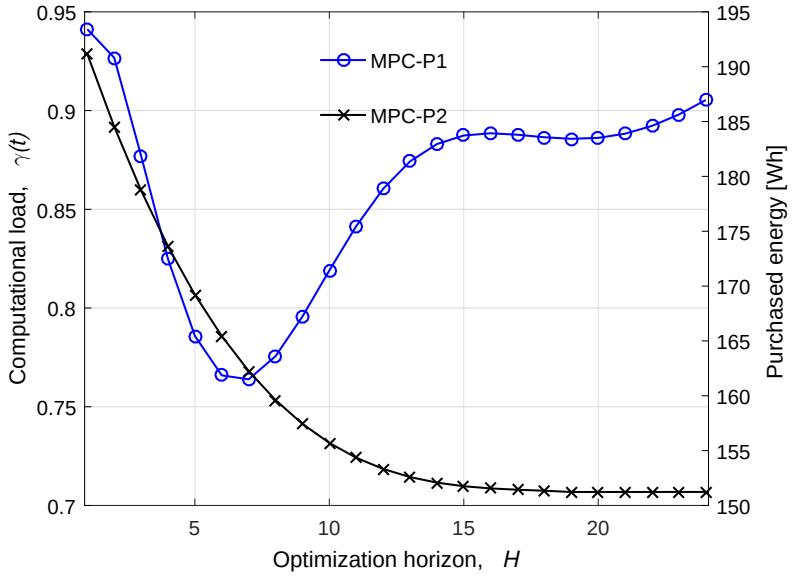

Figure 5.13: Optimization horizon evaluation.

for both problems **P1** and **P2** in Fig. 5.13. It can be observed how the better performance is achieved when $\tau = 7$ for **P1** and $\tau = 24$ for **P2**. After reaching the minimum, both curves start growing up due to the increasing uncertainties in the forecasting procedure, although the slope for **P2** is much less pronounced than in **P1**. The different optimal horizon value comes from the fact that **P1** only uses forecasts regarding the BSs traffic load, while **P2** also uses energy harvesting predictions together with the traffic load ones.

5.6. Conclusions

In this chapter, we have combined EH and MEC paradigms within a shared infrastructure equipped with a solar EH farm for energy sustainability together with a MEC server for low-latency computation. Two main goals are pursued: (i) decreasing the monetary cost incurred by energy purchases from the power grid; and (ii) maximize the exploitation of the available resources at the edge in a fair fashion among BSs belonging to different operators. To do so, we have devised an online framework combining pattern forecasting via an LSTM RNN that learns energy harvesting and traffic load profiles over time, and adaptive control though MPC for dynamic resource allocation. Numerical results, obtained with real-world harvested energy, traffic load, and energy price traces, show that our proposal is able to reduce the amount of purchased energy from the electrical grid of more than 50% with respect to the case where no EH is considered, and about 30% with respect to the case where the optimization is performed disregarding future energy and traffic load forecasts. Moreover, it is capable of reducing the energy consumption related to edge computation about 20% with respect to two benchmarks.

6

Conclusions

In this thesis, we have discussed the role of energy in the design of eco-friendly cost-effective sustainable mobile networks and, in particular, we have elaborated on the use of energy harvesting technology as a means to decrease the environmental footprint of the 5G network. Specifically, we have devised energy management strategies for the 5G mobile network with the main goals of: (i) improving the energy balance across base stations and other network elements, (ii) understanding how the energy can be exchanged either among network elements and the electrical grid, and (iii) investigating how renewable energy sources can be utilized within network elements to provide better performance to the end users (e.g., throughput, coverage, etc.), and reduce the energy consumption (i.e., carbon footprint) within the 5G network infrastructure.

Therefore, we have addressed, formulated and solved some of the problems related to the energy management in different scenarios within the 5G mobile network, covering the following topics: (i) *Wireless Energy Transfer* where we have investigated the tradeoffs involved in the recharging process from base stations to end users; (ii) *Energy Cooperation in Mobile Networks* where we have targeted deployments featuring BSs with EH capabilities that are able to transfer energy among them; (iii) *Energy Trading with the Electrical Grid* where schemes to diminish the cost incurred in the energy purchases from the electrical grid have been proposed; and (iv) *Energy Harvesting and Edge Computing Resource Management* where EH and MEC paradigms have been combined within a multi-operator infrastructure sharing scenario to maximize the exploitation of the network resources while decreasing monetary costs.

Extensive literature has been surveyed in Chapter 2, highlighting open issues and challenges of which some of them have been assessed throughout the several chapters of this thesis. Specifically, the energy transfer from base stations to end users by using transmit beamforming to wirelessly charge mobile UEs in densely-deployed MISO femtocell networks has been tackled in Chapter 3. We have designed several policies to assess which users are to be charged and when, while prioritizing them based on their location and on their battery level. The main conclusions are that: (i) UE location estimation allows heuristic policies to perform very close to the optimum; (ii) mobility helps to increase the power transfer efficiency and best results are achieved when users move in groups; (iii) wireless charging can substantially reduce the fraction of nodes with depleted battery. However, this comes at the expense of constantly transmitting power and transfer efficiencies are too low under any scenario to make WPT technology a viable solution when distances exceed a few meters.

In Chapter 4, the energy cooperation among EH BSs in mobile networks is addressed to provide energy self-sustainability through the use of own-generated energy and carefully planned energy transfers among BSs. This amounts to a combined learning and optimization problem, where learning is carried out on energy arrival (harvested ambient energy) and traffic load traces and this knowledge is exploited, at runtime, for the computation of optimal energy transfer policies

among the distributed energy buffers. This foresighted optimization is performed combining model predictive control and convex optimization techniques. Numerical results reveal great advantages over the case where energy transfer schedules are optimized disregarding future energy and load forecasts: the amount of energy purchased from the power grid is reduced by more than 50% and the outage probability is lowered to zero in nearly all scenarios.

Finally, infrastructure sharing among mobile network operators is exploited in Chapter 5, combining EH and MEC paradigms towards energy sustainability and low-latency computation at the edge. We have devised an online framework combining pattern forecasting via an LSTM RNN that learns energy harvesting and traffic load profiles over time, and adaptive control though MPC for dynamic resource allocation. Our proposal is able to reduce the amount of purchased energy from the electrical grid of more than 50% with respect to the case where no EH is considered, and about 30% with respect to the case where the optimization is performed disregarding future energy and traffic load forecasts. Moreover, it is capable of reducing the energy consumption related to edge computation about 20% with respect to two benchmarks.

To summarize, we have focused on the design of energy management strategies to build sustainable mobile networks where the application of learning techniques along with adaptive control tools and foresighted optimization have provided remarkable results in decreasing energy costs related to purchases from the power grid and efficiency among network elements.

Acknowledgments

This work has received funding from the European Union's Horizon 2020 research and innovation programme under the Marie Sklodowska-Curie grant agreement No. 675891 (SCAVENGE).

List of Publications

This thesis summarizes the work developed over three years where the main outcomes are the following articles.

Journal papers:

[**J1**] N. Piovesan, **A. F. Gambin**, M. Miozzo, M. Rossi, P. Dini, "Energy Sustainable Paradigms and Methods for Future Mobile Networks: a Survey", *Special Issue on Energy-aware Design for Sustainable 5G Networks (Elsevier Computer Communications)*, vol. 119, pp. 101–117, April 2018.

[**J2**] T. Dlamini, **A. F. Gambin**, D. Munaretto, M. Rossi, "Online Supervisory Control and Resource Management for Energy Harvesting BS Sites Empowered with Computation Capabilities", *Journal on Wireless Communication and Mobile Computing, Hindawi*, vol. 2019, February 2019.

[**J3**] **A. F. Gambin**, M. Scalabrin, M. Rossi, "Online Power Management Strategies for Energy Harvesting Mobile Networks", *IEEE Transactions on Green Communications and Networking*, vol. 3, no. 3, pp. 721-738, March 2019.

[**J4**] H. Trinh, **A. F. Gambin**, L. Giupponi, M. Rossi, P. Dini, "Classification of Mobile Services and Apps through Physical Channel Fingerprinting: a Deep Learning Approach", submitted to *IEEE Transactions on Mobile Computing*, April 2019.

[**J5**] **A. F. Gambin**, M. Rossi, "Energy Harvesting and Edge Computing Sharing Framework in Multi-Operator Mobile Networks", submitted to *IEEE Transactions on Network and Service Management*, April 2019.

Conference papers:

[**C1**] L. Bonati, **A. F. Gambin**, M. Rossi, "Wireless Power Transfer under the Spotlight: Charging Terminals amid Dense Cellular Networks," in *IEEE International Symposium on a World of Wireless Mobile and Multimedia Networks (WoWMoM)*. Macao, China: IEEE, Jun 2017.

[**C2**] **A. F. Gambin**, M. Rossi, "Energy Cooperation for Sustainable Base Station Deployments: Principles and Algorithms," in *IEEE Global Communications Conference (GLOBECOM)*. Singapore, Singapore: IEEE, Dec 2017. **Best Paper Award in Green Communications Systems and Networks Symposium.**

[**C3**] **A. F. Gambin**, E. Gindullina, L.Badia, M. Rossi, "Energy Cooperation for Sustainable IoT Services within Smart Cities", in *IEEE Wireless Communications and Networking Conference*

(WCNC). Barcelona, Spain: IEEE, April 2018.

[C4] A. F. Gambin, M. Rossi, "Energy Cooperation Strategies for Sustainable Mobile Networks", in *1st CTTC Workshop.* Barcelona, Spain: Sept 2018.

[C5] T. Dlamini, **A. F. Gambin**, M. Rossi, "Online Resource Management in Energy Harvesting BS Sites through Prediction and Soft-Scaling of Computing Resources", in *IEEE International Symposium on Personal, Indoor and Mobile Radio Communications (PIMRC).* Bologna, Italy: IEEE, Sept 2018.

[C6] A. F. Gambin, M. Rossi, "Smart Energy Policies for Sustainable Mobile Networks via Forecasting and Adaptive Control", in *IEEE Global Communications Conference (GLOBECOM).* Abu Dhabi, EAU: IEEE Dec 2018.

[C7] T. Dlamini, **A. F. Gambin**, "Adaptive Resource Management for a Virtualized Computing Platform in Edge Computing", in *IEEE SECON 2019 workshop on Edge Computing for Cyber Physical Systems (CyberEdge).* Boston, MA, USA: IEEE June 2019.

[C8] A. F. Gambin, "Energy Management Towards Sustainable Mobile Networks", in *IEEE SoftCOM 2019 SCAVENGE Workshop.* Split, Croatia: IEEE Sept 2019.

Remark: in addition to the main topics presented throughout the thesis, our research activity also covered another relevant topic summarized in the following.

Data Analytics and Traffic Characterization for Usage Patterns in LTE Mobile Networks

The automatic classification of applications and services is an invaluable feature for new generation mobile networks. In **[J4]** publication (see above), we propose and validate algorithms to perform this task, at *runtime*, from the *raw physical channel* of an *operative mobile network*, without having to decode and/or decrypt the transmitted flows. Towards this, we decode Downlink Control Information (DCI) messages carried within the Long Term Evolution Physical Downlink Control CHannel (PDCCH). DCI messages are sent by the radio cell in clear text and, in this paper, are utilized to classify the applications and services executed at the connected mobile terminals. Two datasets are collected through a large measurement campaign: one labeled, used to train the classification algorithms, and one unlabeled, collected from four radio cells in the metropolitan area of Barcelona (Spain). Among other approaches, our Convolutional Neural Network (CNN) classifier provides the highest classification accuracy of 99%. The CNN classifier is then augmented with the capability of rejecting sessions whose patterns do not conform to those learned during the training phase, and is subsequently utilized to attain a fine grained decomposition of the traffic for the four monitored radio cells, in an *online* and *unsupervised* fashion.

This activity is the result of a collaboration within the Communication Networks Division at Centre Tecnològic Telecomunicacions Catalunya (CTTC), Castelldefels (Spain). See **[J4]** publication for more details.

References

[1] C. R. Valenta and G. D. Durgin, "Harvesting wireless power: Survey of energy-harvester conversion efficiency in far-field, wireless power transfer systems," *IEEE Microwave Magazine*, vol. 15, no. 4, pp. 108–120, June 2014.

[2] F. Bai and A. Helmy, "A Survey of Mobility Models," *Wireless Adhoc Networks*, vol. 206, pp. 147–176, June 2004.

[3] A. Carroll and G. Heiser, "The systems hacker's guide to the galaxy energy usage in a modern smartphone," in *ACM Proceedings of the 4th Asia-Pacific Workshop on Systems*, Singapore, Singapore, July 2013.

[4] P. Cerwall, P. Jonsson, and R. Möller, "Q3 2018 Ericsson Mobility Report," *Ericsson, Sweden, Tech. Rep.*, Nov 2018.

[5] International Telecommunication Union, "ICT Facts & Figures 2016," [Online]. Available: http://www.itu.int/en/ITU-D/Statistics/Documents/facts/ICTFactsFigures2016.pdf, June 2016 (accessed April, 2019).

[6] A. S. Andrae and T. Edler, "On global electricity usage of communication technology: trends to 2030," *Challenges*, vol. 6, no. 1, pp. 117–157, April 2015.

[7] A. Antonopoulos, E. Kartsakli, A. Bousia, L. Alonso, and C. Verikoukis, "Energy-efficient infrastructure sharing in multi-operator mobile networks," *IEEE Communications Magazine*, vol. 53, no. 5, pp. 242–249, 2015.

[8] A. Fehske, J. Malmodin, G. Biczók, and G. Fettweis, "The Global Footprint of Mobile Communications: The Ecological and Economic Perspective," *IEEE Communications Magazine, issue on Green Communications*, vol. 49, no. 8, pp. 55–62, August 2011.

[9] X. Lu, D. Niyato, P. Wang, D. I. Kim, and Z. Han, "Wireless charger networking for mobile devices: fundamentals, standards, and applications," *IEEE Wireless Communications*, vol. 22, no. 2, pp. 126–135, Apr 2015.

[10] S. Bi, C. K. Ho, and R. Zhang, "Wireless powered communication: opportunities and challenges," *IEEE Communications Magazine*, vol. 53, no. 4, pp. 117–125, April 2015.

[11] Y. Zeng and R. Zhang, "Optimized training design for wireless energy transfer," *IEEE Transactions on Communications*, vol. 63, no. 2, pp. 536–550, February 2015.

[12] R. Zhang and C. K. Ho, "MIMO broadcasting for simultaneous wireless information and power transfer," *IEEE Transactions on Wireless Communications*, vol. 12, no. 5, pp. 1989–2001, May 2013.

[13] Z. Xiang and M. Tao, "Robust beamforming for wireless information and power transmission," *IEEE Wireless Communications Letters*, vol. 1, no. 4, pp. 372–375, August 2012.

[14] A. M. Fouladgar and O. Simeone, "On the transfer of information and energy in multi-user systems," *IEEE Communications Letters*, vol. 16, no. 11, pp. 1733–1736, November 2012.

[15] B. K. Chalise, Y. D. Zhang, and M. G. Amin, "Energy harvesting in an OSTBC based amplify-and-forward MIMO relay system," in *IEEE International Conference on Acoustics, Speech and Signal Processing (ICASSP)*, Kyoto, Japan, March 2012, pp. 3201–3204.

[16] P. V. Mekikis, A. Antonopoulos, E. Kartsakli, A. S. Lalos, L. Alonso, and C. Verikoukis, "Information Exchange in Randomly Deployed Dense WSNs With Wireless Energy Harvesting Capabilities," *IEEE Transactions on Wireless Communications*, vol. 15, no. 4, pp. 3008–3018, April 2016.

[17] P. V. Mekikis, A. Antonopoulos, E. Kartsakli, L. Alonso, and C. Verikoukis, "Connectivity Analysis in Wireless-Powered Sensor Networks with Battery-Less Devices," in *IEEE Global Communications Conference (GLOBECOM)*, Washington DC, USA, Dec 2016, pp. 1–6.

[18] H. Ju and R. Zhang, "User cooperation in wireless powered communication networks," in *IEEE Global Communications Conference (GLOBECOM)*, Austin, TX, USA, December 2014, pp. 1430–1435.

[19] L. Liu, R. Zhang, and K. C. Chua, "Multi-antenna wireless powered communication with energy beamforming," *IEEE Transactions on Communications*, vol. 62, no. 12, pp. 4349–4361, December 2014.

[20] G. Yang, C. K. Ho, R. Zhang, and Y. L. Guan, "Throughput Optimization for Massive MIMO Systems Powered by Wireless Energy Transfer," *IEEE Journal on Selected Areas in Communications*, vol. 33, no. 8, pp. 1640–1650, August 2015.

[21] L. Bonati, A. F. Gambin, and M. Rossi, "Wireless Power Transfer under the Spotlight: Charging Terminals amid Dense Cellular Networks," in *IEEE International Symposium on a World of Wireless Mobile and Multimedia Networks (WoWMoM).* Macao, China: IEEE, Jun 2017.

[22] Y. K. Chia, S. Sun, and R. Zhang, "Energy Cooperation in Cellular Networks with Renewable Powered Base Stations," *IEEE Transactions on Wireless Communications*, vol. 13, no. 12, pp. 6996–7010, December 2014.

[23] S. Hur, T. Kim, D. J. Love, J. V. Krogmeier, T. A. Thomas, and A. Ghosh, "Millimeter wave beamforming for wireless backhaul and access in small cell networks," *IEEE Transactions on Communications*, vol. 61, no. 10, pp. 4391–4403, October 2013.

[24] B. Gurakan, O. Ozel, J. Yang, and S. Ulukus, "Energy cooperation in energy harvesting communications," *IEEE Transactions on Communications*, vol. 61, no. 12, pp. 4884–4898, December 2013.

[25] E. Gelenbe and E. T. Ceran, "Energy Packet Networks With Energy Harvesting," *IEEE Access*, vol. 4, pp. 1321–1331, March 2016.

[26] B. Kreiner and J. Reeves, "Packetized power," [Online]. Available: http://google.com/patents/US20140013146, January 2014 (accessed May, 2019), US Patent App. 14/010,674.

[27] G. Zheng, Z. Ho, E. A. Jorswieck, and B. Ottersten, "Information and energy cooperation in cognitive radio networks," *IEEE Transactions on Signal Processing*, vol. 62, no. 9, pp. 2290–2303, May 2014.

[28] J. Xu, L. Duan, and R. Zhang, "Cost-aware green cellular networks with energy and communication cooperation," *IEEE Communications Magazine*, vol. 53, no. 5, pp. 257–263, May 2015.

[29] J. Xu and R. Zhang, "CoMP Meets Smart Grid: A New Communication and Energy Cooperation Paradigm," *IEEE Transactions on Vehicular Technology*, vol. 64, no. 6, pp. 2476–2488, June 2015.

[30] M. Oikonomakou, A. Antonopoulos, L. Alonso, and C. Verikoukis, "Fairness in multi-operator energy sharing," in *IEEE International Conference on Communications (ICC).* Paris, France: IEEE, May 2017, pp. 1–6.

[31] D. Zordan, M. Miozzo, P. Dini, and M. Rossi, "When telecommunications networks meet energy grids: cellular networks with energy harvesting and trading capabilities," *IEEE Communications Magazine*, vol. 53, no. 6, pp. 117–123, June 2015.

[32] H. S. Dhillon, Y. Li, P. Nuggehalli, Z. Pi, and J. G. Andrews, "Fundamentals of heterogeneous cellular networks with energy harvesting," *IEEE Transactions on Wireless Communications*, vol. 13, no. 5, pp. 2782–2797, May 2014.

[33] M. A. Marsan, G. Bucalo, A. D. Caro, M. Meo, and Y. Zhang, "Towards zero grid electricity networking: Powering BSs with renewable energy sources," in *IEEE International Conference on Communications Workshops (ICC)*, Budapest, Hungary, June 2013, pp. 596–601.

[34] G. Lee, W. Saad, M. Bennis, A. Mehbodniya, and F. Adachi, "Online Ski Rental for ON/OFF Scheduling of Energy Harvesting Base Stations," *IEEE Transactions on Wireless Communications*, vol. 16, no. 5, pp. 2976–2990, May 2017.

[35] M. Miozzo, D. Zordan, P. Dini, and M. Rossi, "SolarStat: Modeling photovoltaic sources through stochastic markov processes," in *IEEE International Energy Conference (ENERGYCON).* Cavtat, Croatia: IEEE, May 2014, pp. 688–695.

[36] N. Piovesan and P. Dini, "Optimal direct load control of renewable powered small cells: A shortest path approach," *Internet Technology Letters*, pp. e7–n/a, 2017, e7.

[37] M. Miozzo, L. Giupponi, M. Rossi, and P. Dini, "Distributed Q-learning for energy harvesting Heterogeneous Networks," in *IEEE International Conference on Communication Workshop (ICCW)*, London, UK, June 2015, pp. 2006–2011.

[38] J. S. Vardakas, N. Zorba, and C. V. Verikoukis, "A survey on demand response programs in smart grids: Pricing methods and optimization algorithms," *IEEE Communications Surveys & Tutorials*, vol. 17, no. 1, pp. 152–178, Firstquarter 2015.

[39] L. P. Qian, Y. J. A. Zhang, J. Huang, and Y. Wu, "Demand response management via real-time electricity price control in smart grids," *IEEE Journal on Selected Areas in Communications*, vol. 31, no. 7, pp. 1268–1280, July 2013.

[40] I. S. Bayram, M. Z. Shakir, M. Abdallah, and K. Qaraqe, "A survey on energy trading in smart grid," in *IEEE Global Conference on Signal and Information Processing (GlobalSIP)*, Atlanta, GA, USA, December 2014, pp. 258–262.

[41] W. Wei, F. Liu, and S. Mei, "Energy pricing and dispatch for smart grid retailers under demand response and market price uncertainty," *IEEE Transactions on Smart Grid*, vol. 6, no. 3, pp. 1364–1374, May 2015.

[42] C. Huang and S. Sarkar, "Dynamic pricing for distributed generation in smart grid," in *IEEE Green Technologies Conference*, Denver, USA, April 2013, pp. 422–429.

[43] A.-H. Mohsenian-Rad, V. W. Wong, J. Jatskevich, R. Schober, and A. Leon-Garcia, "Autonomous demand-side management based on game-theoretic energy consumption scheduling for the future smart grid," *IEEE Transactions on Smart Grid*, vol. 1, no. 3, pp. 320–331, December 2010.

[44] I. Zenginis, J. S. Vardakas, C. Echave, M. Morató, J. Abadal, and C. V. Verikoukis, "Cooperation in microgrids through power exchange: An optimal sizing and operation approach," *Applied Energy*, vol. 203, no. Supplement C, pp. 972 – 981, 2017.

[45] Q. Dong, L. Yu, W.-Z. Song, L. Tong, and S. Tang, "Distributed demand and response algorithm for optimizing social-welfare in smart grid," in *IEEE International Parallel & Distributed Processing Symposium (IPDPS)*, Shanghai, China, May 2012, pp. 1228–1239.

[46] P. D. Lund, J. Lindgren, J. Mikkola, and J. Salpakari, "Review of energy system flexibility measures to enable high levels of variable renewable electricity," *Renewable and Sustainable Energy Reviews*, vol. 45, pp. 785–807, May 2015.

[47] K. Zhang, Y. Mao, and S. Leng, "Poster paper: A green transmission power control scheme for cellular networks in smart grid," in *IEEE International Conference on Communications and Networking in China (CHINACOM)*, Maoming, China, August 2014, pp. 638–639.

[48] S. Bu, F. R. Yu, and Y. Qian, "Energy-efficient cognitive heterogeneous networks powered by the smart grid," in *IEEE International Conference on Computer Communications (INFOCOM)*, Turin, Italy, April 2013, pp. 980–988.

[49] M. J. Farooq, H. Ghazzai, and A. Kadri, "A stochastic geometry-based demand response management framework for cellular networks powered by smart grid," in *IEEE Wireless Communications and Networking Conference (WCNC)*, Doha, Qatar, April 2016, pp. 1–6.

[50] H. Ghazzai, E. Yaacoub, and M. s. Alouin, "A game theoretical approach for cooperative environmentally friendly cellular networks powered by the smart grid," in *IEEE Online Conference on Green Communications (OnlineGreenComm)*, November 2014, pp. 1–6.

[51] D. Niyato, X. Lu, and P. Wang, "Adaptive Power Management for Wireless Base Stations in a Smart Grid Environment," *IEEE Wireless Communications*, vol. 19, no. 6, pp. 44–51, December 2012.

[52] J. Leithon, S. Sun, and T. J. Lim, "Energy management strategies for base stations in a smart grid environment," *Transactions on Emerging Telecommunications Technologies*, vol. 28, no. 1, Aug 2014.

[53] J. Leithon, T. J. Lim, and S. Sun, "Energy exchange among base stations in a cellular network through the smart grid," in *IEEE International Conference on Communications (ICC)*, Sydney, Australia, June 2014, pp. 4036–4041.

[54] N. Reyhanian, B. Maham, V. Shah-Mansouri, and C. Yuen, "Double-auction-based energy trading for small cell networks with energy harvesting," in *IEEE International Conference on Communications (ICC)*, Kuala Lumpur, Malaysia, May 2016, pp. 1–6.

[55] M. Mendil, A. D. Domenico, V. Heiries, R. Caire, and N. Hadj-said, "Fuzzy Q-Learning based energy management of small cells powered by the smart grid," in *IEEE Annual International Symposium on Personal, Indoor, and Mobile Radio Communications (PIMRC)*, Valencia, Spain, September 2016, pp. 1–6.

[56] M. J. Farooq, H. Ghazzai, A. Kadri, H. ElSawy, and M.-S. Alouini, "A hybrid energy sharing framework for green cellular networks," *IEEE Transactions on Communications*, vol. 65, no. 2, pp. 918–934, Feb 2017.

[57] InternetLiveStats.com, "Internet Live Stats," [Online]. Available: http://www.internetlivestats.com/, Dec 2016 (accessed May, 2019).

[58] A. Kurs, A. Karalis, R. Moffatt, J. D. Joannopoulos, P. Fisher, and M. Soljačić, "Wireless power transfer via strongly coupled magnetic resonances," *Science*, vol. 317, no. 5834, pp. 83–86, July 2007.

[59] A. Kurs, R. Moffatt, and M. Soljačić, "Simultaneous mid-range power transfer to multiple devices," *Applied Physics Letters*, vol. 96, no. 4, pp. 044 102:1–044 102:3, Jan 2010.

[60] L. R. Varshney, "Transporting information and energy simultaneously," in *IEEE International Symposium on Information Theory*, Toronto, ON, CA, July 2008.

[61] R. Zhang and C. K. Ho, "MIMO Broadcasting for Simultaneous Wireless Information and Power Transfer," in *IEEE Global Telecommunications Conference*, Houston, TX, US, Dec 2011.

[62] J. Yang and S. Ulukus, "Optimal Packet Scheduling in an Energy Harvesting Communication System," *IEEE Transactions on Communications*, vol. 60, no. 1, pp. 220–230, Jan 2012.

[63] A. A. Nasir, X. Zhou, S. Durrani, and R. A. Kennedy, "Relaying Protocols for Wireless Energy Harvesting and Information Processing," *IEEE Transactions on Wireless Communications*, vol. 12, no. 7, pp. 3622–3636, July 2013.

[64] J. Jadidian and D. Katabi, "Magnetic MIMO: How to Charge Your Phone in Your Pocket," in *Annual International Conference on Mobile Computing and Networking*, Maui, HI, US, Sept 2014.

[65] M. Sheng, L. Wang, X. Wang, Y. Zhang, C. Xu, and J. Li, "Energy Efficient Beamforming in MISO Heterogeneous Cellular Networks With Wireless Information and Power Transfer," *IEEE Journal on Selected Areas in Communications*, vol. 34, no. 4, pp. 954–968, Apr 2016.

[66] S. Akbar, Y. Deng, A. Nallanathan, M. Elkashlan, and A.-H. Aghvami, "Simultaneous Wireless Information and Power Transfer in K-Tier Heterogeneous Cellular Networks," *IEEE Transactions on Wireless Communications*, vol. 15, no. 8, pp. 5804–5818, Aug 2016.

[67] A. Goldsmith, *Wireless Communications*. New York, NY, US: Cambridge University Press, 2005.

[68] C. Xiao, Y. R. Zheng, and N. C. Beaulieu, "Novel Sum-of-Sinusoids Simulation Models for Rayleigh and Rician Fading Channels," *IEEE Transactions on Wireless Communications*, vol. 5, no. 12, pp. 3667–3679, Dec 2006.

[69] E. V. Denardo, *Dynamic Programming: Models and Applications*. Mineola, NY, US: Dover Publications, 2003.

[70] J. Broch, D. A. Maltz, D. B. Johnson, Y.-C. Hu, and J. Jetcheva, "A performance comparison of multi-hop wireless ad hoc network routing protocols," in *ACM/IEEE international conference on Mobile computing and networking*, Dallas, TX, US, Oct 1998.

[71] D. B. Johnson and D. A. Maltz, *Dynamic Source Routing in Ad Hoc Wireless Networks*. Boston, MA, US: Springer US, 1996, pp. 153–181.

[72] H. Sugiyama, "Packet switched power network with decentralized control based on synchronized QoS routing," *ICT&Applications and Collocated Events*, pp. 147–152, Nov 2012.

[73] V. Krylov, D. Ponomarev, and A. Loskutov, "Toward the power InterGrid," in *IEEE International Energy Conference and Exhibition (ENERGYCON)*. Manama, Bahrain: IEEE, May 2010, pp. 351–356.

[74] J. Ma, L. Song, and Y. Li, "Optimal power dispatching for local area packetized power network," *IEEE Transactions on Smart Grid*, 2017.

[75] A. F. Gambin and M. Rossi, "Energy Cooperation for Sustainable Base Station Deployments: Principles and Algorithms," in *IEEE Global Communications Conference (GLOBECOM)*. Singapore, Singapore: IEEE, Dec 2017.

[76] X. Huang, T. Han, and N. Ansari, "Smart grid enabled mobile networks: Jointly optimizing BS operation and power distribution," *IEEE/ACM Transactions on Networking*, 2017.

[77] T. Han and N. Ansari, "On optimizing green energy utilization for cellular networks with hybrid energy supplies," *IEEE Transactions on Wireless Communications*, vol. 12, no. 8, pp. 3872–3882, 2013.

[78] Z. Guo, T. J. Lim, and M. Motani, "Base station energy cooperation in green cellular networks," in *IEEE Global Conference on Signal and Information Processing (GlobalSIP)*. Austin, Texas, US: IEEE, Dec 2013, pp. 349–352.

[79] M. J. Farooq, H. Ghazzai, A. Kadri, H. ElSawy, and M.-S. Alouini, "Energy sharing framework for microgrid-powered cellular base stations," in *IEEE Global Communications Conference (GLOBECOM)*. Washington, DC, USA: IEEE, Dec 2016, pp. 1–7.

[80] J. Xu, L. Duan, and R. Zhang, "Energy group buying with loading sharing for green cellular networks," *IEEE Journal on Selected Areas in Communications*, vol. 34, no. 4, pp. 786–799, 2016.

[81] B. Gurakan, O. Ozel, and S. Ulukus, "Optimal energy and data routing in networks with energy cooperation," *IEEE Transactions on Wireless Communications*, vol. 15, no. 2, pp. 857–870, 2016.

[82] Z. Wang, V. Aggarwal, and X. Wang, "Joint energy-bandwidth allocation in multiple broadcast channels with energy harvesting," *IEEE Transactions on Communications*, vol. 63, no. 10, pp. 3842–3855, 2015.

[83] V. Aggarwal, M. R. Bell, A. Elgabli, X. Wang, and S. Zhong, "Joint energy-bandwidth allocation for multiuser channels with cooperating hybrid energy nodes," *IEEE Transactions on Vehicular Technology*, vol. 66, no. 11, pp. 9880–9889, 2017.

[84] J. B. Rawlings and D. Q. Mayne, *Model predictive control: Theory and design*. Nob Hill Pub., 2009.

[85] Y. Fang and A. Armaou, "Nonlinear model predictive control using a bilinear Carleman linearization-based formulation for chemical processes," in *American Control Conference (ACC)*. Chicago, IL, US: IEEE, July 2015, pp. 5629–5634.

[86] J. W. Eaton and J. B. Rawlings, "Model predictive control of chemical processes," in *American Control Conference (ACC)*. Boston, MA, US: IEEE, June 1991, pp. 1790–1795.

[87] M. Arefi, A. Montazeri, J. Poshtan, and M. Jahed-Motlagh, "Nonlinear model predictive control of chemical processes with a Wiener identification approach," in *IEEE International Conference on Industrial Technology*. Mumbai, India: IEEE, Dec 2006, pp. 1735–1740.

[88] K. Nejadkazemi and A. Fakharian, "Pressure control in gas oil pipeline: A supervisory model predictive control approach," in *4th International Conference on Control, Instrumentation, and Automation (ICCIA)*. Qazvin, Iran: IEEE, Jan 2016, pp. 396–400.

[89] A. Pavlov, D. Krishnamoorthy, K. Fjalestad, E. Aske, and M. Fredriksen, "Modelling and model predictive control of oil wells with electric submersible pumps," in *IEEE Conference on Control Applications (CCA)*. Nize, France: IEEE, Oct 2014, pp. 586–592.

[90] R. Halvgaard, L. Vandenberghe, N. K. Poulsen, H. Madsen, and J. B. Jørgensen, "Distributed model predictive control for smart energy systems," *IEEE Transactions on Smart Grid*, vol. 7, no. 3, pp. 1675–1682, 2016.

[91] P. Stadler, A. Ashouri, and F. Maréchal, "Distributed model predictive control of energy systems in microgrids," in *Annual IEEE Systems Conference (SysCon).* Orlando, FL, US: IEEE, April 2016, pp. 1–6.

[92] K. Meng, Z. Y. Dong, Z. Xu, and S. R. Weller, "Cooperation-driven distributed model predictive control for energy storage systems," *IEEE Transactions on Smart Grid*, vol. 6, no. 6, pp. 2583–2585, 2015.

[93] S. G. Tzafestas, P. Borne, and L. Grandinetti, *Parallel and Distributed Computing in Engineering Systems: Proceedings of the IMACS/IFAC International Symposium on Parallel and Distributed Computing in Engineering Systems, Corfu, Greece, 23-28 June 1991.* North Holland, 1992.

[94] E. Perea-Lopez, B. E. Ydstie, and I. E. Grossmann, "A model predictive control strategy for supply chain optimization," *Computers & Chemical Engineering*, vol. 27, no. 8, pp. 1201–1218, 2003.

[95] M. W. Braun, D. E. Rivera, M. Flores, W. M. Carlyle, and K. G. Kempf, "A model predictive control framework for robust management of multi-product, multi-echelon demand networks," *Annual Reviews in Control*, vol. 27, no. 2, pp. 229–245, 2003.

[96] P.-H. Lin, S.-S. Jang, and D. S.-H. Wong, "Predictive control of a decentralized supply chain unit," *Industrial & engineering chemistry research*, vol. 44, no. 24, pp. 9120–9128, 2005.

[97] P. Doganis, E. Aggelogiannaki, and H. Sarimveis, "A combined model predictive control and time series forecasting framework for production-inventory systems," *International Journal of Production Research*, vol. 46, no. 24, pp. 6841–6853, 2008.

[98] G. E. Box, G. M. Jenkins, G. C. Reinsel, and G. M. Ljung, *Time series analysis: forecasting and control.* John Wiley & Sons, 2015.

[99] G. P. Zhang and M. Qi, "Neural network forecasting for seasonal and trend time series," *European Journal of Operational Research*, vol. 160, no. 2, pp. 501–514, 2005.

[100] G. P. Zhang, "Time series forecasting using a hybrid arima and neural network model," *Neurocomputing*, vol. 50, pp. 159–175, 2003.

[101] I. Khandelwal, R. Adhikari, and G. Verma, "Time series forecasting using hybrid arima and ann models based on dwt decomposition," *Procedia Computer Science*, vol. 48, pp. 173–179, 2015.

[102] D. J. MacKay, "Gaussian processes-a replacement for supervised neural networks?" 1997.

[103] C. K. Williams, "Prediction with Gaussian processes: From linear regression to linear prediction and beyond," *NATO ASI. Series D, Behavioural and Social Sciences*, vol. 89, pp. 599–621, 1998.

[104] D. J. Leith, M. Heidl, and J. V. Ringwood, "Gaussian process prior models for electrical load forecasting," in *International Conference on Probabilistic Methods Applied to Power Systems*, Ames, IA, USA, Sept 2004, pp. 112–117.

[105] M. Blum and M. Riedmiller, "Electricity demand forecasting using gaussian processes," *Power*, vol. 10, p. 104, 2013.

[106] J. W. Taylor, "Short-term electricity demand forecasting using double seasonal exponential smoothing," *Journal of the Operational Research Society*, vol. 54, no. 8, pp. 799–805, 2003.

[107] J. W. Taylor, L. M. De Menezes, and P. E. McSharry, "A comparison of univariate methods for forecasting electricity demand up to a day ahead," *International Journal of Forecasting*, vol. 22, no. 1, pp. 1–16, 2006.

[108] W. Ketter, J. Collins, and P. Reddy, "Power tac: A competitive economic simulation of the smart grid," *Energy Economics*, vol. 39, pp. 262–270, 2013.

[109] J. Kocijan, R. Murray-Smith, C. E. Rasmussen, and B. Likar, "Predictive control with Gaussian process models," in *EUROCON 2003. Computer as a Tool. The IEEE Region 8*, vol. 1. IEEE, 2003, pp. 352–356.

[110] A. Pawlowski, J. L. Guzmán, F. Rodríguez, M. Berenguel, and J. E. Normey-Rico, "Predictive control with disturbance forecasting for greenhouse diurnal temperature control," *IFAC Proceedings Volumes*, vol. 44, no. 1, pp. 1779–1784, 2011.

[111] B. Likar and J. Kocijan, "Predictive control of a gas–liquid separation plant based on a Gaussian process model," *Computers & Chemical Engineering*, vol. 31, no. 3, pp. 142–152, 2007.

[112] A. Grancharova, J. Kocijan, and T. A. Johansen, "Explicit stochastic predictive control of combustion plants based on Gaussian process models," *Automatica*, vol. 44, no. 6, pp. 1621–1631, 2008.

[113] R. Palm, "Multiple-step-ahead prediction in control systems with Gaussian process models and TS-fuzzy models," *Engineering Applications of Artificial Intelligence*, vol. 20, no. 8, pp. 1023–1035, 2007.

[114] J. Ko, D. J. Klein, D. Fox, and D. Haehnel, "Gaussian processes and reinforcement learning for identification and control of an autonomous blimp," in *IEEE International Conference on Robotics and Automation*. Roma, Italy: IEEE, April 2007, pp. 742–747.

[115] J. M. Maciejowski and X. Yang, "Fault tolerant control using Gaussian processes and model predictive control," in *Conference on Control and Fault-Tolerant Systems (SysTol)*. Nice, France: IEEE, Oct 2013, pp. 1–12.

[116] Y. Wang, C. Ocampo-Martínez, V. Puig, and J. Quevedo, "Gaussian-process-based demand forecasting for predictive control of drinking water networks," in *International Conference on Critical Information Infrastructures Security.* Limassol, Cyprus: Springer, October 2014, pp. 69–80.

[117] A. Von Meier, *Electric power systems: a conceptual introduction.* John Wiley & Sons, 2006.

[118] Telecom Italia (TIM), "Open Big Data Challenge," [Online]. Available: https://dandelion.eu/datamine/open-big-data/, 2015 (accessed April, 2019).

[119] M. Ester, H.-P. Kriegel, J. Sander, X. Xu *et al.*, "A density-based algorithm for discovering clusters in large spatial databases with noise," in *KDD*, vol. 96, no. 34, 1996, pp. 226–231.

[120] G. Auer, O. Blume, V. Giannini, I. Godor, M. Imran, Y. Jading, E. Katranaras, M. Olsson, D. Sabella, P. Skillermark *et al.*, "D2. 3: Energy efficiency analysis of the reference systems, areas of improvements and target breakdown," *EARTH*, pp. 1–69, Dec 2010.

[121] A. Biason and M. Zorzi, "On the Effects of Battery Imperfections in an Energy Harvesting Device," in *2016 International Conference on Computing, Networking and Communications.* Hawaii, USA: IEEE, Feb 2016.

[122] E. Hadoux, A. Beynier, and P. Weng, "Generalization and reuse of machine learning models over multiple contexts," in *International Workshop on Learning over Multiple Contexts (ECML)*, Nancy, France, Sept 2014.

[123] C. E. Rasmussen and C. K. Williams, *Gaussian processes for machine learning.* MIT press Cambridge, 2006, vol. 1.

[124] R. Murray-Smith, T. A. Johansen, and R. Shorten, "On transient dynamics, off-equilibrium behaviour and identification in blended multiple model structures," in *Control Conference (ECC), 1999 European.* IEEE, 1999, pp. 3569–3574.

[125] D. Leith, R. Murray-Smith, and W. Leithead, "Nonlinear structure identification: A Gaussian Process prior/Velocity-based approach," 2000.

[126] D. Duvenaud, J. R. Lloyd, R. Grosse, J. B. Tenenbaum, and Z. Ghahramani, "Structure discovery in nonparametric regression through compositional kernel search," *arXiv preprint arXiv:1302.4922*, 2013.

[127] C. E. R. . H. Nickisch, "The GPML Toolbox version 4.0," [Online]. Available: http://www.gaussianprocess.org/gpml/code/matlab/doc/manual.pdf, 2018 (accessed April, 2019).

[128] Y. Wang, C. Ocampo-Martinez, and V. Puig, "Stochastic model predictive control based on Gaussian processes applied to drinking water networks," *IET Control Theory & Applications*, vol. 10, no. 8, pp. 947–955, 2016.

[129] M. Grant, S. Boyd, and Y. Ye, "CVX: Matlab software for disciplined convex programming," [Online]. Available: http://cvxr.com/cvx/, 2008 (accessed April, 2019).

[130] T. Zhang, Y. Zhang, H. Lei, B. Guo, and Y. Zha, "Optimal microgrid operation based on model predictive control framework," in *3rd International Conference on Control, Automation and Robotics (ICCAR).* Nagoya, Japan: IEEE, Apr 2017, pp. 575–581.

[131] H. W. Kuhn, "The Hungarian method for the assignment problem," *Naval research logistics quarterly*, vol. 2, no. 1-2, pp. 83–97, Mar 1955.

[132] A. Lieder, D. Briskorn, and R. Stolletz, "A Dynamic Programming Approach for the Aircraft Landing Problem with Aircraft Classes," *European Journal of Operational Research*, vol. 243, pp. 61–69, July 2015.

[133] R. Morabito, "Power Consumption of Virtualization Technologies: An Empirical Investigation," in *IEEE International Conference on Utility and Cloud Computing (UCC)*, Limassol, Cyprus, Dec 2015.

[134] Y. Jin, Y. Wen, and Q. Chen, "Energy efficiency and server virtualization in data centers: An empirical investigation," in *IEEE Conference on Computer Communications Workshops (INFOCOM Workshops)*, Orlando, USA, Mar 2012.

[135] T. Dlamini, A. F. Gambin, D. Munaretto, and M. Rossi, "Online Supervisory Control and Resource Management for Energy Harvesting BS Sites Empowered with Computation Capabilities," *Hindawi Wireless Communications and Mobile Computing*, 2019.

[136] I. Goodfellow, Y. Bengio, A. Courville, and Y. Bengio, *Deep learning.* MIT press Cambridge, 2016, vol. 1.

[137] T. Frisanco, P. Tafertshofer, P. Lurin, and R. Ang, "Infrastructure sharing and shared operations for mobile network operators from a deployment and operations view," in *IEEE Network Operations and Management Symposium (NOMS).* Salvador, Bahia, Brazil: IEEE, April 2008, pp. 129–136.

[138] J. Markendahl and A. Ghanbari, "Shared smallcell networks multi-operator or third party solutions-or both?" in *11th International symposium and workshops on modeling and optimization in mobile, Ad Hoc and wireless networks (WiOpt).* Tsukuba Science City, Japan: IEEE, May 2013, pp. 41–48.

[139] L. Cano, A. Capone, G. Carello, M. Cesana, and M. Passacantando, "On optimal infrastructure sharing strategies in mobile radio networks," *IEEE Transactions on Wireless Communications*, vol. 16, no. 5, pp. 3003–3016, 2017.

[140] Z. Zhu, J. Peng, X. Gu, H. Li, K. Liu, Z. Zhou, and W. Liu, "Fair resource allocation for system throughput maximization in mobile edge computing," *IEEE Access*, vol. 6, pp. 5332–5340, 2018.

[141] C. Wang, C. Liang, F. R. Yu, Q. Chen, and L. Tang, "Computation offloading and resource allocation in wireless cellular networks with mobile edge computing," *IEEE Transactions on Wireless Communications*, vol. 16, no. 8, pp. 4924–4938, 2017.

[142] J. Zhang, W. Xia, F. Yan, and L. Shen, "Joint computation offloading and resource allocation optimization in heterogeneous networks with mobile edge computing," *IEEE Access*, vol. 6, pp. 19 324–19 337, 2018.

[143] J. Xu and S. Ren, "Online Learning for Offloading and Autoscaling in Renewable-Powered Mobile Edge Computing," in *IEEE Global Communications Conference (GLOBECOM)*, Washington, USA, Dec 2016.

[144] A. Beloglazov, J. Abawajy, and R. Buyya, "Energy-aware Resource Allocation Heuristics for Efficient Management of Data Centers for Cloud Computing," *Future Generation Computer Systems*, vol. 28, no. 5, pp. 755–768, 2012.

[145] R. Nathuji and K. Schwan, "VirtualPower: coordinated power management in virtualized enterprise systems," in *Proceedings of twenty-first ACM SIGOPS symposium on Operating systems principles*, Washington, USA, Oct 2007.

[146] M. Nelson, B.-H. Lim, and G. Hutchins, "Fast Transparent Migration for Virtual Machines," in *Proceedings of the Annual Conference on USENIX Annual Technical Conference*, Berkeley, USA, Apr 2005.

[147] C. Jeffrey, A. Darrell, T. Prachi, V. Amin, and D. Ronald, "Managing energy and server resources in hosting centers," in *Proceedings of the 18th ACM Symposium on Operating Systems Principles*, Alberta, Canada, Oct 2001.

[148] J. R. Lorch and A. J. Smith, "PACE: A new approach to dynamic voltage scaling," *IEEE Transactions on Computers*, vol. 53, no. 7, pp. 856–869, 2004.

[149] "Five Trends to Small Cells 2020," Huawei Technologies, Helsinki, Finland, Tech. Rep., Feb 2016.

[150] D. Pelleg, A. W. Moore *et al.*, "X-means: Extending K-means with efficient estimation of the number of clusters," in *Proceedings of the Seventeenth International Conference on Machine Learning (ICML)*, vol. 1, San Francisco, CA, USA, June 2000, pp. 727–734.

[151] T. Dlamini, A. F. Gambin, D. Munaretto, and M. Rossi, "Online Resource Management in Energy Harvesting BS Sites through Prediction and Soft-Scaling of Computing Resources," in *IEEE International Symposium on Personal, Indoor and Mobile Radio Communications (PIMRC)*, Bologna, Italy, Sept 2018.

[152] National Grid USA Service Company, "US National Grid - Electric Service," [Online]. Available: https://www9.nationalgridus.com/niagaramohawk/business/rates/3˙elec.asp, January 2015 (accessed May, 2019).

[153] S. Hochreiter and J. Schmidhuber, "Long Short-Term Memory," *Neural Computation*, vol. 9, no. 8, pp. 1735–1780, Nov 1997.

[154] F. A. Gers, J. Schmidhuber, and F. Cummins, "Learning to forget: Continual prediction with LSTM," 1999.

[155] D. P. Kingma and J. Ba, "Adam: A method for stochastic optimization," in *International Conference on Learning Representations (ICLR).* San Diego, CA, USA: IEEE, May 2015.

[156] F. Chollet *et al.*, "Keras," [Online]. Available: https://github.com/keras-team/keras, 2015 (accessed May, 2019).

[157] M. Abadi *et al.*, "TensorFlow: Large-Scale Machine Learning on Heterogeneous Systems," [Online]. Available: https://www.tensorflow.org/, 2015 (accessed May, 2019).